Dolphin Bones in Mawaki Archaeological Site : Holocene Paleoenvironmental Changes in Far East

Yasuto Itoh   Hideki Takada   Keiji Takemura

Dolphin Bones in Mawaki Archaeological Site:

Holocene Paleoenvironmental Changes in Far East

Dolphin Bones in Mawaki Archaeological Site: Holocene Paleoenvironmental Changes in Far East

Edited by

Yasuto Itoh

Hideki Takada

Keiji Takemura

List of Authors

Yasuto Itoh (Editor, Chapter 1, 3, 6)

Department of Physical Sciences, Graduate School of Science, Osaka Prefecture University (Gakuen-cho 1-1, Naka-ku, Sakai, Osaka 599-8531, Japan)

itoh@p.s.osakafu-u.ac.jp

Keiji Takemura (Editor, Chapter 1, 2, 3, 6)

Beppu Geothermal Research Laboratory, Institute for Geothermal Sciences, Graduate School of Science, Kyoto University (Noguchibaru, Beppu, Oita 874-0903, Japan)

takemura@bep.vgs.kyoto-u.ac.jp

Hideki Takada (Editor, Chapter 2, 3, 4, 5, 6)

The Mawaki Jomon Museum (Mawaki 48-100, Noto-cho, Ishikawa 927-0562, Japan)

takada-h@town.noto.lg.jp

Shigekazu Kusumoto (Chapter 1)

Graduate School of Science and Engineering for Research, University of Toyama (3190 Gofuku, Toyama 930-8555, Japan)

kusu@sci.u-toyama.ac.jp

Tsuyoshi Haraguchi (Chapter 3)

Graduate School of Science, Osaka City University (3-3-138 Sugimoto, Sumiyoshi-ku, Osaka 558-8585, Japan)

haraguti@sci.osaka-cu.ac.jp

Toshio Nakamura (Chapter 4)

Division of Chronological Research, Institute for Space-Earth Environmental Research, Nagoya University (Chikusa, Nagoya 464-8601, Japan)

nakamura@nendai.nagoya-u.ac.jp

Masaaki Kanehara (Chapter 5)

Nara University of Education (Takabatake-cho, Nara 630-8528, Japan)

kanehara@nara-edu.ac.jp

Preface

This book presents the fruits of interdisciplinary study conducted on an early Holocene archaeological site upon the Noto Peninsula of central Japan. From the famous Mawaki archaeological site, countless dolphin bones have been excavated, which are associated with various stone artifacts (arrowheads, knives and scrapers) and ritual wood columns, indicating the presence of a longstanding fishery on the Sea of Japan coast, a fact which reflects regional sea-level and paleoenvironmental changes. Affluent information on the climatic and geologic phenomena during the Holocene time was pursued by means of stratigraphy, paleontology, geochronology and geophysics.

In Chapter 1, Itoh, Y. and others present the outline of Noto Peninsula and Toyama Bay based on geophysical, geological and geomorphological information. They provide the readers with tectonic and geological perspective of the study area. Takada, H. and Takemura, K. focus on the archaeological significance of the Mawaki site (Chapter 2). Chapter 3 by Takemura, K. and others is dedicated to describing Holocene stratigraphy around the study area putting emphasis on the occurrence and significance of dolphin bones. Chronological constraints on the paleoenvironmental discussion are given by radiocarbon dating with accelerator mass spectrometry of Holocene sediments at the Mawaki site by Nakamura, T. and Takada, H. (Chapter 4). A paleontological evaluation of the Mawaki environment is shown by Kanehara, M. and Takada, H. based on analyses of pollen and diatoms (Chapter 5). Finally, an estimate of the Holocene sea level changes on the coastal area is presented by Takemura, K. and others in Chapter 6.

Through such intensive multidisciplinary approaches, the authors attempt to describe life of the ancients on post-glacial Far East, which has never been understood in the framework of long-term environmental changes.

We thank Dr. T. Sato (Geological Survey, Japan) for inputs pertaining to the sea

http://www.sciencepublishinggroup.com

Contents

Contents

Contents

Chapter 1

Outline of Noto Peninsula and Toyama Bay: Tectonic and Geological Framework

Yasuto Itoh

Shigekazu Kusumoto

Keiji Takemura

Abstract

Outline of the attractive archaeological site is overviewed from the geomorphological, geological and geophysical points of view. Categorized landforms of the Japanese Archipelago indicate that the Mawaki site is placed on a stable plateau facing the Japan Sea backarc basin. Large facies variety in volcaniclastic and marine sedimentary sequence around the site records long-term paleoenvironmental changes after the rifting event in the Miocene. Sharp contrasts in gravity and geomagnetic anomalies delineate deep-rooted structure related with cumulative crustal deformation under strong tectonic stress, which has concurrently enhanced recent activities on remarkable reverse fault zones. Three-dimensional perspective of the study area surrounded by such deformation front is presented utilizing new datasets of reflection seismic survey.
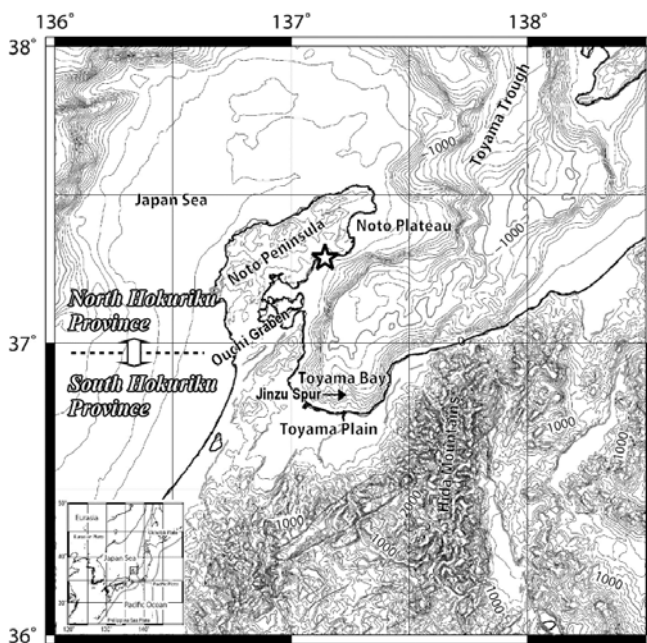
Figure 1.1 *Landforms of the Hokuriku Province. Star denotes the Mawaki archaeological site. Summit level contours are in 100 m interval. Inset shows plate tectonic configuration around southwest Japan.*

1.1   Landforms

The Mawaki archaeological site is located on the eastern coast of the Noto Peninsula in Hokuriku Province, central Japan (Figure 1.1). Regional characteristics from the viewpoints of earth science are summarized in this chapter, which should help readers to cultivate perspective view on the longstanding attractive ancient ruins.

Noto Peninsula looks like a forearm embracing the Toyama Bay, which is an 1,000-m deep basin fringed with 3,000-m mountains of the Japan Alps. Divided by NE-SW Ouchi Graben, the root of the peninsula constitutes a part of active geomorphic block that is referred to as South Hokuriku Province in this chapter, whereas its tip including the Mawaki site has a feature of peneplain and referred to as North Hokuriku Province.

Active landforms of the South Hokuriku Province are summarized based on concise description by Fujii (1988) as follows. The Hida Mountains act as eastern and southern border of the province and supply enormous amount of detritus to form grand alluvial fans in the Toyama Plain. Active uplift of the mountainous range reaches 5 mm/year. Active deformation is also reflected in tilted surface of river terraces, altitude and gradient of which are getting larger with age. In sharp contrast, the Toyama Bay (Figure 1.1) is actively subsiding during the Quaternary. Its shelf is quite narrow as a result of progradation of alluvial fans and vigorous coastal erosion. Beyond fault-related rugged slope, its basal area is divided by the Jinzu Spur into eastern and western portions and merged northeastward into mouth of the Toyama Trough.

North Hokuriku Province is interpreted as a low-relief continental fragment in the Japan Sea largely immune to tectonic movements throughout the Neogene and Quaternary, and the shelf that surrounds it is quite narrow. Around the Mawaki site, altitudes of marine terraces correlated with oxygen isotope stages 5e, 7, and 9 are about 40 m, 60 m to 70 m, and 100 m, respectively

(Koike and Machida, 2001), and the average uplift rate is 0.3 mm/year.

1.2　Geology

We first set focus on the North Hokuriku Province (Figure 1.2), and present a brief geologic summary. Most of its surface consists of altered early Miocene volcanic rocks (Anamizu and Yanagida Formations), which is underlain by sporadic exposures of the Mesozoic Funatsu Granites accompanied with metamorphic rocks and overlain by middle to late Miocene diatomaceous mudstone. The Mawaki site is surrounded by the Neogene volcaniclastic hills about 100 m high and is located on an alluvial plain between 4 m and 12 m above sea level.

Thick piles of volcaniclastic and marine sediments burying an enormous basin of the South Hokuriku Province are cut by numerous active faults (Figure 1.3). It is noted that the NE-SW trending faults constitute some bunches of neotectonic zones, of which characteristics will be discussed in the following 'Tectonics' section.
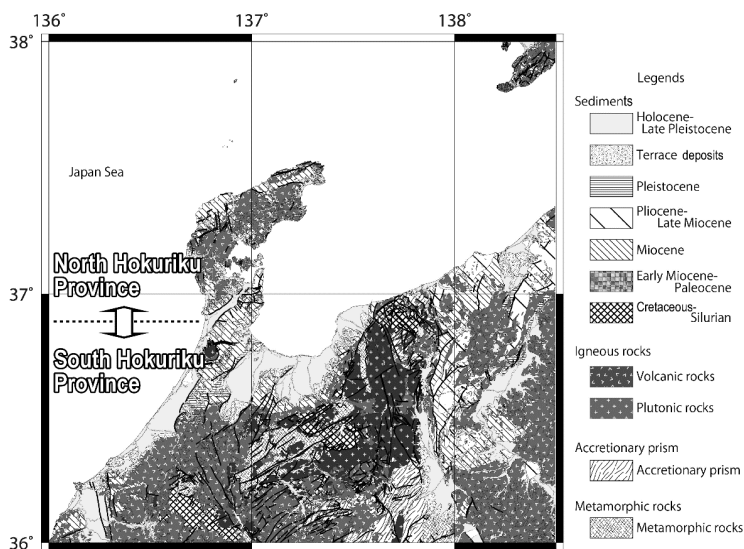
Figure 1.2　*Simplified geologic map of the Hokuriku Province in central Japan.*
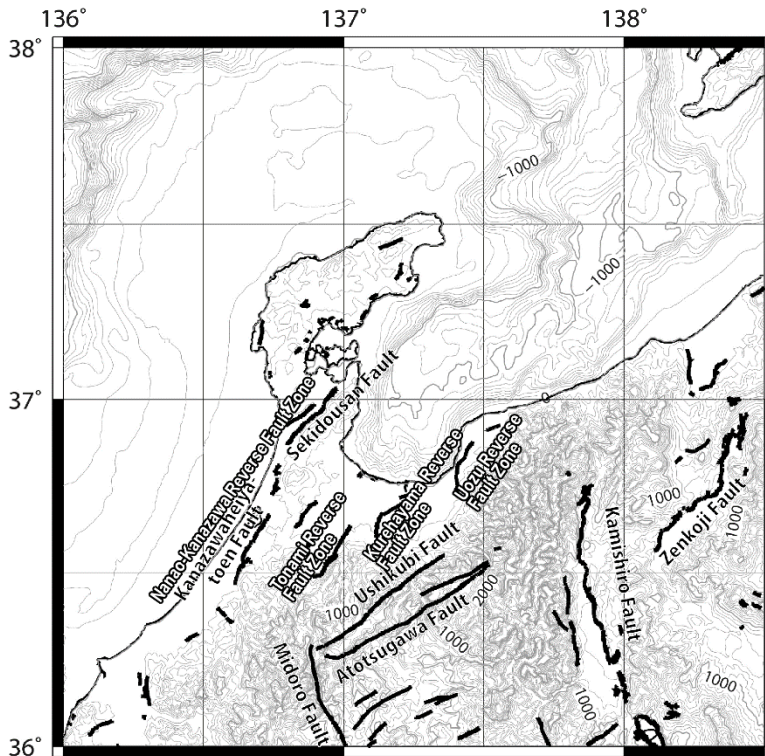
Figure 1.3 *Active faults around the Hokuriku Province.*

1.3　Geophysics

1.3.1　Gravity Anomaly

In Figure 1.4, we show gravity anomaly map assuming the Bouguer density of 2670 kg/m^3. The Bouguer gravity anomaly map shown in Figure 1.4 is the residual Bouguer gravity anomaly map of which the first trend surface estimated by the least square method was removed from the original Bouguer gravity anomaly.
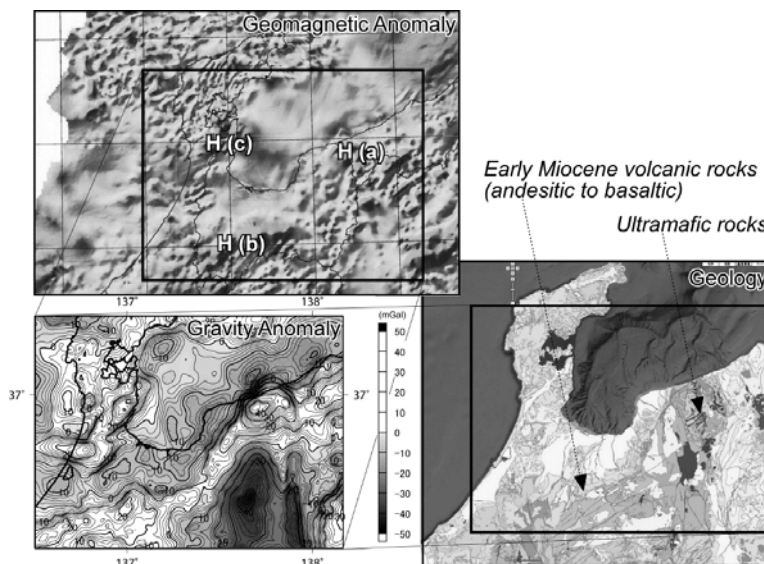
Figure 1.4 *Geomagnetic anomaly trend around the Hokuriku Province (Nakatsuka and Okuma, 2005) together with Bouguer gravity anomaly (Komazawa, 2004) and geologic (Geological Survey of Japan, 2012) maps. Annotation 'H' in geomagnetic anomaly map corresponds to area accompanied by remarkable high (positive) anomaly.*

Low gravity anomalies in the southeast region in the study area are corresponding to the northern part of mountain range in central Japan and might be caused by isostasy due to the loads of mountains because they have heights beyond 3,000 m. In addition, the north-south long and narrow low gravity anomaly is caused by Matsumoto Basin which is the tectonic basin with thick sedimentary layer (e.g., Okubo et al., 1990).

Toyama Basin and Toyama Bay are characterized by low gravity anomalies, which are caused by low density materials such as fan and Quaternary sediments. On the other hand, the Noto Peninsula including Mawaki and the eastern part of the Toyama Basin are characterized by high gravity anomalies. These high gravity anomalies are close to low gravity area and there are steep gradients between these gravity anomalies. The steep gradient in the eastern part of Toyama Basin is corresponding to the Kurobishi-Yama Fault (Tsujimura,

1926). The southern part of the steep gravity gradient in the western Toyama is corresponding to the Tonami-Heiya Seien Fault Zone including Isurugi Fault (e.g., Ikebe, 1949).

The northern part of the steep gradient in the western part of the basin was found by dense gravity survey (e.g., Sunami and Kono, 1988; Hagita et al., 1997). Although tectonic lines and fault topographies such as fault scarps have not been confirmed around this steep gradient zone, they have suggested that concealed faults (e.g., Himi Fault) would exist in this zone. Sutou et al. (2004) showed that epicentres of micro-earthquakes distributed in the steep zone, and that this steep gradient can be explained by basement deformation reaching 1 km. In their subsurface modelling, they considered the characteristics of the surface geology and explained the steep gravity gradient by deformation of basement without deformation of the Quaternary sediment near the surface.

1.3.2   Geomagnetic Anomaly
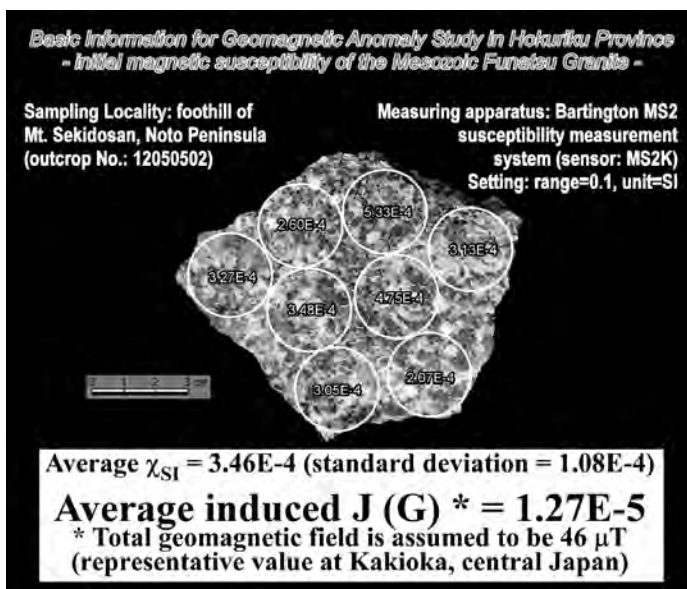
Figure 1.5   *Results of measurement of initial magnetic susceptibility of the Funatsu Granites exposed in the Noto Peninsula.*

Reflecting inhomogeneity in basement rocks, there are several conspicuous highs of geomagnetic anomaly around the study area (Figure 1.4). Geomagnetic anomalies on the eastern (H(a) in Figure 1.4) and southern (H(b)) margins of the South Hokuriku Province are accompanied with positive Bouguer gravity anomaly and probably originated from ultramafic complex in the Hida Marginal Belt and widely-exposed early Miocene volcanics.

Origin of another domal anomaly around the border of the North and South Hokuriku Provinces (H(c)) remains unsolved. To evaluate contribution of the sporadic Funatsu Granites as an anomaly source, we undertook a rock magnetic experiment. A hand-specimen was taken at the foothill of Mt. Sekidosan located on the positive anomaly, and its initial magnetic susceptibility was measured on a flat surface using a Bartington MS2 susceptibility meter equipped with a contact sensor (MS2K). Results summarized in Figure 1.5 clearly demonstrate that induced magnetization of the Funatsu Granites is too weak to generate the observed anomaly. As for the plutonic body, Hirooka et al. (1983) showed that natural remanent magnetization is also scored quite low and ruled out of candidates.

Alternative possible theory for the conspicuous positive anomaly is a hypothetical failed rift around the North Hokuriku Province. Itoh et al. (2006) submitted a paleogeographic reconstruction before the event of backarc opening of the Japan Sea. They assumed a failed rift around the area of the present analysis based on distribution of the early Miocene rift-margin type volcanism (Figure 1.6). We, then, propose that a bunch of syn-rifting volcanics are buried under the North Hokuriku Province, generating clustered geomagnetic anomalies in the area.
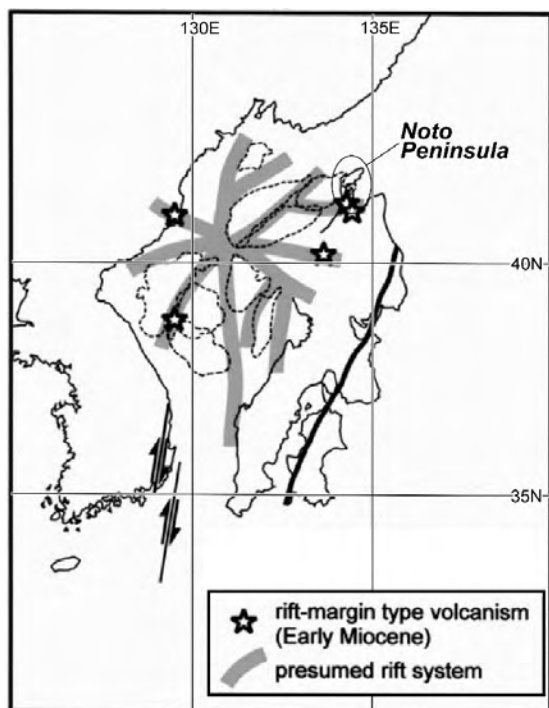
Figure 1.6 *Paleogeographic reconstruction of southwest Japan in an initial rifting stage of the Japan Sea after Itoh et al. (2006).*

1.3.3 Seismic Survey

In 1987, an offshore seismic survey (Nishitsugaru-Niigata-Oki) was conducted on the backarc shelf of northeast Japan using M/V KAIYO, by MITI (Ministry of International Trade and Industry). During the shooting of 4,010 km seismic lines, 96 channels of hydrophones (with an interval of 25 m) recorded the energy released from a 70 l (4,244 in.^{3}) tuned airgun array, shot at 25 m interval. Raw seismic data were stacked and then subjected to a post-stack processing sequence in order to enhance the resolution.
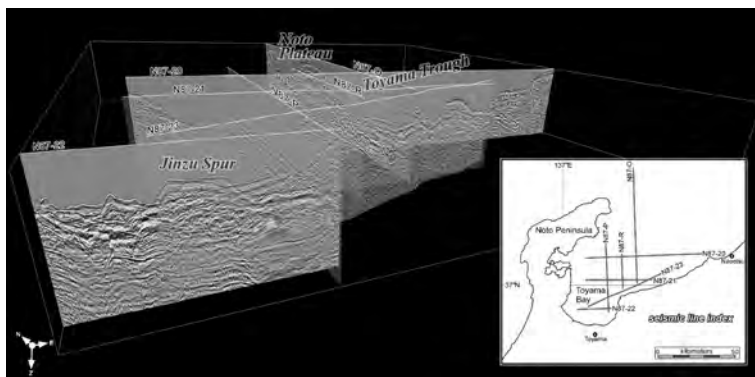
Figure 1.7 *A bird's-eye image of submarine topographic and structural architectures around the Toyama Bay based on reflection seismic profiles of the Nishitsugaru-Niigata-Oki offshore survey.*

Figure 1.7 presents a bird's-eye view of submarine topographic and structural architectures around the Toyama Bay based on the reflection seismic profiles. The Noto Plateau, Toyama Trough and Jinzu Spur are delineated as an undeformed basement high, a longstanding channel and a fault-bounded horst, respectively. Flat sedimentary top of the Jinzu Spur is partly tilted, implying active deformation.

Figure 1.8 shows depth-converted seismic profiles of the N-S line N87-O. It is noted that some discontinuous but strong reflectors are identified within acoustic basement of the Noto Plateau. It may be originated from syn-rifting intrusive bodies, which are responsible for conspicuous geomagnetic anomalies in the area (see Figure 1.4). Depth-converted profile of the E-W line N87-22 (Figure 1.9) is highly provocative. The Jinzu Spur is a horst bounded by normal faults. Separation of seismic horizons and lateral change in thickness of interpreted geologic units clearly demonstrate that the extensional feature has developed since the Pliocene. Controversial point is that the regional tectonic stress during the period was compressive as discussed in the next section. To understand the complex structural trend, numerical deformation modeling of upper crust may be effective.
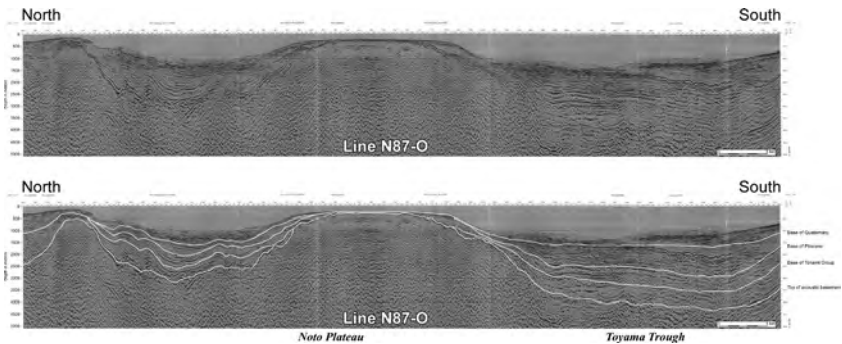
Figure 1.8 *Depth-converted seismic profiles (top, raw; bottom, interpreted) of the N-S line N87-O. See Figure 1.7 for line location.*
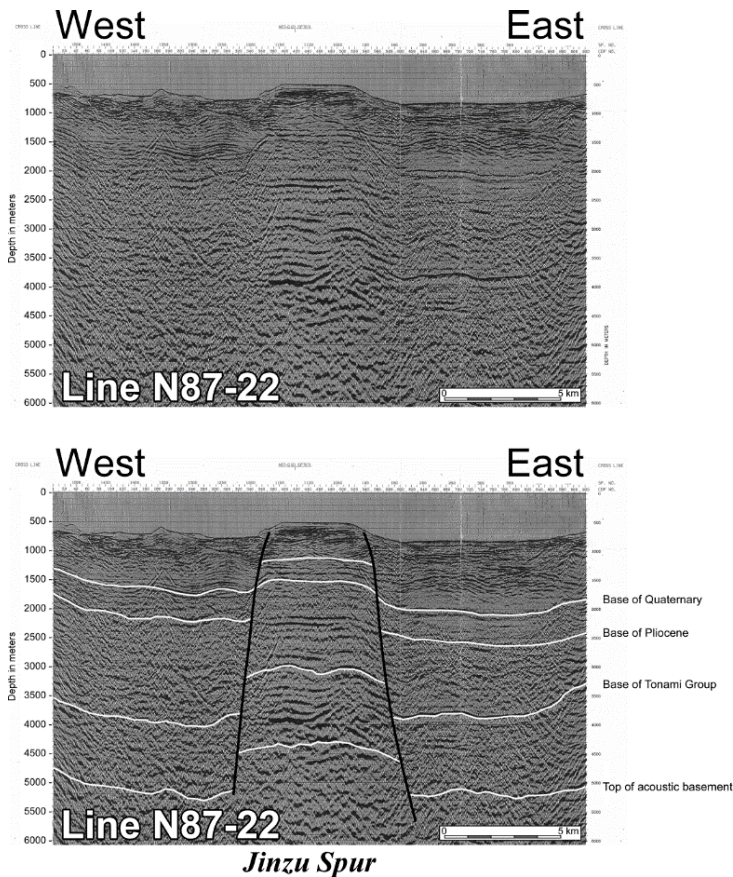
Figure 1.9 *Depth-converted seismic profiles (top, raw; bottom, interpreted) of the E-W line N87-22. See Figure 1.7 for line location.*

Figures 1.10, 1.11 and 1.12 are isopach maps around the Toyama Bay for the total sediment thickness, Miocene sediments and Plio- / Pleistocene sediments, respectively. Sedimentary layers are thickest around the deepest portion of the bay (Figure 1.10), a fact which is suggestive of deficit in the balance of subsidence / burial in spite of enormous clastic influx from the Japan Alps hinterland. Miocene isopach (Figure 1.11) indicates that northeastern part of the bay was under stagnant subsidence, whereas prominent depocenters developed in the southwestern portion. Although coeval sediments on adjacent land are rather thin, the confined depression may have relation with deep-rooted structure along the western coast of the bay delineated through gravity analysis. Sedimentation pattern in recent periods (Figure 1.12) represents shrinkage of basin as a result of rising compressive regime around the South Hokuriku Province.
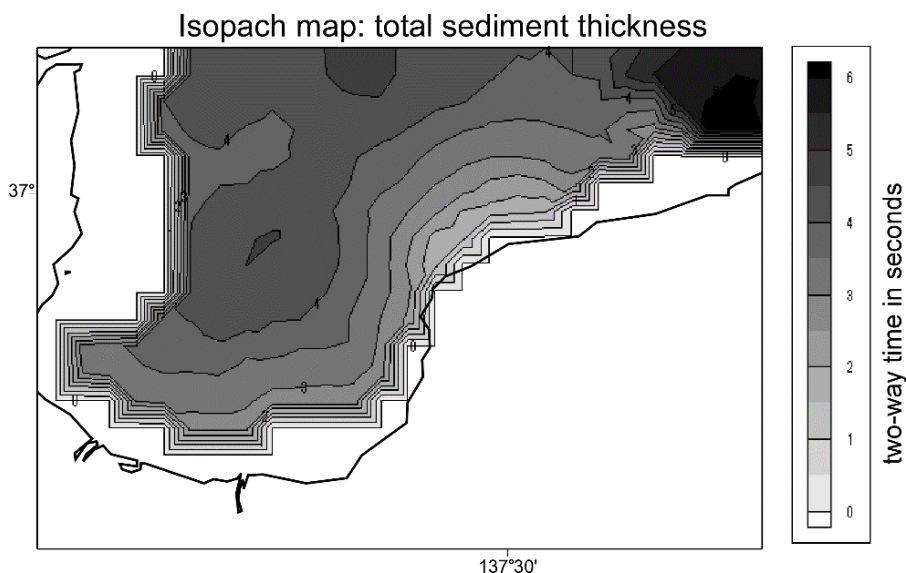
Figure 1.10   *Two-way time isopach map around the Toyama Bay: total sediment thickness.*

Isopach map: Miocene sediments
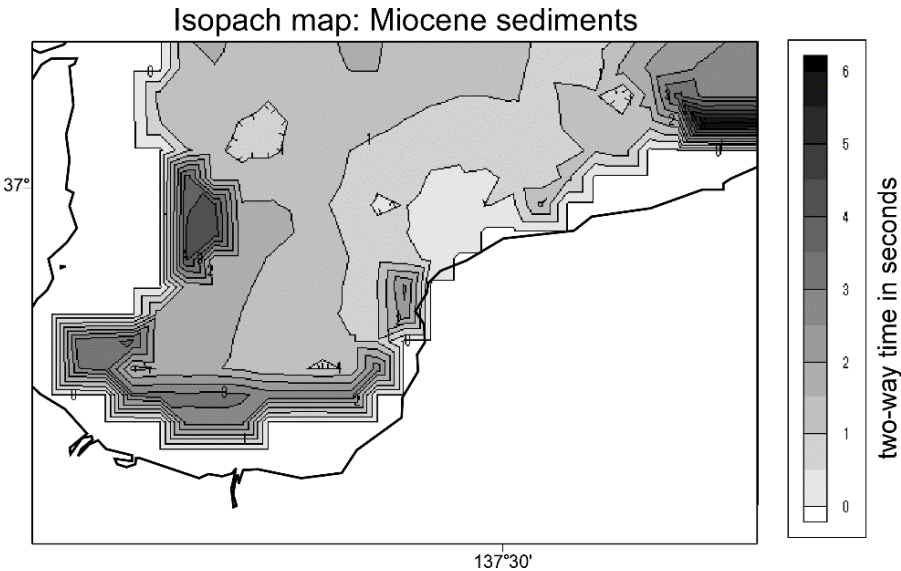
Figure 1.11 *Two-way time isopach map around the Toyama Bay: Miocene sediments.*

Isopach map: Plio- / Pleistocene
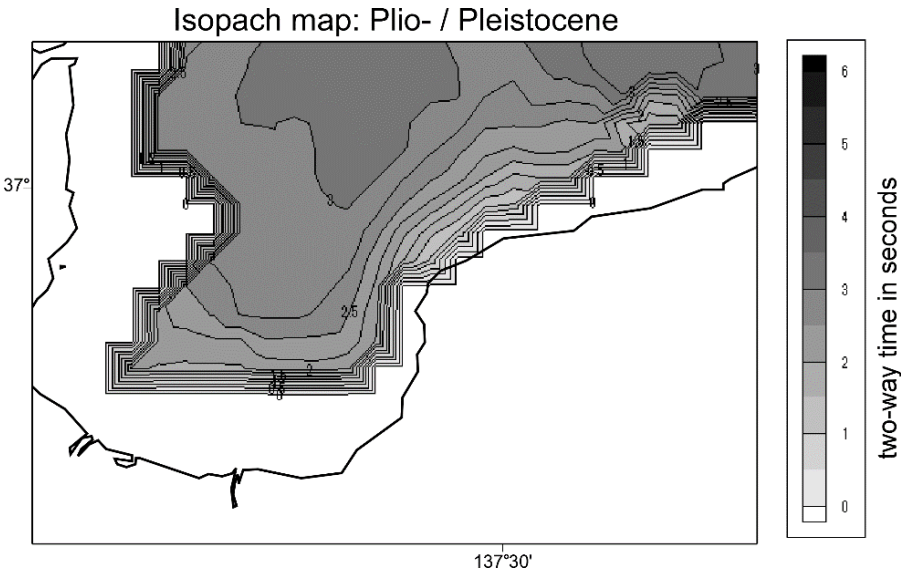
Figure 1.12 *Two-way time isopach map around the Toyama Bay:*
Plio- / Pleistocene sediments.

1.4 Tectonics

1.4.1 Miocene Backarc Rifting

Most important tectonic event governing geomorphic and paleoenvironmental changes around the Hokuriku Province is the Miocene backarc rifting of the Japan Sea. Since 1980s, numerous researchers have studied the remarkable event by any possible means of analysis. Although fruits of marine geological surveys were summarized by Jolivet and Tamaki (1992) and Tada and Tamaki (1992), survey sites were chosen excluding basin center because frequent discharge of flammable gases cannot be controlled by using a non-riser drilling vessel. Hence we describe features of the event on firm ground data.

I Geological Evidence

Hayakawa and Takemura (1987) described an event sequence in the Yatsuo area, a prominent hilly area in central part of the South Hokuriku Province (Figure 1.2). They showed that the early to middle Miocene Yatsuo Group is a cycle of transgressive unit accompanied with intensive volcanism. Paleoenvironmental analysis revealed that the initial littoral to shelf settings had deepened into slope to basin floor settings simultaneously with accumulation of the marine sediments as thick as 1,500 m. It is inevitably postulated that the massive subsidence was linked to thinning of backarc crust and vigorous faulting along rift zones during the Japan Sea opening event, because the Yatsuo Group is one of the lowermost marine Cenozoic strata upon the backarc margin. Their investigation also showed that the Yatsuo Group was unconformably overlain by non-volcanic clastics of the Tonami Group, base of which constitutes a continuous seismic horizon in the Toyama Bay as mentioned above, suggesting a drastic change in basin configuration and stagnant subsidence since the late Miocene. Away from the backarc rift zones, Neogene strata in the North Hokuriku Province are much thinner than those in the southern domain.

II   Paleomagnetic Analysis

Formation process of the western Japan Sea is characterized by fan-shaped backarc spreading as a result of rapid clockwise rotation of southwest Japan, which was elucidated through pioneering paleomagnetic studies by Otofuji and his colleagues. For example, Otofuji and Matsuda (1987) estimated amount of the early Miocene tectonic rotation and submitted the first-time reliable paleogeographic reconstruction before rifting. Their kinematic model, however, did not contain the Hokuriku Province reflecting incomplete dataset at that point in time.

Itoh (1988) presented paleomagnetic data sufficient to evaluate the Cenozoic tectonic episodes around the Hokuriku Province. He pointed out that the clockwise rotation angle of the study area is smaller than that of the main part of southwest Japan, presumably related to regional bending in an arc-arc collision event. Based on along-arc declination changes determined for the early Miocene rocks in Hokuriku, Itoh and Ito (1989) submitted a model of ductile deformation of the crust in a short period.

Magnetostratigraphy was first studied by Itoh and Hayakawa (1988) for the thick Neogene sequence in the Yatsuo area, and their numerical estimation of sedimentation rates lent support to the paleoenvironmental model after Hayakawa and Takemura (1987). These research results during two decades was summed up by Tamaki et al. (2006), who presented a complete paleomagnetic dataset of the Yatsuo Group and most reliable stratigraphic correlation.

1.4.2   Neotectonic Events

As suggested by Huzita (1980), southwest Japan in late Cenozoic has been suffering progressive E-W tectonic stress in general, which is often regarded as an effect of accelerated subduction of the Pacific Plate. Since recent events are directly linked to environmental and/or geographical circumstances of the

Mawaki site, we investigate neotectonic episodes specific for the Hokuriku Province in the following sections.

I   Emergence of Compressive Regime Around Hokuriku

Itoh et al. (1997) presented the Neogene to Quaternary burial history on the backarc shelf of southwest Japan based on stratigraphic data obtained from deep exploration boreholes. Although their age determination was not precise enough to evaluate the Quaternary change in tectonic regimes, ubiquitous accelerated subsidence since 5 Ma has been confirmed in the backarc basin including the Hokuriku Province. Fujii et al. (1976) pointed out that contemporaneous uplift of hilly province was under way. Thus the recent landforms in Hokuriku may have developed under a compressive regime.

In reference to remarkable gradient in Bouguer anomaly around the Toyama Bay (Section 1.3.1), Ohkubo et al. (2000) stated that the Pliocene strata along the western coast is unconformably overlain by the Junicho Formation, which is assigned to the early Quaternary (Satoguchi and Nagahashi, 2012). Hayakawa and Takemura (1987) presumed a hiatus between the Pliocene and Pleistocene units in the Yatsuo area. Itoh (1985) found that the Pleistocene Yokoo Formation on the northeastern point of the South Hokuriku Province is settled on the middle Miocene units, with a 10 m.y.-long hiatus. The stratigraphic gap implies change of tectonic stress and basin configuration.

II   Active Faults

Ikeda et al. (2002) recognized the Uozu, Kurehayama, Tonami and Nanao-Kanazawa in Figure 1.3 as major reverse fault zones in the Hokuriku Province, which are unexceptionally characterized by NE-SW trend. The Ouchi Graben, defined as boundary between the North and South Hokuriku Provinces, is a part of the Nanao-Kanazawa reverse fault zone. Research Group for Active Faults of Japan (1991) gave detailed description of constituent ruptures of those

fault zones, and confirmed dominant vertical slips.

It seems, however, that the geomorphological approaches have not shown comprehensive view of the neotectonic deformation. For instance, quite steep gravity gradient and grand inclined terrace around the eastern part of the province are much larger tectonic features than the adjoining Uozu fault zone. Subsurface structure inferred from the Bouguer anomaly seems to accord with trend of prominent faults along the foothills of mountainous range as described by Tsujimura (1926). Based on paleomagnetic analysis, Itoh and Watanabe (1988) revealed that the sedimentary rocks on the northeastern point of the South Hokuriku Province have suffered significant rotation during the Quaternary under strong E-W compressive stress. Further interdisciplinary research should be organized for construction of realistic model of the tectonic zone.

1.4.3   Origin of Paradoxical Bouguer Anomaly Around the Jinzu Spur

As shown in seismic profiles (Figures 1.7 and 1.9), the Jinzu Spur is convex upward. In general, high gravity anomalies should be obtained over these structures, but here low gravity anomaly was observed over the spur.

There are two possible interpretations for the conspicuous gravity trend on the Jinzu Spur. As shown in Figure 1.9, geologic units constituting the horst are cut by small faults in the course of structural build-up. Such mechanical disturbance may result in decrease of effective density of the topographic high. Another option is to assume inherent density contrast of sedimentary layers between crest and foothills of the active structure. Figure 1.1 suggests that the western and eastern flanks of the spur are the pathway of voluminous clastics derived from large rivers, Jinzu and Joganji, respectively. Density of the fluvial units burying the channel probably tends to be higher than fine-grained levee sediments, reflecting prompt compaction. Thus the specific negative anomaly is

attributed to difference in material property of shallow geologic units.

We adopt the latter assumption that the Quaternary sediments on both sides of the Jinzu Spur would have higher density than the spur, and estimated density contrast which would make meaningful low gravity anomaly over the upward convex structure by Talwani's method (Talwani et al., 1959). As a result, it was found that the density contrast of 50 kg/m^3 (0.05 g/cm^3) led to meaningful decrease of gravity anomaly (about 1.5 mGal) over the spur.

References

[1]   Fujii, S. (1988). Marine Geology - Toyama Bay. In N. Yamashita, Y. Kaseno, & J. Itoigawa (Eds.), Regional Geology of Japan - Part 5 Chubu II (pp. 202-204). Tokyo: Kyoritsu Shuppan Co (in Japanese).

[2]   Fujii, S., Takemura, T., & Yamamoto, O. (1976). Isurugi Movement - Quaternary tectonic event in the Toyama basin. Abstracts of Annual Meeting of the Geological Society of Japan, 83, 110 (in Japanese).

[3]   Geological Survey of Japan, AIST (Ed.) (2012). Seamless Digital Geological Map of Japan 1:200,000 - Research Information Database DB084. Tsukuba: National Institute of Advanced Science and Technology.

[4]   Hagita, N., Adachi, M., & Shichi, R. (1997). Himi fault revealed by gravity survey in the west of the Toyama Plain, central Japan. The Journal of Earth and Planetary Sciences, Nagoya University, 44, 29-59.

[5]   Hayakawa, H., & Takemura, A. (1987). The Neogene system in the Yatsuo area, Toyama Prefecture, central Japan. Journal of the Geological Society of Japan, 93, 717-732 (in Japanese with English abstract).

[6]   Hirooka, K., Nakajima, T., Sakai, H., Date, T., Nittamachi, K., & Hattori, I. (1983). Accretion tectonics inferred from paleomagnetic measurements of Paleozoic and Mesozoic rocks in central Japan. In M. Hashimoto, & S. Uyeda (Eds.), Accretion Tectonics in the Circum-Pacific Regions (pp. 179-194). Tokyo: Terra Scientific Publishing Co.

[7]   Huzita, K. (1980). Role of the Median Tectonic Line in the Quaternary tectonics of the Japanese islands. Memoir of the Geological Society of Japan, 18, 129-153.

[8]   Ikebe, N. (1949). Tertiary stratigraphy of western Toyama and eastern Ishikawa Prefectures. Science of the Earth, 1, 14-26.

[9]   Ikeda, Y., Imaizumi, T., Sato, H., Togo, M., Hirakawa, K., & Miyauchi, T. (Eds.) (2002). Atlas of Quaternary Thrust Faults in Japan. Tokyo: University of Tokyo Press (in Japanese with English summary).

[10]   Itoh, Y. (1985). Stratigraphy and geochronology of the Neogene in the Tomari area, Toyama Prefecture, Central Japan. News of Osaka Micropaleontologists, 13, 1-12 (in Japanese with English abstract).

[11]   Itoh, Y. (1988). Differential rotation of the eastern part of southwest Japan inferred from paleomagnetism of Cretaceous and Neogene rocks. Journal of Geophysical Research, 93, 3401-3411.

[12]   Itoh, Y., & Hayakawa, H. (1988). Magnetostratigraphy of Neogene rocks around the Yatsuo area in Toyama Prefecture, Japan. Journal of the Geological Society of Japan, 94, 515-525 (in Japanese with English abstract).

[13]   Itoh, Y., & Ito, Y. (1989). Confined ductile deformation in the Japan arc inferred from paleomagnetic studies. Tectonophysics, 167, 57-73.

[14]   Itoh, Y., Nakajima, T., & Takemura, A. (1997). Neogene deformation of the back-arc shelf of Southwest Japan and its impact on the palaeoenvironments of the Japan Sea. Tectonophysics, 281, 71-82.

[15]   Itoh, Y., & Watanabe, M. (1988). Tectonic rotation of the Tomari area, easternmost part of Toyama Prefecture, inferred from paleomagnetic study. Journal of the Geological Society of Japan, 94, 457-460 (in Japanese).

[16]   Itoh, Y., Uno, K., & Arato, H. (2006). Seismic evidence of divergent rifting and subsequent deformation in the southern Japan Sea, and a Cenozoic tectonic synthesis of the eastern Eurasian margin. Journal of Asian Earth Sciences, 27, 933-942.

[17]   Jolivet, L., & Tamaki, K. (1992). Neogene kinematics in the Japan Sea region and volcanic activity of the northeast Japan arc. In K. Tamaki, K. Suyehiro, J. Allan, M. McWilliams et al. (Eds.), Proceedings of the Ocean Drilling Program, Scientific Results, vol. 127/128, Part 2 (pp. 1311-1331). TX: Ocean Drilling Program, College Station.

[18]   Koike, K., & Machida, H. (Eds.) (2001). Atlas of Quaternary Marine Terraces in

the Japanese Islands. Tokyo: University of Tokyo Press.

[19] Komazawa, M. (2004). Gravity Grid Database of Japan, Gravity CD-ROM of Japan, ver.2 - Digital Geoscience Map P-2. Tsukuba: Geological Survey of Japan.

[20] Nakatsuka, T., & Okuma, S. (2005). Aeromagnetic Anomalies Database of Japan - Digital Geoscience Map P-6. Tsukuba: Geological Survey of Japan.

[21] Ohkubo, H., Sato, T., & Watanabe, M. (2000). Stratigraphic correlation between the Plio-Pleistocene Yabuta and Junicho Formations using volcanic ash beds, and diatom and calcareous nannofossil biostratigraphy of lower part of the Junicho Formation in northwestern Toyama Prefecture, Central Japan. Journal of the Geological Society of Japan, 106, 583-596 (in Japanese with English abstract).

[22] Okubo, S., Nagasawa, K., Murata, I., & Sheu, H. C. (1990). Gravity observations along the Itoigawa-Shizuoka Geotectonic Line (III) - Bouguer anomaly around the northern part of Matsumoto Bonchi Toen Fault. Bulletin of the Earthquake Research Institute, University of Tokyo, 65, 649-663.

[23] Otofuji, Y., & Matsuda, T. (1987). Amount of clockwise rotation of Southwest Japan - fan shape opening of the southwestern part of the Japan Sea. Earth and Planetary Science Letters, 85, 289-301.

[24] Research Group for Active Faults of Japan (1991). Active Faults in Japan: Sheet Maps and Inventories, Rev. ed. Tokyo: University of Tokyo Press (in Japanese with English summary).

[25] Satoguchi, Y., & Nagahashi, Y. (2012). Tephrostratigraphy of the Pliocene to Middle Pleistocene Series in Honshu and Kyushu Islands, Japan. Island Arc, 21, 149-169.

[26] Sunami, M., & Kono, Y. (1988). Gravity structure around the Ochi Depression in the Noto Peninsula, Central Japan. Journal of the Seismological Society of Japan, 2nd Ser., 41, 173-178.

[27] Sutou, H., Kitaguchi, Y., Yamamoto, K., & Kono, Y. (2004). Gravity anomalies and basement structures in southern part of the Noto Peninsula, Japan - Relationship among gravity anomalies, active faults and seismicity. Journal of the Seismological Society of Japan, 2nd Ser., 56, 363-377.

[28] Tada, R., & Tamaki, K. (1992). Scientific results of ODP Japan Sea Legs, and their implication for stratigraphy. Journal of the Japanese Association for Petroleum

Technology, 57, 103-111 (in Japanese with English abstract).

[29] Talwani, M., Worzel, J. L., & Landisman, M. (1959). Rapid gravity computations for two-dimensional bodies with application to the Mendocino submarine fracture zone. Journal of Geophysical Research, 64, 49-59.

[30] Tamaki, M., Itoh, Y., & Watanabe, M. (2006). Paleomagnetism of the Lower to Middle Miocene Series in the Yatsuo area, eastern part of southwest Japan: clockwise rotation and marine transgression during a short period. Bulletin of the Geological Survey of Japan, 57, 73-88.

[31] Tsujimura, T. (1926). A peculiar type of fault scarp on the northern border of the Hida Range. Geographical Review of Japan, 2, 679-695 (in Japanese).

Chapter 2

An Overview of the Mawaki Archaeological Site with a Focus on Its Archaeological Significance

Hideki Takada

Keiji Takemura

Abstract

The archaeological site of Mawaki is famous for its long history of occupation from the Jomon period to the present. In particular, the discovery of abundant dolphin bones is a significant source of information on lifeways during this period. The history of excavations may be divided into two phases. The Early Phase was one marked by the discovery of Jomon pottery associated with abundant dolphin bones and other archaeological remains. The Late Phase is marked by its designation as a National Historic Site post 1987; this phase included research on the distribution of deposits with dolphin bones, and the discovery of a circular array of wooden columns from the late Jomon period, as also tombs and human bones from the middle Jomon period.
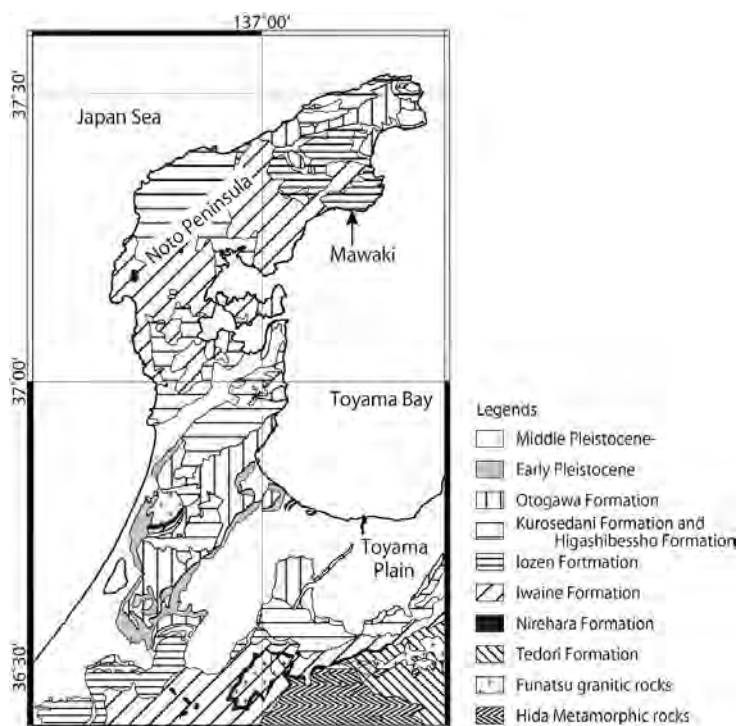
Figure 2.1 *The location of the Mawaki site at the Noto Peninsula with geological information.*

2.1   Introduction: The Significance of the Site of Mawaki

Mawaki is located on the eastern coast of the Noto Peninsula in central Japan (Figure 2.1). In 1982 and 1983, this important discovery occurred owing to farmland consolidation (The Integrated Improvement Act of the Agricultural Foundation), and many dolphin bones were discovered with remains of Jomon pottery. This was a very important discovery as regards evidence of past human subsistence strategies.

The site represents a village with evidence of habitation from around 7000 to 2500 cal. yr B.P. This period was marked by an early Holocene high sea level, as compared to the larger regional chronology of 15,000 years with evidence of various sea level fluctuations. The period corresponds to the Early through Final Jomon periods of the Japanese archaeological timescale. The Jomon period is divided into six ages characterized by differing pottery remains; these are shown in Table 2.1 (Kobayashi, 2008). The Mawaki site is surrounded by hills about 100 m high, and is located on an alluvial plain between 4 m and 12 m above sea level. As shown in Figure 2.2, this archaeological site was found beneath cultivated fields and is located between a hilly terrain and the present day coastal residential area.

Table 2.1   *Archaeological timescale in Japan.*

Age Name (Japanese)	Age Name (English)	Calendar Age
Jomon Sosoki	Incipient Jomon	15,700 - 11,550 cal. yr B.P.
Jomon Soki	Initial Jomon	11,450 - 6,950 cal. yr B.P.
Jomon Zenki	Early Jomon	6,950 - 5,470 cal. yr B.P.
Jomon Chuki	Middle Jomon	5,470 - 4,420 cal yr B.P.
Jomon Koki	Late Jomon	4,420 - 3,220 cal. yr B.P.
Jomon Banki	Final Jomon	3,220 - 2,350 cal. yr B.P.

The surrounding archeological sites during the Jomon periods are distributed as shown in Figure 2.3. However, only Mawaki was continuously occupied from the early to final Jomon periods. The site of Himenishiueno (No. 2 in

Figure 2.3) is located on a marine terrace of the Last Interglacial (Koike and Machida, 2001) and has three pit dwelling dugouts with several kinds of early Jomon pottery remains. This site is about 400 m to the east, and is located on the shore of an inlet of Mawaki Bay. These two sites may have had close and strong relationships in this region in the past. Mawaki must have been a very significant region for human occupation during the Jomon period.

2A: View from North

2B: View from South

2C: View from hill-side

Figure 2.2 *The modern embayment and adjacent Mawaki archaeological site on the alluvial plain.*
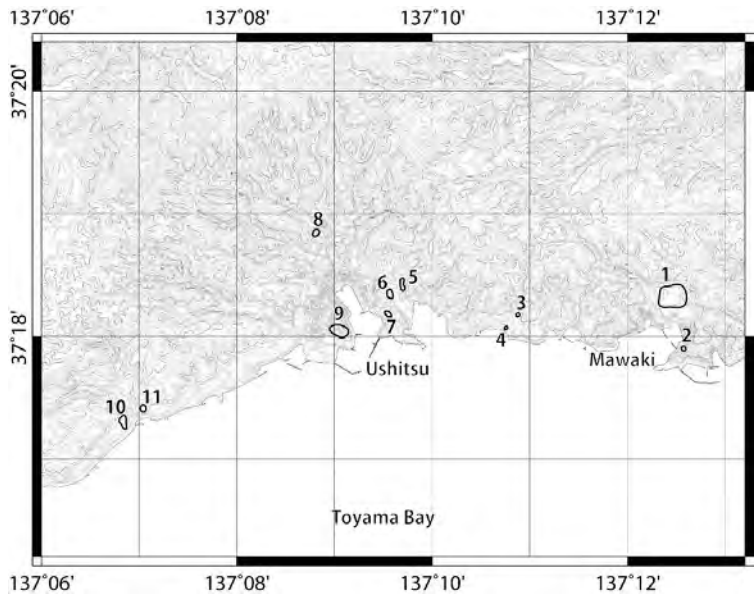
Figure 2.3 *Surrounding archaeological sites around Mawaki site during Jomon period. 1: Mawaki site, 2: Himenishiuwano site, 3: Hane C site, 4: Hane site, 5: Tanoura-koyada site, 6: Ushitsu-Shironomachi site, 7: Toshimayama site, 8: Urushiwara site, 9: Ushitsu-Sakiyama site, 10: Donoue site, 11: Nishinoue site.*

2.2   History of Excavations Since 1982 at Mawaki

2.2.1   The Early Phase Excavations: Phase of New Discoveries

4A: The length of the dolphin skull near the center of the photograph is ca. 40 cm.

4B: Dolphin bones and Jomon pottery from the Mawaki archaeological site.
The diameter of the pottery is ca. 30 cm.

4C: Human bones and related tombs.

Figure 2.4   *Dolphin bones in the sedimentary record at Mawaki.*

Farmland consolidation (The Integrated Improvement Act of the Agricultural Foundation) planed by the government was an opportunity for finding important archaeological sites from the Jomon period to the present. The first and second stage excavations were carried out in 1982 and 1983 (Figure 2.4). The most important discoveries were those of numerous dolphin bones and of Jomon pottery. These excavation reports were published in 1986 (Board of Education of Noto Town and Investigating Commission for Mawaki Site, 1986). In 1987, after the publication of reports on the new discovery of the coexistence of numerous dolphin bones and Jomon pottery, the Mawaki archaeological site was designated as a National Historic Site.

2.2.2 The Late Phase Excavation: The Establishment of Mawaki as a National Historic Site

The third to sixth stages of excavations were carried out from 1998 to 2002. Before excavation, a committee on Further Excavation for Effective Settlement as a National Historic Site was established. The excavations were restarted under the leadership by this committee. The results of this stage were summarized in a report published in 2002 (Board of Education of Noto Town and Investigating Commission for Mawaki Site, 2002). The main discoveries of this phase are human bones and related tombs (Figure 2.4C).

The seventh to ninth stages of excavations were carried out in 2003 to 2005. The results of this stage were summarized in a report published in 2006 (Board of Education of Noto Town and Investigating Commission for Mawaki Site, 2006). The main discoveries are archaeological relics, such as a circular array of wooden columns from the late Jomon period. Further, bore samples were extracted for purposes of investigating deposits associated with dolphin bones.

The tenth to thirteenth stages of excavations were carried out from 2006 to 2009. The results of this stage were summarized in a report published in 2010

(Board of Education of Noto Town and Investigating Commission for Mawaki Site, 2010). The main discoveries include those of a dwelling site (a prehistoric settlement) during the Middle Jomon period.

2.3   Overview of Its Archaeological Significance

Archaeological relics, such as the circular array of wooden columns from the late Jomon period and tombs and human bones from the middle Jomon period, have been excavated here. The strata at the site contain large amounts of pottery, stone artifacts and animal bones. Jomon pottery excavated from the Mawaki site is categorized into as many as 23 types. The historical transition of pottery types in central Japan along the Japan Sea can be recognized within this single site (e.g., Board of Education of Noto Town and Investigating Commission for Mawaki Site, 1986, 2002, 2006). As the ceramic sequence is exceptionally well preserved in this region, excavation and geoarchaeological surveys are still in progress.

As Mawaki is an archaeological site in an embayment buried during the Holocene marine transgression, it is characterized by marine animal remains. Numerous dolphin bones (Figure 2.4) were excavated in 1982 and 1983 occurring within the late early to earliest middle sequences of the Jomon period, along with abundant Jomon pottery (Figure 2.4) and other remains. In many cases, dolphin bones were found as a consolidated, stratified occurrence. Over 286 individual dolphins were counted. No other occurrence of this size has been reported from any coeval coastal archaeological sites in East Asia. Six species of dolphin are represented here (e.g., Hiraguchi and Miyazaki, 1986; Hiraguchi, 1986, 1989, 1992, 2006): *Lagenorhynchus obliquidens*, *Delphinus delphis*, *Tursiops truncatus*, *Pseudorca crassidens*, *Globicephala macroynchus*, and *Grampus griseus*. *Lagenorhynchus obliquidens* accounted for 60% of the dolphin bones found here. Stone artifacts within these strata comprise numerous chert arrowheads, arrows, knives, and scrapers. Dolphin bones at the Mawaki

site are thought to be the result of dolphin fishing, as reported in archaeological discussion on dolphin fishery (e.g., Hiraguchi, 1992; Yamamoto, 1997). A key aim of our geoarchaeological investigations is understanding the relationship between the formation of the layer intercalated with many dolphin bones and the site's paleoenvironment in relation to sea-level changes (Itoh et al., 2011).

References

[1] Board of Education of Noto Town and Investigating Commission for Mawaki Site (1986). Mawaki site in Noto Town, Ishikawa Prefecture: Excavation report related to the integrated improvement act of agricultural foundation (in Japanese).

[2] Board of Education of Noto Town and Investigating Commission for Mawaki Site (2002). Mawaki site in Noto Town, Ishikawa Prefecture: Outline of excavation report at three to six stages related to the improvement act of site environment as a historical site (in Japanese).

[3] Board of Education of Noto Town and Investigating Commission for Mawaki Site (2006). Mawaki site in Noto Town, Ishikawa Prefecture: Outline of excavation report at seven to nine stages related to the improvement act of site environment as a historical site (in Japanese).

[4] Board of Education of Noto Town and Investigating Commission for Mawaki Site (2010). Mawaki site in Noto Town, Ishikawa Prefecture: Outline of excavation report at ten to thirteen stages related to the improvement act of site environment as a historical site (in Japanese).

[5] Hiraguchi, T. (1986). Catching dolphins at the coast of Toyama Bay in the Jomon period. Ozakai (Journal of Archeological Society of Toyama), 10, 51-68 (in Japanese).

[6] Hiraguchi, T. (1989). Catching dolphins of the Jomon period: Concerning a regional characteristic of the Hokuriku. Journal of Archaeological Society of Ishikawa, 32, 19-38 (in Japanese).

[7] Hiraguchi, T. (1992). Catching dolphins at the Mawaki site central Japan, and its contribution to Jomon Society. In C. M. Aikens & S. N. Rhee (Eds.), Pacific northeast Asia in prehistory (pp. 35-45). Pullman: Washington State University Press.

[8]   Hiraguchi, T. (2006). People at Mawaki site with dolphin fishery. In Board of Education of Noto Town & Investigating Commission for Mawaki Site (Eds.), Mawaki site in Noto Town, Ishikawa Prefecture: Outline of excavation report at seven to nine stages related to the improvement act of site environment as a historical site (pp. 147-158) (in Japanese).

[9]   Hiraguchi, T., & Miyazaki, N. (1986). Animal remains. In Board of Education of Noto Town (Ed.), Mawaki site (pp. 346-400) (in Japanese).

[10] Itoh, Y., Takemura, K., Nakamura, T., Hasegawa, S., & Takada, H. (2011). Paleoenvironmental analysis of the Mawaki archaeological site, central Japan, in relation to stratigraphic position of dolphin bones. Geoarchaeology, 26 (4), 461-478.

[11] Kobayashi, K. (2008). Age determination, calendar age of Jomon period. In Y. Kosugi et al. (Eds.), Rekishino - Monosashi, Jomon-Jidai no Hennen Taikei. Doseisha (in Japanese).

[12] Koike, K., & Machida, H. (Eds.) (2001). Atlas of Quaternary marine terraces in the Japanese islands. Tokyo: University of Tokyo Press (in Japanese).

[13] Yamamoto, N. (1997). Residence form and dolphin fisheries at Mawaki Site, Ishikawa Prefecture. Annals of Prehistoric Archaeology (Senshi-Kokogaku Ronshu), 6, 55-78 (in Japanese).

Chapter 3

Holocene Stratigraphy from the Mawaki Archaeological Site and the Occurrence and Significance of Dolphin Bones

Keiji Takemura

Hideki Takada

Tsuyoshi Haraguchi

Yasuto Itoh

Abstract

The Mawaki archaeological site area comprises thick Holocene sediments, which were deposited as a series of marine transgressive and regressive cycles. From the sedimentary sequence, a shallow estuarine sedimentation system is recognized and is seen to be associated with a coastal environment. The distribution of the sediments, intercalated with many dolphin bones, is concordant with the sedimentation processes recorded in the borehole sequence.

3.1 Introduction
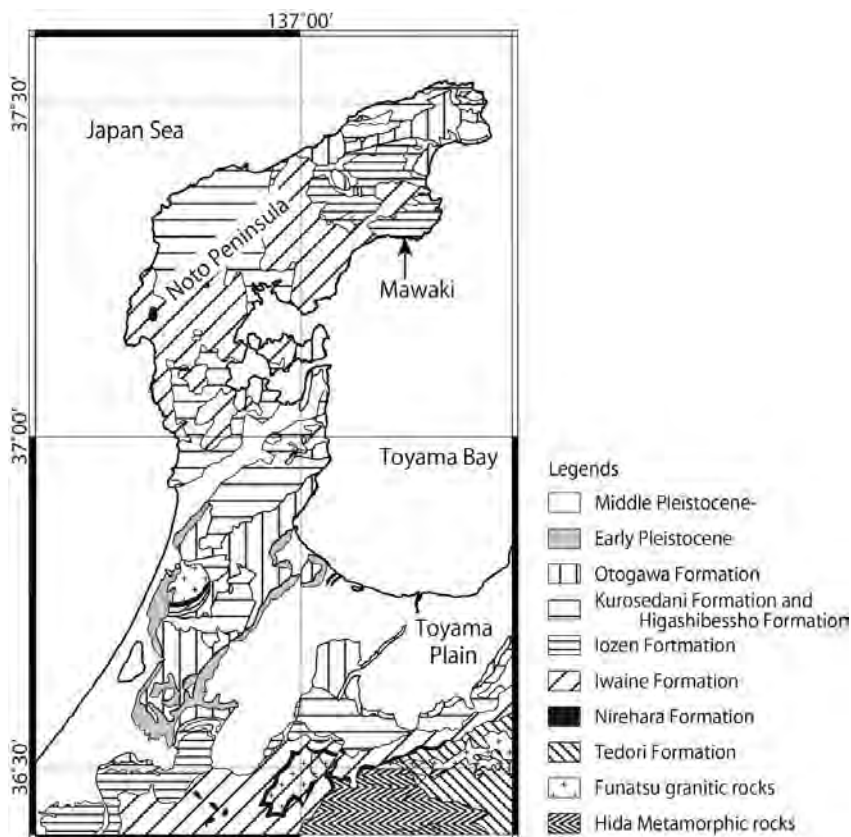
Figure 3.1 *Location of Mawaki Site of the Noto Peninsula with geological information.*

The Mawaki archaeological site is located in the northern part of Noto Peninsula, and faces Toyama Bay to the south (Figure 3.1). Following the early phase of excavation from 1980 to 1983 (Board of Education of Noto Town and Investigating Commission for Mawaki Site, 1986), the Mawaki site was designated as a National Historic Site on the basis of its significance for the Jomon culture along the Japan Sea coast. The late phase of excavation started in 1997 during which fundamental geological drilling, geoslicer coring, and geoarchaeological research was carried out. Pollen and diatom analyses and precise ^{14}C dating were undertaken in order to fully understand the distribution of sediments intercalated with dolphin bones. This work contributed to an understanding of the significance of the Mawaki site and the distribution of human remains during the Holocene (Board of Education of Noto Town and Investigating Commission for Mawaki Site, 2002; 2006; 2010).

In this section, we summarize the stratigraphy of drilled core samples and geoslicer coring sediments samples from above the Miocene basement rocks. Geoslicer coring is an operational system of directly oriented coring using sheet piles ("YAITA" in Japanese) and obtains vertical thin sections of unconsolidated soil layers (Nakata and Shimazaki, 1997; Haraguchi et al., 1998).
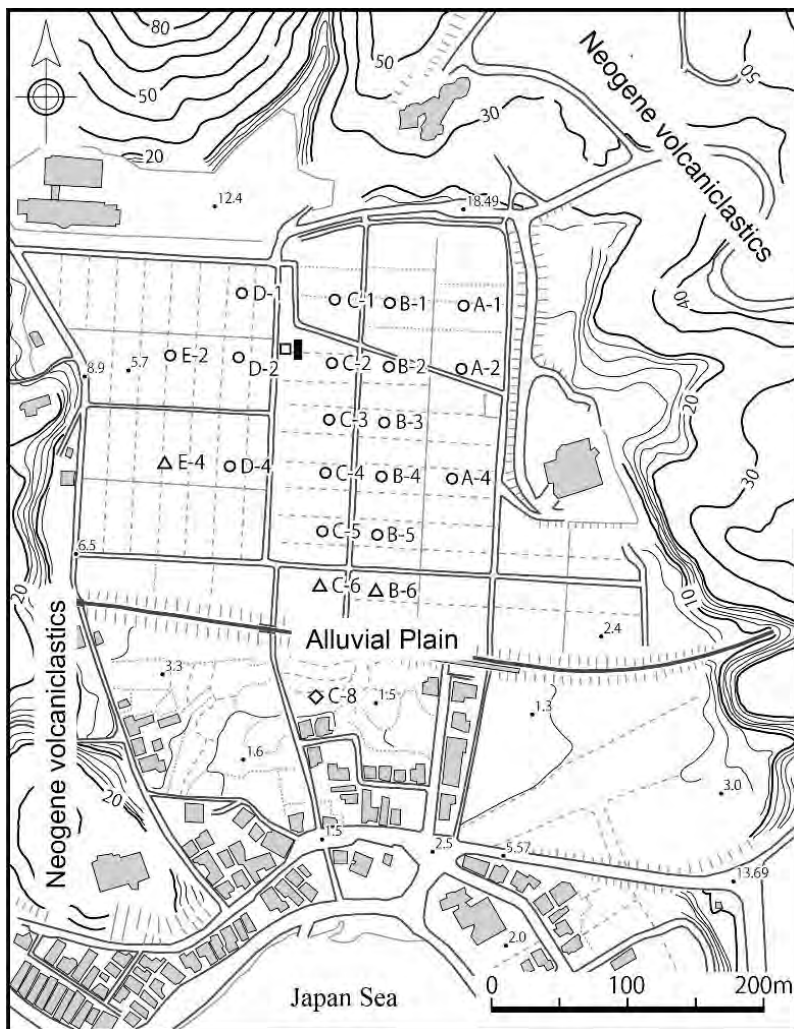
Figure 3.2 *Borehole and geoslicer locations around the Mawaki archaeological site. Open circle: drilling in 1997 & 1998, open triangle: drilling in 2002, open rhombus: drilling in 2005, solid rectangle: geoslicer coring.*

3.2 Drilling Operations and Geoslicer Sampling at the Mawaki Site

During the late phase at the Mawaki site, drilled cores were obtained in order to study the distribution of the strata intercalated with dolphin bones. The borehole

locations are shown in Figure 3.2. In 1997 and 1998, boring operations were carried out at 17 points, and the complete sequence of sediments was obtained (Photo 3.1: coring, Photo 3.2: core sediments). In 2001, we carried out further boring operations near the present shoreline in order to better understand the continuity from the present shoreline to the Mawaki archaeological site. Geoslicer coring was carried out to check the sedimentary facies along the former shoreline during the Jomon period, and its relation to the dolphin bone occurrences (Photo 3.3: geoslicer coring, Photo 3.4: geoslicer sediments).

Photo 3.1   *Coring.*
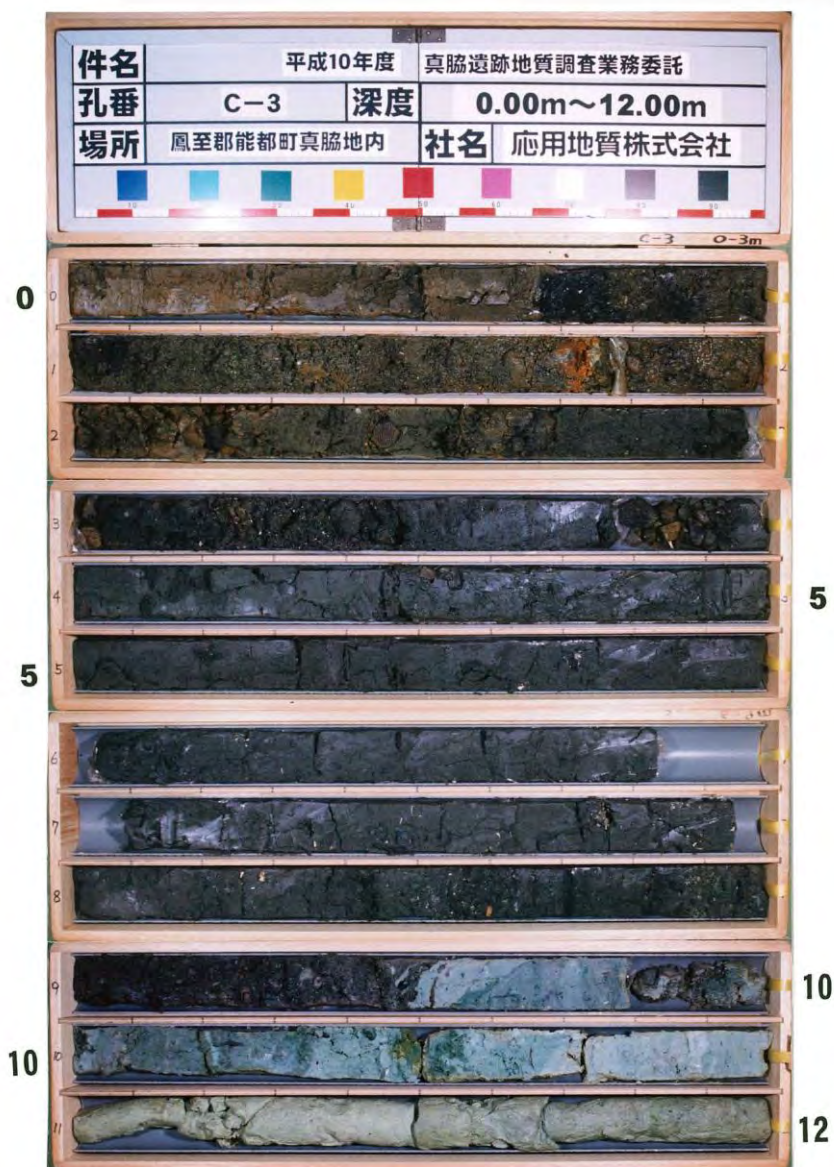
Photo 3.2 *Core sediment samples. Japanese explanations on the core box: Subject: Geological Research at Mawaki Site (2008), Borehole No.: C-3, Depth: 0.00m – 12.00m, Location: Mawaki, Noto Town, Operation: Oyo Corporation Co., Ltd.*

Photo 3.3 *Geoslicer sampling.*

Photo 3.4 *Geoslicer sample.*

3.3 Stratigraphy of Drilled Core and Geoslicer Sediment Samples

The Mawaki site faces the sea and is surrounded by low hills composed of Miocene andesitic volcaniclastics. These volcaniclastics form the basement to the late Quaternary sediments at Mawaki. On the basis of the sediment core observations, the stratigraphy can be summarized as five units (units A to E in ascending order) above the Miocene volcaniclastic basement (Figure 3.2 and Figure 3.3). The lithological unit nomenclature is that of Itoh et al. (2011).
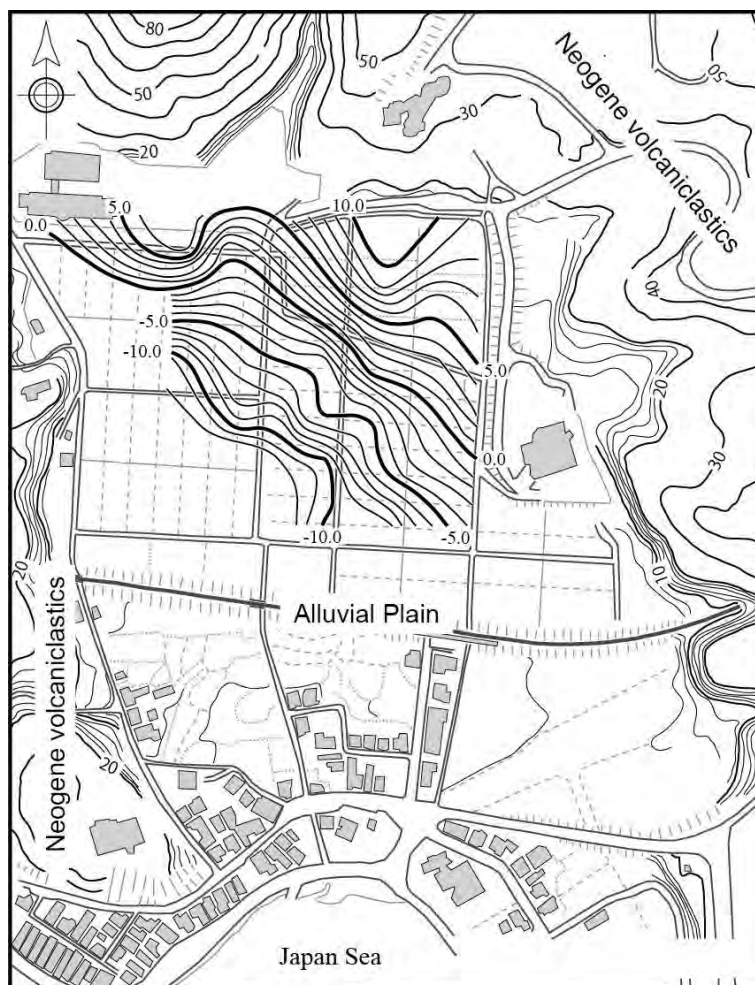
Figure 3.3 *Basement topography. Contours delineate the buried topography of basement rocks (the elevation of the surface of the Miocene volcaniclastics).*

Basement: Miocene volcaniclastics composed of tuff and tuffaceous mudstone.

Unit A: Sands and gravels, poorly sorted, containing charcoal grains.

Unit B: Clays and silts with abundant remains of marine organisms, intercalations of well-sorted sandy layers, containing shell and plant fragments.

Unit C: Silty sands with gravels, well-sorted medium sands, containing

abundant shells and plant fragments.

Unit D: Sands and gravels, poorly sorted, containing pottery fragments and charcoal grains.

Unit E: Cultivated soil.
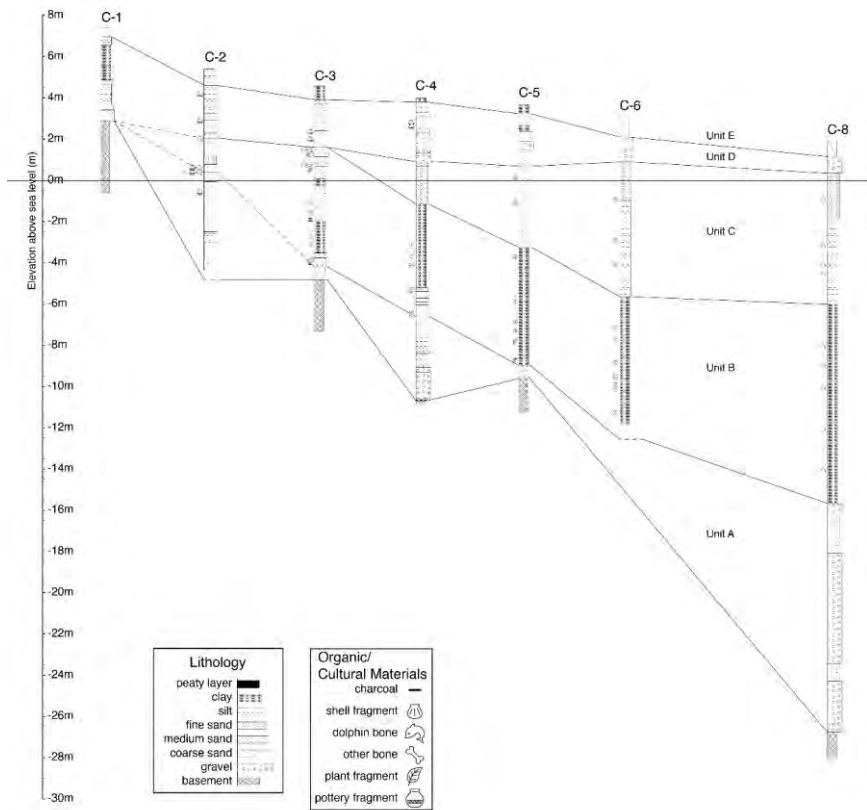
Figure 3.4 *Geological profile along cross section of C-Line.*

The cross section along the C-Line (Figure 3.4) clearly shows that the clays and silty sands with abundant marine organisms were deposited in marine environments (units B & C). The deposits in marine environments are thicker on the coastal side and the bottom horizon is lower.
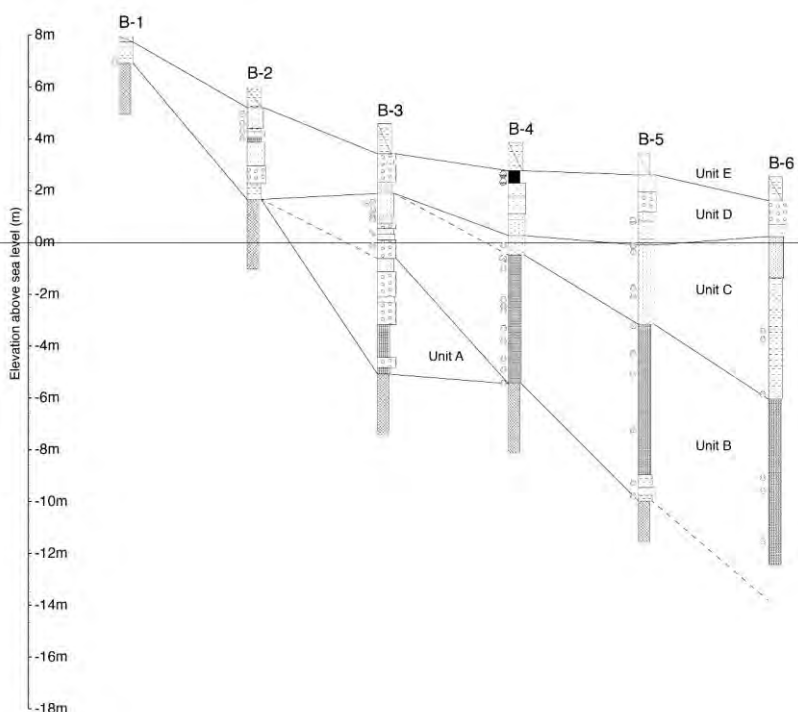
Figure 3.5   *Geological profile along cross section of B-Line.*

The cross section along the B-Line (Figure 3.5) also clearly indicates that the clays and silty sands with abundant marine organisms were deposited in marine environments (units B & C) and they are thicker on the coastal side; the basal horizon is shallower towards the shoreline.

The cross section along the 2-Line (Figure 3.6), at a higher elevation, shows that the sediments are mainly composed of poorly sorted sands and gravels with intercalations of coaly silts and sands from Unit D. At this elevation, the marine transgressive sediments seen in units B & C are recognized at narrow horizons. The boundary between the sedimentary sequence and the basement rocks is irregular in shape due to erosion, the topography being deeper to the west, with the thick sediments of Unit A indicating the former valley before the marine transgression.

The cross section along the 4-Line (Figure 3.7), at a middle elevation, shows a thick marine sequence composed of silts and clays with abundant shell fragments, and also an irregular basement topography, deeper to west with thick subaerial sediments (Unit A) indicating the conditions before the marine transgression.
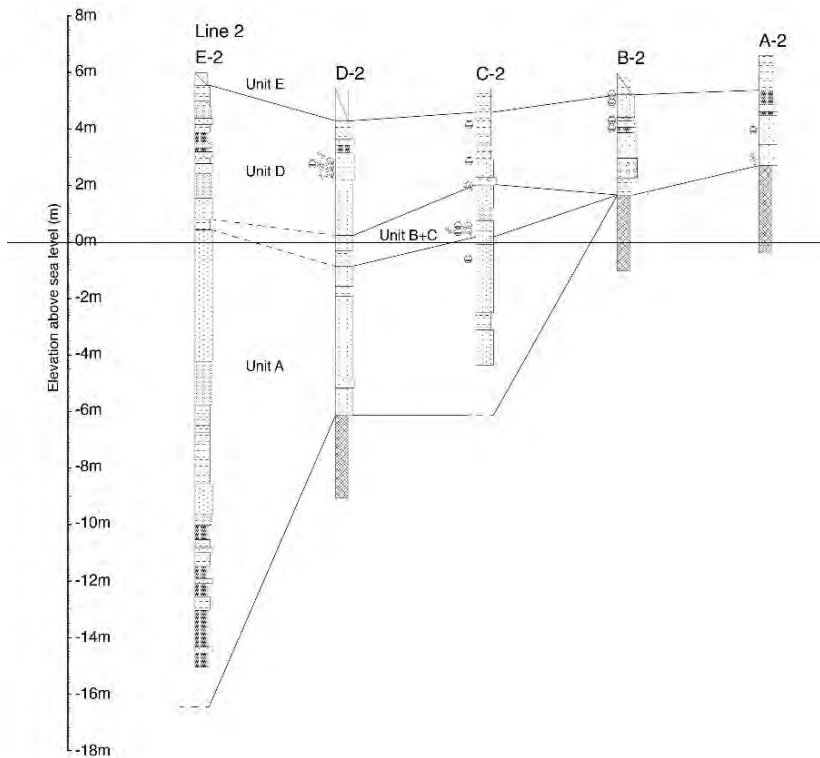
Figure 3.6 *Geological profile along cross section of 2 Line.*
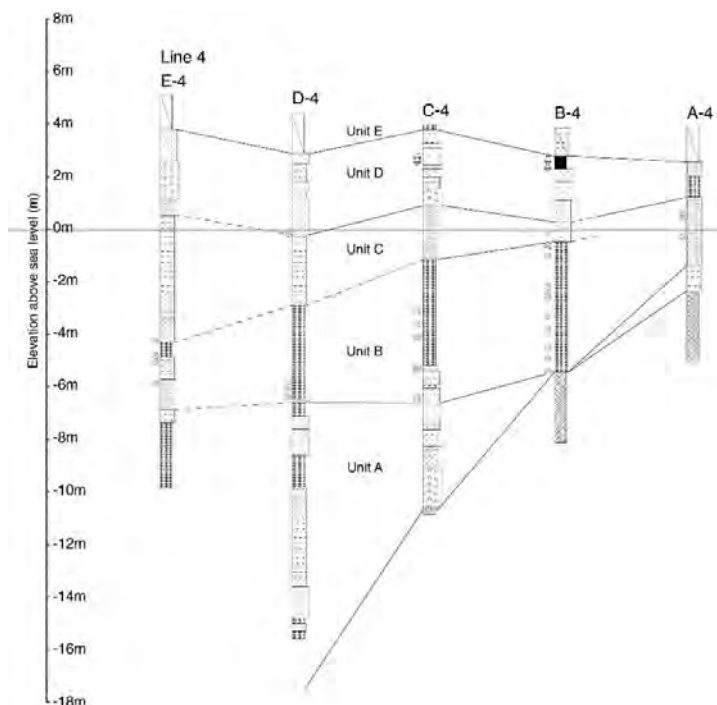
Figure 3.7   *Geological profile along cross section of 4 Line.*

Geoslicer coring was carried out in order to study the sedimentary facies of coastal area, including the dolphin bones. The lithology of the samples is complicated; the sediments are composed of poorly sorted silts and sands, with plant fragments, pottery and dolphin bones.

3.4   Holocene Lithostratigraphy to the Shoreline at Mawaki

3.4.1   Basement Structure

The basement relief (Figure 3.3) indicates the surface of the Miocene volcaniclastics and shows the topography before the Holocene marine transgression. The relief is steeper than that of the present-day valley slopes, and this is a result of erosion in Last Glacial times.

3.4.2   Sedimentary Facies and Sedimentary Environment Change

Sedimentary facies are characterized upward in time, and spatial distribution (Figs 3.4, 3.5, 3.6 and 3.7). The thick marine clays of Unit B indicate rapid sedimentation in bay environments, and the upper part of Unit B is intercalated with alternations of silts and sands with plant fragments typical of estuarine environments. The sand sequence of Unit C indicates the development of a sand bar at that time. The distribution of lithologies at the Mawaki site in space and time, show thick clay sediments of bay environments, followed by estuarine sediments to shoreline deposits related to the development of the sand bar shown in Unit C.

3.4.3   Facies of Transgression and Regression

The sequence at the Mawaki Site is composed of lower terrestrial, middle marine, and upper terrestrial environments. This indicates a series of marine transgressions and regressions during the Holocene. The distribution of marine environments was developed at an elevation of 3m above present-day sea level. This indicates that the former sea level was higher than that in the present day.

3.4.4   Characteristics of Sediments Including Dolphin Bones Horizon

Abundant dolphin bones are distributed in a narrow horizon within the sedimentary sequence, which includes poorly sorted silty sands with plant fragments of a near marine environments (Figs 3.4, 3.5 and 3.8). The data indicate that the areal distribution is limited. The distribution and occurrence of the horizons are the subject of further discussion related to sea level rise, sedimentation processes, paleogeographical change, and human activities.
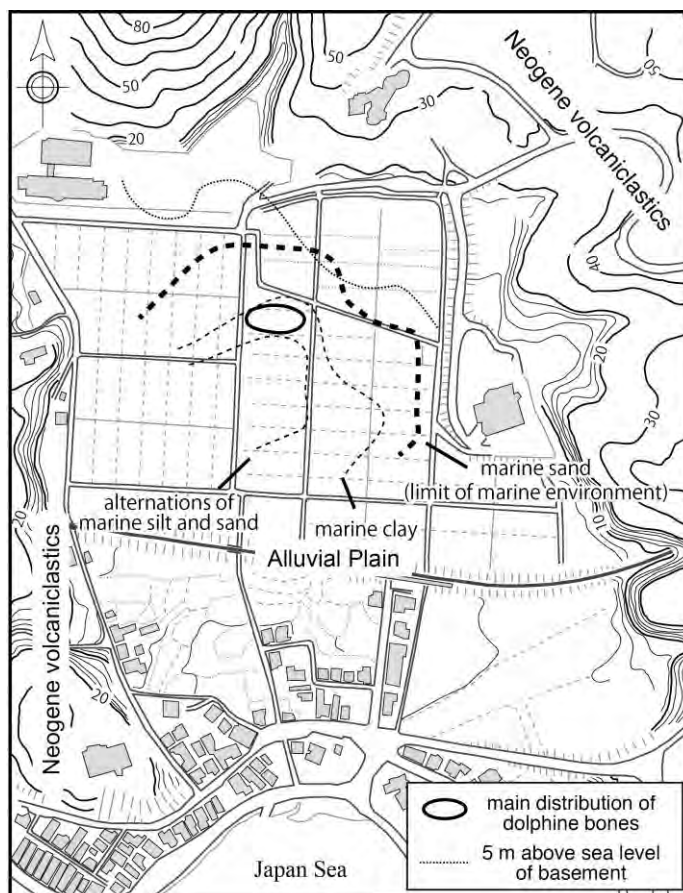
Figure 3.8 *Distribution of sediments intercalated dolphin bones and sediments of marine environments.*

3.4.5 Development of Terrestrial Topography and Transition of Human Relics

The distribution of human relics represented by pottery and bones is characteristics (Figure 3.9). Human relics belonging to the Early Jomon period are distributed more abundantly in higher elevation than that from other periods. This means that the sea level rise and marine transgression was larger in the Early Jomon period.
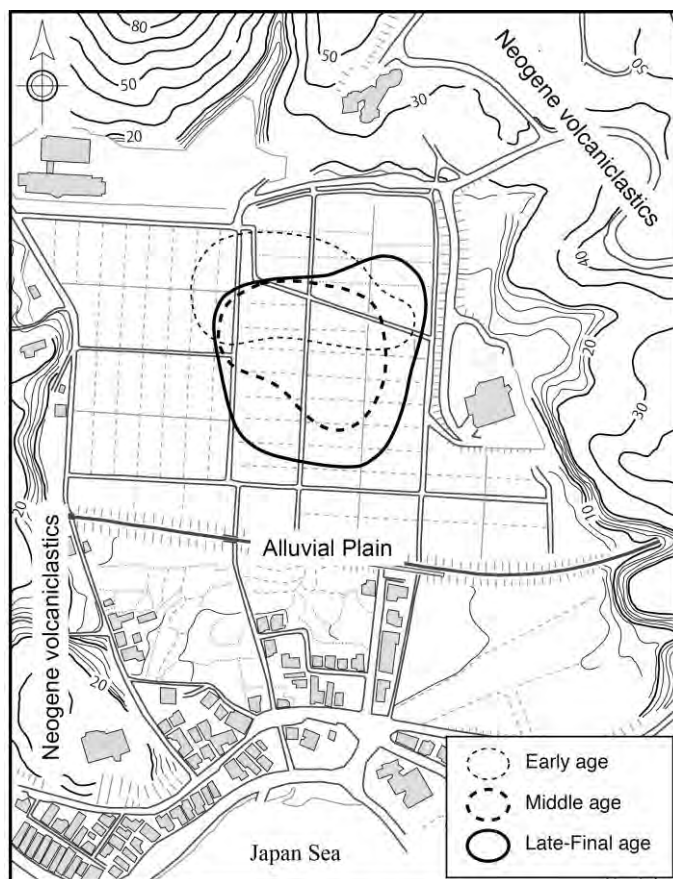
Figure 3.9 *Distribution of Jomon relics at each ages of Jomon period.*

3.5 Summary

The stratigraphy of Mawaki site comprises mainly five sequences of alluvial unconsolidated sediments above the Miocene basement rocks. The sediments are divided into five units, A to E in ascending order, typical of terrestrial and marine (bay and estuarine) environments. Around the Mawaki site a bay environments developed, and in the late stages of Early to Middle Jomon period, sea level was stable and the bay comprises barrier sediments composed of well-sorted fine to medium sands and silts with dolphin bones found at the

shoreline during this stage.

References

[1] Board of Education of Noto Town and Investigating Commission for Mawaki Site (1986). Mawaki site in Noto Town, Ishikawa Prefecture: Excavation report related to the integrated improvement act of agricultural foundation (in Japanese).

[2] Board of Education of Noto Town and Investigating Commission for Mawaki Site (2002). Mawaki site in Noto Town, Ishikawa Prefecture: Outline of excavation report at three to six stages related to the improvement act of site environment as a historical site (in Japanese).

[3] Board of Education of Noto Town and Investigating Commission for Mawaki Site (2006). Mawaki site in Noto Town, Ishikawa Prefecture: Outline of excavation report at seven to nine stages related to the improvement act of site environment as a historical site (in Japanese).

[4] Board of Education of Noto Town and Investigating Commission for Mawaki Site (2010). Mawaki site in Noto Town, Ishikawa Prefecture: Outline of excavation report at ten to thirteen stages related to the improvement act of site environment as a historical site (in Japanese).

[5] Haraguchi, T., Nakata, T., Shimazaki, K., Imaizumi, T., Kojima, K., & Imuimaru, K. (1998). A new sampling method of unconsolidated sediments by long Geo-slicer, a pile-type soil sampler. Jour. Japan Soc. Eng. Geol., 39, (3), 306-314. (in Japanese with English Abstract).

[6] Itoh, Y., Takemura, K., Nakamura, T., Hasegawa, S., & Takada, H. (2011). Paleoenvironmental analysis of the Mawaki archaeological site, central Japan, in relation to stratigraphic position of dolphin bones. Geoarchaeology, 26 (4), 461-478.

[7] Nakata, T., & Shimazaki, K. (1997). Geo-slicer, a newly inverted soil sampler, for high-resolution active fault studies. Journal of Geography, 106, 59-69 (in Japanese with English abstract).

Chapter 4

Radiocarbon Dating of Holocene Sediments at the Mawaki Site by Accelerator Mass Spectrometry

Toshio Nakamura

Hideki Takada

Abstract

^{14}C dating by accelerator mass spectrometry was conducted for sediment cores B3, C3, C4, C5, C6 and C8, as well as for wood samples collected from an outcrop of trench site along C-Line (D2), around the Mawaki archeological site, middle of the Noto Peninsula, in Noto-town, Hosu-gun, Ishikawa Prefecture, to analyze paleoenvironmental change, especially the temporal progression of the Holocene marine transgression and the successive retreat. The calibrated ^{14}C ages of the cored sediments ranged from 10,400 cal BP to 900 cal BP. Additionally, several carbonaceous fractions were separated from dolphin bones excavated at the Mawaki site for ^{14}C dating. The ^{14}C ages and their calibrated ages for the alkali-treated fractions from the dolphin bone ranged around 5,230-5,270 BP and 5,580-5,650 cal BP, respectively. The temporal change of the correction value for the local marine carbon reservoir effect, ΔR, was analyzed using the ^{14}C ages measured for sediments from cores C4, C5 and C6, and it was recognized that the ΔR values tended to be more negative during the Holocene marine transgression period (6,000~7,000 cal BP). It means that the ^{14}C age differences between marine and terrestrial samples are smaller here at the Mawaki site compared with the average difference value established worldwide. The negative trend of the ΔR values can be explained by a higher supply of well-mixed surface ocean water from the warm Kuroshio Current.

4.1   Introduction

Age determination is very important for understanding the chronological sequence of environmental changes and human activities at archaeological sites. The chronological sequence of transitions of pottery types constructed by archaeologists is very effective for establishing the chronology of the site and comparing its order to with that of other sites. However, numerical age determination is more useful and important than estimating chronological order

because it allows determination of the specific ages of material or strata. Radiocarbon (^{14}C) dating is one of the most trustworthy age determination methods for establishing absolute ages from several tens of thousands of years ago to present. ^{14}C age determination began in the late 1940's, when Professor Willard Libby detected ^{14}C in nature (Figure 4.1), confirmed a relation known as the decay curve of ^{14}C abundance in a carbon sample, and determined the age of the sample, the time passed since the living material became dead (Arnold and Libby, 1949; Figure 4.2). ^{14}C dating can be applied to carbon containing materials such as wood, other plant material, shell, and so on. Since that time, the techniques for implementing the ^{14}C method have advanced greatly. In this section, we briefly describe the principles and application techniques of the ^{14}C dating method. We then report the results of an application of the ^{14}C dating method using accelerator mass spectrometry (AMS) to several types of remains excavated at the Mawaki Archaeological Site.

Galactic cosmic ray (p^{1+}, He^{2+},---) + Earth's air (N, O) => X + n

$$n + ^{14}N \quad => \quad ^{14}C + p$$
$$^{14}C + O + O \quad => \quad ^{14}CO_2$$
$$^{14}CO_2 + (sun\ light\ + H_2O) \quad => \quad living\ material(^{14}C, ^{13}C, ^{12}C)$$

$$^{12}CO_2:^{13}CO_2:^{14}CO_2 = 0.989: 0.011:1.2 \times 10^{-12}$$
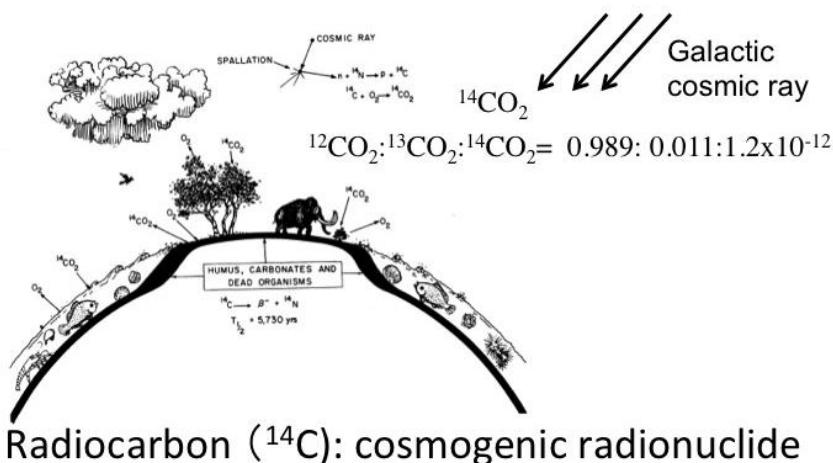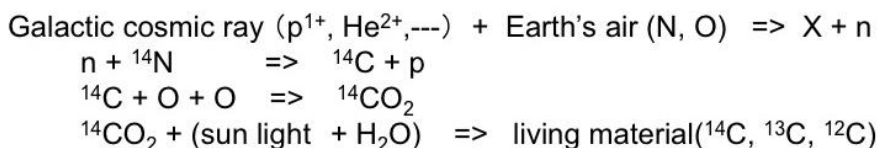
Radiocarbon (^{14}C): cosmogenic radionuclide

Figure 4.1 *Production, decay and distribution of ^{14}C on the earth.*
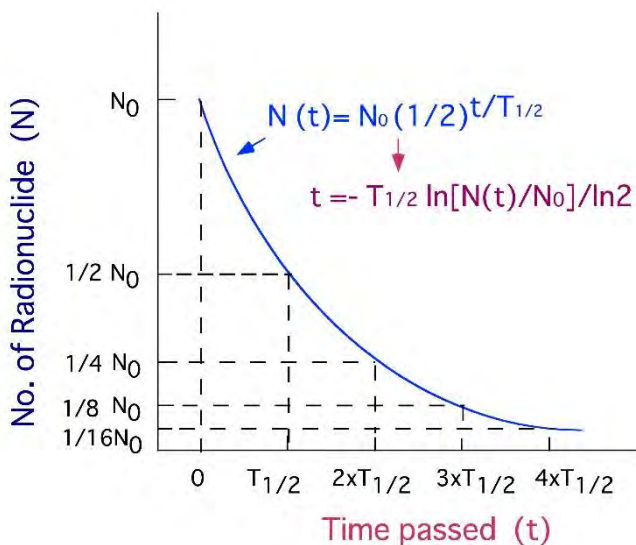
Figure 4.2 *Relationship between number of radionuclide and time passed.*

4.2 Two Methods of ^{14}C Dating

^{14}C dating is one of the radiometric methods based on the radioactive decay of radionuclides in the environment. The method utilizes the cosmogenic radionuclide, ^{14}C, which has a half life of 5,730±30 years. ^{14}C is produced continuously in the Earth's atmosphere by galactic cosmic rays, at a rate of almost two atoms per second per cm^2 of earth surface. Measurement of ^{14}C in nature was first conducted first by Prof. Libby and his colleagues at the University of Chicago during the late 1940s. To be a suitable material for ^{14}C dating, a sample must contain carbon originally fixed by the incorporation of atmospheric CO_2 through photosynthesis and must have a clear relationship in its geological context to the event to be dated. The material also must have been preserved well during the time period from carbon fixation to ^{14}C measurement. Materials commonly measured include wood (cellulose), seeds, pollen, charcoal, bone, peat, chitin, and carbonate shells (Figure 4.3).
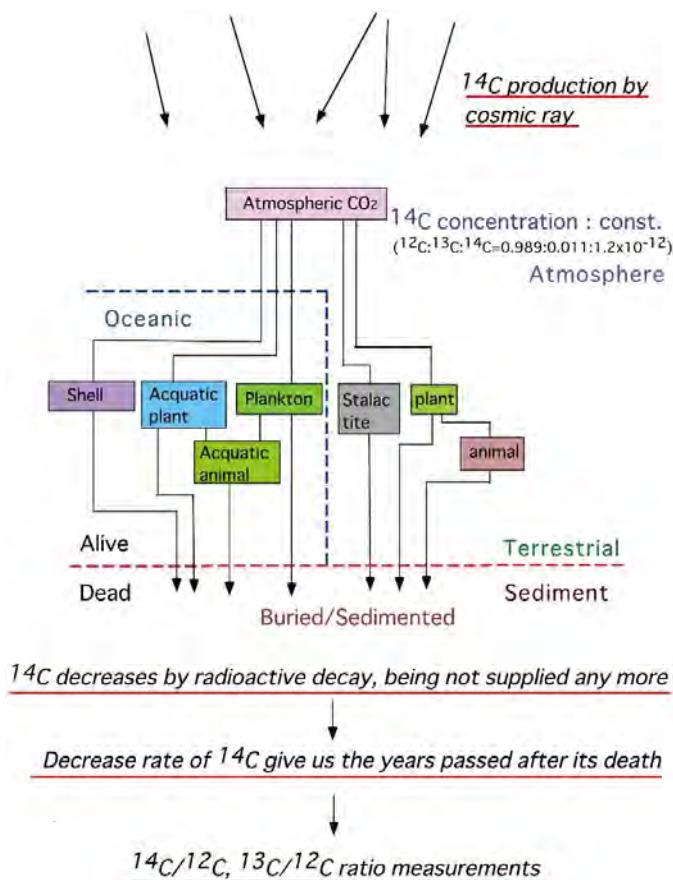
Figure 4.3 *Principle of ^{14}C dating for carbonaceous materials on the earth.*

^{14}C dating is applicable to organic matter containing carbon that was fixed photosynthetically from atmospheric CO_2 within the past 50,000 to 60,000 years. The reliability of age determination by the ^{14}C dating method has been improved by calibration of ^{14}C ages to calendar dates and by taking account of the inevitable temporal variations of the ^{14}C content of atmospheric CO_2 in the past (Reimer et al., 2013). Additionally, improved accuracy of ^{14}C content analysis and appropriate selection of specific samples during the field surveys have contributed to the high reliability of ^{14}C dating analysis.

Two different methods for measuring the ^{14}C content of carbonaceous

materials are in use. In the first method, the ^{14}C activity of a sample is measured by counting the beta particles emitted through the decay of ^{14}C, by using a gas proportional counter for carbonaceous gases such as CO_2, CH_4, C_2H_2, or rarely C_2H_6, or by using a liquid scintillation counter using benzene or ethanol synthetized from sample carbon. The second method, which has been in use since 1977, is direct ion counting of three carbon isotopes, ^{12}C, ^{13}C and ^{14}C of the carbon sample using accelerator mass spectrometry (AMS) (Figures 4.4, 4.5 and 4.6). AMS uses a tandem electrostatic accelerator to obtain individual carbon ions of ^{12}C, ^{13}C and ^{14}C with energies high enough (several MeV) to be separated clearly from background ions with a mass-analyzing magnet. Individual ions of ^{14}C, which has quite low abundance compared to stable ^{12}C and ^{13}C (even a contemporaneous carbon sample has ^{14}C/^{12}C ratio as low as 10^{-12}), are finally identified and counted by a heavy ion ionization detector.
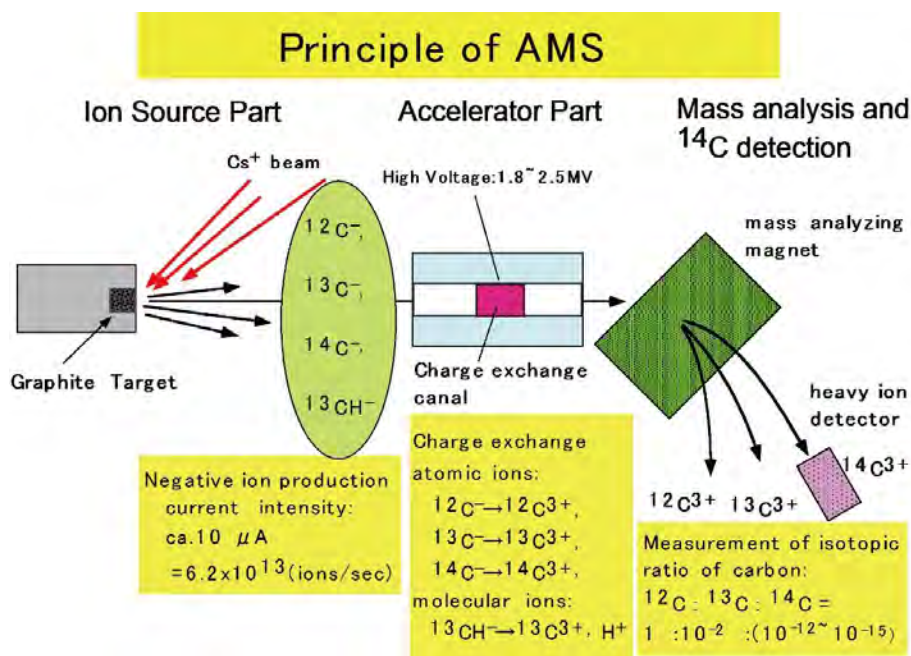
Figure 4.4 *Process of measuring three carbon isotopes, ^{12}C, ^{13}C and ^{14}C with AMS.*

Figure 4.5 *Photo of Tandetron AMS System (Model 4130-AMS) at Nagoya University.*
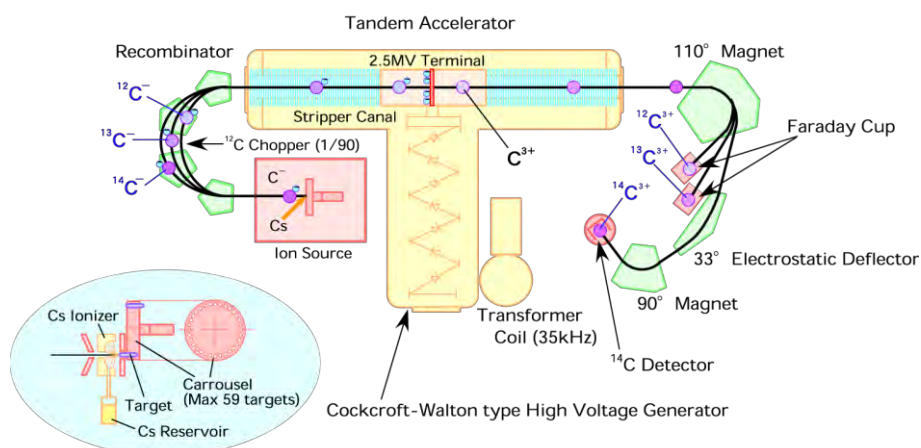
Figure 4.6 *Layout of Tandetron AMS System (Model 4130-AMS) at Nagoya University.*

The characteristics and advantages of AMS ^{14}C age determination compared with beta-ray counting methods include the following; (1) The sample volume required for the AMS method is far less (by three orders of magnitude) than that required for decay counting methods (Figure 4.7). AMS allows routine measurements for carbon samples ranging from 100 μg and 1.5 mg, whereas decay counting methods usually require a minimum of several grams of carbon. (2) Because a small amount of sample can be used in AMS, replicate measurements of the same sample and measurements of specific fractions of the sample are possible. (3) AMS can also measure older material (ca. 50 to 60 ka BP). The procedures required for ^{14}C dating of geological and archeological samples are summarized in Figure 4.8, which describes the processes from selection of adequate sample materials that are deeply related to the events to be dated, to the reporting of the ^{14}C dating results.

Item	AMS system	Radioactivity method
Carbon necessary	0.1 ～ 1.5 mg	2 ～ 5 g
Measurement error (±1σ)	±20 ～ ±40 yr	±80 yr
Oldest age measurable	ca. 60,000 yr BP	35,000 ～ 40,000 yr BP
Measurement time	20 ～ 40 min. (for sample only)	16 ～ 20 hr (for sample only)

Figure 4.7   *Comparison of performances in ^{14}C dating by AMS system and radioactivity method.*

Process	Checks and operations
Selection of sample material to be dated	・sample material that clearly shows the event to be solved ・selection of carbonaceous materials suitable for dating ・removal of foreign carbon contamination ・sample preparation
^{14}C measurement	・high precision measurement ・high accuracy measurement ・reduction of ^{14}C blank, as low as possible
Calculation of ^{14}C age	・estimate the initial ^{14}C abundance in the sample material ・correction for carbon isotopic fractionation
Calibration to calendar date	・calibration with an appropriate IntCal dataset ・correction for local ocean carbon reservoir effect, and calibration with Marine dataset
Report of ^{14}C dating results	・conventional ^{14}C age ・δ^{13}C value (carbon stable isotope ratio) ・calibrated calendar dates

Figure 4.8 *Procedure of calendar age determination by AMS ^{14}C dating.*

4.3 Process of Calendar Age Determination and Evaluation of Marine Reservoir Effect

^{14}C ages of terrestrial samples can be calibrated to calendar dates by using international calibration datasets (Reimer et al., 2013), IntCal or SHCal, depending on the location in the Northern or Southern Hemisphere where the sample formed by the incorporation of atmospheric CO_2 through photosynthesis or by the acquisition of carbon via a food chain. On the other hand, the ^{14}C ages of marine samples are calibrated to calendar dates differently than those of terrestrial samples. It is well known that ocean deep water forms in the North Atlantic Ocean and circulates in the deeper layers of the ocean through the Atlantic, Antarctic, Indian, and Pacific oceans before finally upwelling in the northern Pacific Ocean and returning at the ocean surface to the North Atlantic Ocean, with a cycle time of more than 1,500 years (Stuiver and Braziunas, 1993). The circulation of ocean deep water causes marine samples to become eventually depleted in ^{14}C (marine carbon reservoir effect: R in Figure 4.9). The ^{14}C ages of marine materials is globally older by an average of 400 ^{14}C years

(<R>) (Stuiver and Braziunas, 1993), than those of terrestrial samples that incorporate atmospheric CO_2 directly. In areas where the upwelling of deep water is strong, the surface water, and of course the oceanic carbonaceous materials, are more depleted in ^{14}C than the average value of <R>, which is known as the local ^{14}C reservoir effect of surface ocean water. Along with the global average effect, this additional local reservoir effect, i.e., correction value of the local marine reservoir effect denoted as ΔR, is normally not negligible for precise calibration of ^{14}C ages of marine samples (Hughen et al., 2004).
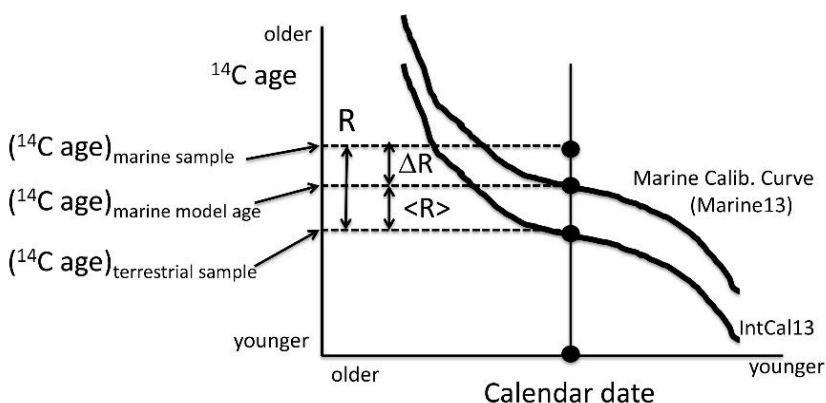
Figure 4.9 *Marine carbon reservoir effect, its local effect and correction value of the local effect.*

The marine carbon reservoir effect R at a local point is expressed by the difference in ^{14}C age between the marine sample and a contemporaneous atmospheric sample collected in the same area (Stuiver and Polach, 1977; Stuiver et al., 1986; Stuiver and Braziunas, 1993). However, the correction

value of the local marine reservoir effect is sometimes expressed by ΔR, as stated above, and defined as (1) the age difference between the local marine reservoir value R and the average value <R> for global contemporaneous ocean materials (Hughen et al., 2004), or more directly, as (2) the difference between the ^{14}C age of the marine sample and the corresponding optimum marine global ^{14}C age at the sample calendar age given by the Marine13 calibration curve (Figure 4.9; Reimer et al., 2013). We used the second calculation method noted as (2) above to calculate the correction value ΔR, as discussed later in this text.

In the southwestern part of the Japanese Archipelago, well-mixed surface ocean water is supplied from the warm Kuroshio Current, which flows northward along the western rim of the Pacific Ocean and partly into the Sea of Japan. The correction value of the local reservoir effect, ΔR, is rather negative in this region.

4.4 Sediment Samples from the Mawaki Site for ^{14}C Dating

Table 4.1 *Organic fractions separated and their yields, CO_2 yields, C/N ratios, $\delta^{13}C$ and ^{14}C age values, calibrated age ranges and Lab. code no. of ^{14}C measurements, for dolphin bone samples collected from the Mawaki site.*

No.	Organic fraction	yield	CO_2 yield	C/N ratio	$\delta^{13}C$ by RIMS	^{14}C age (± 1σ)	calbrated age range (±2σ)	Lab code #
		(%)	(%)		(‰)	(yr BP)	(cal yr BP)	(NUTA2-)
1	SC	0.07	38.20	8.3	-17.5±0.1	4910±35	5318-5065 (95.4%)	1447
2	Insol. Res. after GC ext	-	22.00	4.9	-19.1±0.1	5015±35	5454-5285 (95.4%)	1448
3	GC-DB	1.65	36.80	3.4	-14.4±0.1	5120±35	5578-5388 (94.5%)	1446
4	A-DB(2h)	4.43	22.30	3.5	-15.0±0.1	5220±35	5656-5477 (95.4%)	1448
5	A-DB(48h)	2.34	26.40	3.9	-15.3±0.1	5185±30	5606-5462 (95.4%)	1559
6	GC-A-DB(2h)	1.20	35.10	3.1	-13.5±0.1	5225±30	5656- 5490 (95.4%)	1553

No.	Organic fraction	yield	CO_2 yield	C/N ratio	$\delta^{13}C$ by RIMS	^{14}C age ($\pm 1\sigma$)	calbrated age range ($\pm 2\sigma$)	Lab code #
		(%)	(%)		(‰)	(yr BP)	(cal yr BP)	(NUTA2-)
7	GC-A-DB(48h)	0.35	37.90	-	-13.6±0.1	5275±30	5705- 5574 (95.4%)	1557
8	GC-A-DB(48h-A.C.)	0.48	30.10	3.2	-13.5±0.1	5245±30	5692- 5550 (95.4%)	1560
9	XAD-GC-DB	-	40.70	-	-12.8±0.1	5235±30	5680- 5520 (95.4%)	1561

The Mawaki archeological site, located in the middle of the Noto Peninsula, in Noto-town, Hosu-gun, Ishikawa Prefecture (Figure 4.10), is situated on an alluvial coastal plain with an area of about 1.2×10^5 m^2 bordered in the south by Noto bay, and surrounded by hills in the other three directions. As a result of excavation surveys conducted from 1982 to 1983, it was found that the site had been inhabited by humans almost continuously for about 3,500 years, from the early Jomon (around 6,000 years ago) to the latest Jomon (ca. 2,500 years ago).

Fifteen years after the first excavation survey, in 1997, the second survey program was initiated. To obtain a general understanding of the human settlement and the natural environment at the site, in addition to the essential direct excavations, several sediment cores were collected first from the large alluvial plain, normally composed from bottom to top of a sequence of terrestrial, marine and terrestrial layers. We collected wood and plant fragments, charcoal, shell, and bone samples from top to the bottom of the C3, C4, C5, C6, and C8 boring cores (Figures 4.11 and 4.12, and Tables 4.2~4.6), which were taken at intervals of 10 m from north to south in the middle of the alluvial plain. A few samples were collected from core B3 and from an outcrop at the trench dug along C-line (Figure 4.11 and Table 4.7). The shell samples were mixed, containing both spiral gastropods and bivalves.
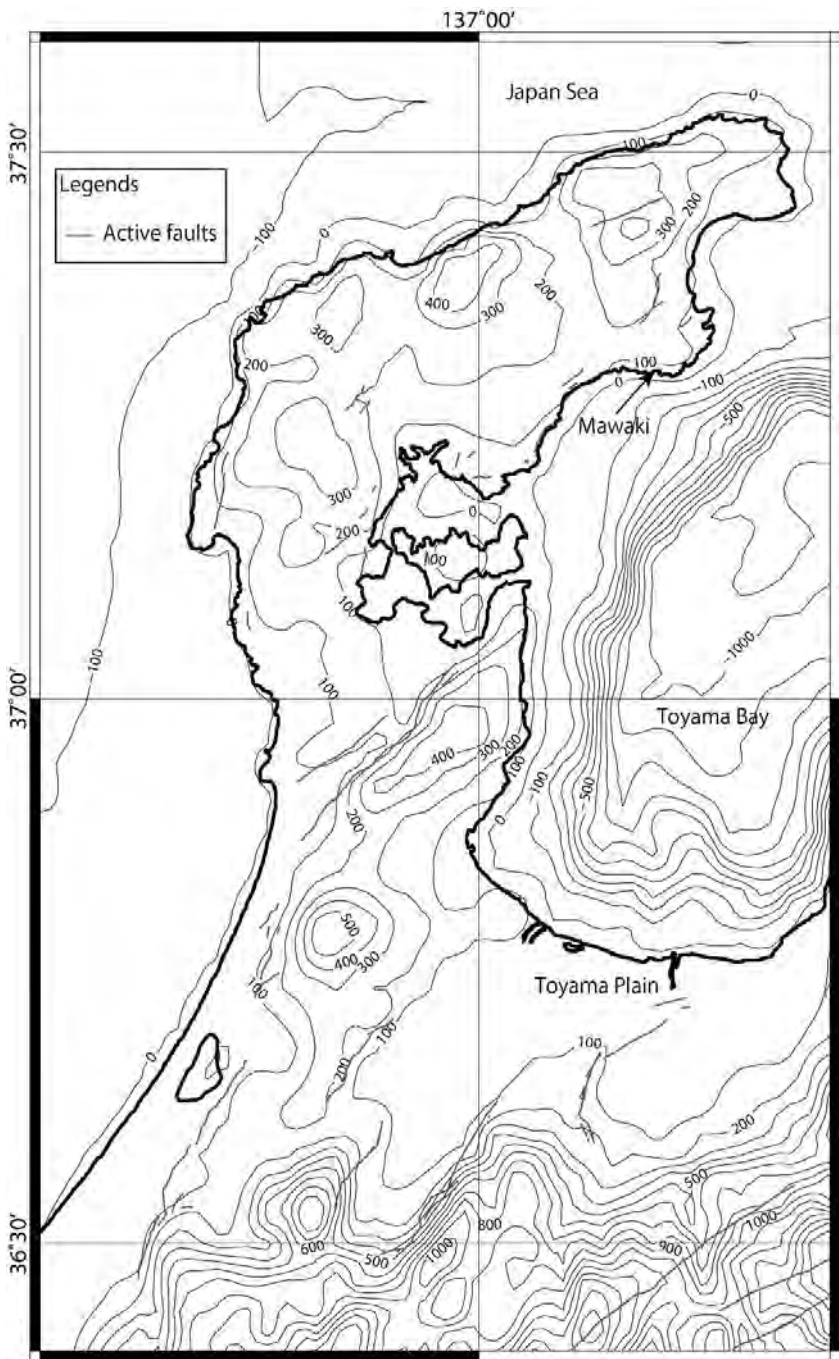
Figure 4.10 *Location of Mawaki archaeological site.*
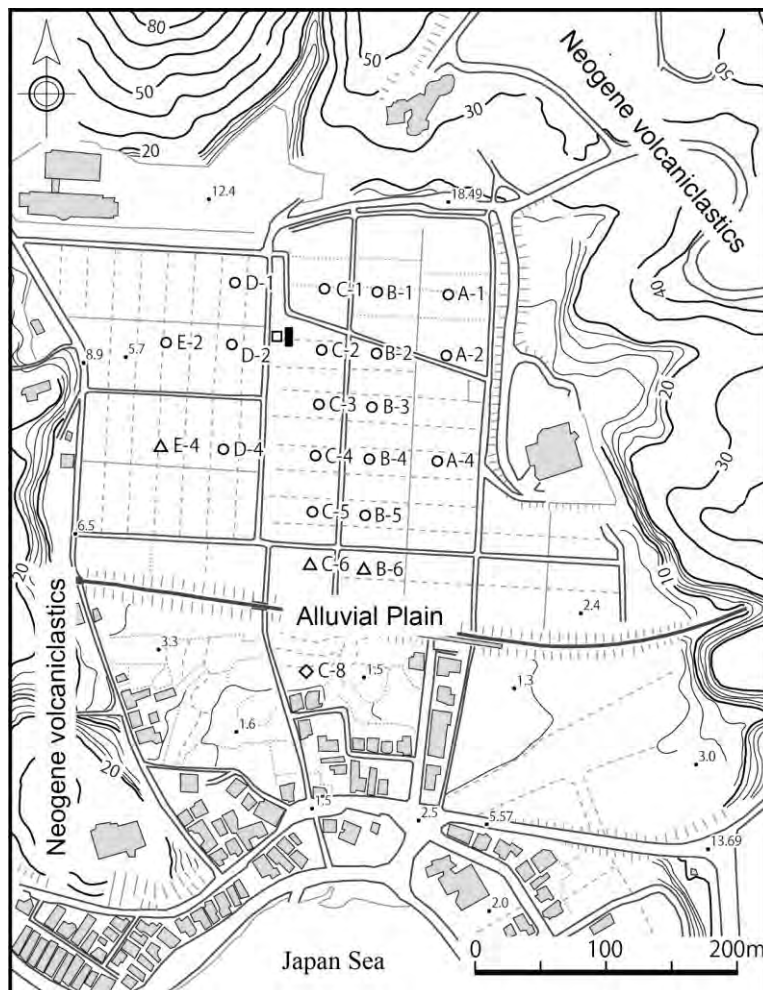
Figure 4.11 *Drilling locations at Mawaki Site.*

Unfortunately, we could not identify the species of the shell samples. Because shell fragments were rare in the cored sediments and no shell mound was observed at the Mawaki site, we assumed that the shell fragments from these core samples were of natural origin and not transported there by human activities. We also collected samples of dolphin bones, which were very common in the deeper sediments. It is considered that the resident people caught dolphins periodically from the sea and used them as food.
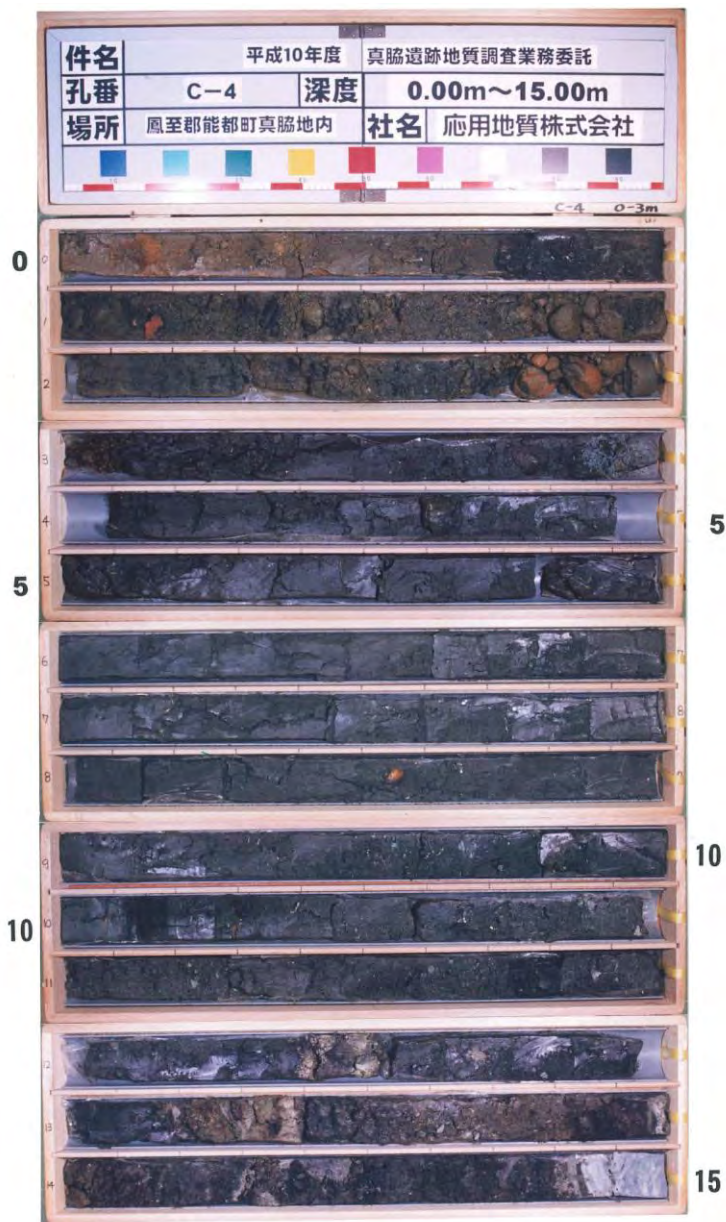
Figure 4.12 *Example of cored sample. Japanese explanations on the core box: Subject: Geological Research at Mawaki Site (2008), Borehole No.: C-4, Depth: 0.00m – 15.00m, Location: Mawaki, Noto Town, Operation: Oyo Corporation Co., Ltd.*

Table 4.2   *Age data from cored sediments of C-3.*

No.	Sample No.	Core No.	Depth	Height above sea level	Sample Material	$\delta^{13}C$ by AMS
			(m)	(m)		(‰)
			0.00	4.59		
1	C3-1W	Core 3	2.53	2.06	Wood	
2	C3-2B	Core 3	3.50	1.09	Bone	
3	C3-3B	Core 3	3.90	0.69	Bone	
4	C3-4C	Core 3	4.40	0.19	Charcoal	
5	C3-5W	Core 3	5.46	-0.87	Wood	
6	C3-6W	Core 3	6.10	-1.51	Wood	
7	C3-7C	Core 3	7.76	-3.17	Charcoal	
8	C3-8W	Core 3	8.43	-3.84	Wood	

Table 4.2   *Continue.*

No.	$\delta^{13}C$ by IRMS	^{14}C age ($\pm\sigma$)	Calibrated age (mean$\pm\sigma$)	Calibrated age range ($\pm2\sigma$)		Lab No.
	(‰)	(yr BP)	(cal yr BP)	(cal yr BP)	(Prob.)	(*Beta-)
1	-28.2±0.1	4310±50	4900±70	5040-4820	(95.4%)	*123714
2	-16.4±0.1	5730±40	6140±60	6255-6014	(95.4%)	*123715
3	-17.1±0.1	5620±50	6020±70	6160-5906	(95.4%)	*123716
4	-28.7±0.1	6080±50	6950±90	7156-7098 7086-7076 7070-7044 7030-6795	(9.8%) (1.0%) (2.7%) (81.9%)	*123717
5	-28.4±0.1	6280±60	7200±80	7408-7401 7325-7005	(0.4%) (95.0%)	*123718
6	-25.2±0.1	6210±60	7110±80	7258-6960	(95.4%)	*123719
7	-27.7±0.1	6700±60	7570±50	7668-7469	(95.4%)	*123720
8	-27.9±0.1	6920±50	7760±60	7918-7904 7858-7664	(1.6%) (93.8%)	*123721

Table 4.3 *Age data from cored sediments of C-4.*

No.	Sample No.	Core No.	Depth	Height above sea level	Sample Material	δ^{13}C by AMS
			(m)	(m)		(‰)
			0.00	4.00		
9	C4-1W	Core C4	3.65	0.35	Wood	-24.2±1.0
10	C4-2S	Core C4	3.65	0.35	Shell	1.2±1.0
11	C4-3S	Core C4	5.05	-1.05	Shell	1.3±1.0
12	C4-4W	Core C4	5.48	-1.48	Wood	-26.4±1.0
13	C4-5S	Core C4	7.15	-3.15	Shell	0.0±1.0
14	C4-6W	Core C4	7.52	-3.52	Wood	-27.3±1.0
15	C4-7W	Core C4	8.28	-4.28	Wood	-26.5±1.0
16	C4-8S	Core C4	8.50	-4.50	Shell	0.3±1.0
17	C4-9W	Core C4	9.30	-5.30	Wood	-29.3±1.0
18	C4-10S	Core C4	9.30	-5.30	Shell	0.9±1.0
19	C4-11W	Core C4	10.30	-6.30	Wood	-27.6±1.0
20	C4-12S	Core C4	10.38	-6.38	Shell	-0.7±1.0

Table 4.3 *Continue.*

No.	δ^{13}C by IRMS	^{14}C age (±σ)	Calibrated age (mean±σ)	Calibrated age range (±2σ)		Lab No.
	(‰)	(yr BP)	(cal yr BP)	(cal yr BP)	(Prob.)	(NUTA2-)
9		5596±30	6370±40	6436-6306	(95.4%)	5608
10		5853±30	6270±40	6350-6190	(95.4%)	946
11		4953±29	5300±50	5423-5228	(95.4%)	945
12		6011±32	6850±50	6944-6777 6764-6754	(93.5%) (1.9%)	5609
13		6445±29	6930±50	7040-6831	(95.4%)	987
14		6139±32	7050±70	7158-6948	(95.4%)	5610
15		6407±32	7350±40	7418-7272	(95.4%)	5613
16		6575±29	7090±50	7188-6990	(95.4%)	990
17		6818±33	7650±30	7694-7589	(95.4%)	5614
18		7106±33	7580±40	7654-7508	(95.4%)	947
19		7107±34	7930±40	8004-7917 7904-7856	(69.4%) (26.0%)	7107
20		7461±30	7920±40	7990-7842	(95.4%)	991

Table 4.4   *Age data from cored sediments of C-5.*

No.	Sample No.	Core No.	Depth	Height above sea level	Sample Material	δ^{13}C by AMS
			(m)	(m)		(‰)
			0.00	3.67		
21	C5-1P	Core 5	4.05	-0.38	Plant	-27.0±1.0
22	C5-2S	Core 5	4.05	-0.38	Shell	1.5±1.0
23	C5-3W	Core 5	4.35	-0.68	Wood	-30.0±1.0
24	C5-4W	Core 5	4.35	-0.68	Wood	-25.5±1.0
25	C5-5S	Core 5	4.97	-1.30	Shell	2.2±1.0
26	C5-6P	Core 5	6.50	-2.83	Plant	-28.9±1.0
27	C5-7S	Core 5	6.50	-2.83	Shell	2.8±1.0
28	C5-8W	Core 5	6.58	-2.91	Wood	
29	C5-9S	Core 5	7.54	-3.87	Shell	2.4±1.0
30	C5-10S	Core 5	8.15	-4.48	Shell	2.2±1.0
31	C5-11P	Core 5	8.43	-4.76	Plant	-28.3±1.0
32	C5-12S	Core 5	8.83	-5.16	Shell	1.5±1.0
33	C5-13P	Core 5	9.10	-5.43	Plant	-27.1±1.0
34	C5-14S	Core 5	9.62	-5.95	Shell	0.9±1.0
35	C5-15S	Core 5	10.63	-6.96	Shell	-0.4±1.0
36	C5-16S	Core 5	11.85	-8.18	Shell	0.9±1.0
37	C5-17S	Core 5	12.13	-8.46	Shell	-0.1±1.0
38	C5-18W	Core 5	12.57	-8.90	Wood	-31.4±1.0
39	C5-19W	Core 5	12.60	-8.93	Wood	

Table 4.4 *Continue.*

No.	δ¹³C by IRMS	¹⁴C age (±σ)	Calibrated age (mean±σ)	Calibrated age range (±2σ)		Lab No.
	(‰)	(yr BP)	(cal yr BP)	(cal yr BP)(Prob.)		(NUTA2-)
21		4373±31	4940±50	5038-4998	(11.9%)	5866
				4982-4857	(83.5%)	
22		4166±28	4250±60	4364-4139	(95.4%)	1205
23		4500±30	5170±80	5296-5046	(95.4%)	5616
24		5291±32	6080±60	6183-5989	(93.1%)	
				5963-5951	(2.3%)	
25		5004±29	5360±40	5440-5285	(95.4%)	1206
26		5228±31	5980±60	6174-6155	(3.4%)	5617
				6112-6079	(6.9%)	
				6022-5914	(85.1%)	
27		5483±29	5860±50	5930-5752	(95.4%)	1207
28	-28.6±0.1	5430±50	6230±60	6314-6172	(85.2%)	*123722
				6155-6110	(6.1%)	
				6079-6058	(1.5%)	
				6052-6020	(2.6%)	
29		6066±30	6490±50	6588-6398	(95.4%)	1208
30		6067±30	6490±50	6588-6398	(95.4%)	1209
31		5933±31	6760±40	6846-6814	(8.3%)	5618
				6801-6672	(87.1%)	
32		6275±30	6730±50	6825-6641	(95.4%)	1210
33		6037±32	6880±50	6970-6790	(95.4%)	5619
34		6545±33	7060±50	7156-6956	(95.4%)	1242
35		6896±34	7410±40	7480-7322	(95.4%)	1251
36		7289±34	7750±50	7837-7662	(95.4%)	1252
37		7337±40	7800±50	7908-7695	(95.4%)	1320
38		7058±32	7890±30	7959-7832	(95.4%)	5622
39	-31.6±0.1	7050±40	7890±40	7958-7818	(91.7%)	*123723
				7812-7794	(3.7%)	

Table 4.5 *Age data from cored sediments of C-6.*

No.	Sample No.	Core No.	Depth	Height above sea level	Sample Material	$\delta^{13}C$ by AMS
			(m)	(m)		(‰)
			0.00	3.10		
40	C6-1P	Core 6	5.89	-2.79	Plant	-27.2±1.0
41	C6-2S	Core 6	5.89	-2.79	Shell	0.8±1.0
42	C6-3P	Core 6	7.16	-4.06	Plant	-25.9±1.0
43	C6-4S	Core 6	7.16	-4.06	Shell	0.8±1.0
44	C6-5P	Core 6	9.31	-6.21	Plant	-27.7±1.0
45	C6-6S	Core 6	9.31	-6.21	Shell	0.6±1.0
46	C6-7P	Core 6	10.28	-7.18	Plant	-31.2±1.0
47	C6-8S	Core 6	10.28	-7.18	Shell	1.1±1.0
48	C6-9P	Core 6	10.88	-7.78	Plant	-40.1±1.0
49	C6-10S	Core 6	10.88	-7.78	Shell	0.4±1.0
50	C6-11P	Core 6	12.03	-8.93	Plant	-37.3±1.0
51	C6-12S	Core 6	12.03	-8.93	Shell	1.8±1.0
52	C6-13P	Core 6	12.58	-9.48	Plant	-30.6±1.0
53	C6-14S	Core 6	12.58	-9.48	Shell	-2.2±1.0
54	C6-15P	Core 6	13.20	-10.10	Plant	-25.8±1.0
55	C6-16S	Core 6	13.20	-10.10	Shell	-0.2±1.0
56	C6-17P	Core 6	14.24	-11.14	Plant	-27.9±1.0
57	C6-18S	Core 6	14.24	-11.14	shell	-0.2±1.0

Table 4.5   Continue.

No.	δ^{13}C by IRMS	^{14}C age (±σ)	Calibrated age (mean±σ)	Calibrated age range (±2σ)		Lab No.
	(‰)	(yr BP)	(cal yr BP)	(cal yr BP)(Prob.)		(NUTA2-)
40		4170±36	4710±70	4834-4780 4770-4580	(20.3%) (75.1%)	5969
41		4468±37	4660±70	4790-4529	(95.4%)	5964
42		4688±36	5420±70	5577-5537 5478-5318	(11.7%) (83.7%)	5972
43		5042±37	5390±50	5505-5291	(95.4%)	5965
44		5687±38	6470±50	6626-6586 6568-6398	(2.7%) (92.7%)	5973
45		5978±38	6390±50	6480-6291	(95.4%)	5966
46		5947±37	6780±50	6880-6870 6860-6676	(2.3%) (93.1%)	6538
47		6099±33	6530±50	6626-6430	(95.4%)	6542
48		6034±58	6890±90	7153-7118 7024-6730	(2.4%) (93.0%)	6539
49		6293±33	6750±50	6848-6654	(95.4%)	6543
50		6619±68	7510±50	7607-7423	(95.4%)	6540
51		6501±34	7010±60	7134-6905	(95.4%)	6544
52		6460±37	7370±40	7434-7292	(95.4%)	6541
53		6781±34	7310±40	7398-7238	(95.4%)	6546
54		7080±39	7910±40	7978-7834	(95.4%)	5974
55		7057±40	7540±40	7618-7454	(95.4%)	5967
56		7061±39	7890±40	7965-7825 7807-7798	(94.1%) (1.3%)	5975
57		7455±40	7910±50	8000-7824	(95.4%)	5968

Table 4.6 *Additional newly measured data from cored sediments of C-8.*

No.	Sample No.	Core No.	Depth	Height above sea level	Sample Material	δ^{13}C by AMS
			(m)	(m)		(‰)
			0.00	1.96		
58	C8-1P	Core C8	0.91	1.05	Plant	-24.4±1.0
59	C8-2P	Core C8	2.26	-0.30	Plant	-24.2±1.0
60	C8-3P	Core C8	7.15	-5.19	Plant	-29.4±1.0
61	C8-4P	Core C8	10.63	-8.67	Plant	-17.6±1.0
62	C8-5P	Core C8	14.62	-12.66	Plant	-26.6±1.0
63	C8-6P	Core C8	15.34	-13.38	Plant	-24.9±1.0
64	C8-7P	Core C8	16.36	-14.40	Plant	-24.3±1.0
65	C8-8P	Core C8	20.76	-18.80	Plant	-26.2±1.0
66	C8-9P	Core C8	27.40	-25.44	Plant	-28.8±1.0

Table 4.6 *Continue.*

No.	δ^{13}C by IRMS	^{14}C age (±σ)	Calibrated age (mean±σ)	Calibrated age range (±2σ)	Lab No.
	(‰)	(yr BP)	(cal yr BP)	(cal yr BP)(Prob.)	(NUTA2-)
58		998±23	910±40	962-904 (80.6%) 858-828 (12.6%) 810-802 (2.2%)	16194
59		2886±25	3020±40	3140-3126 (1.8%) 3108-3094 (1.9%) 3079-2928 (91.7%)	16186
60		4761±28	5510±60	5588-5464 (91.6%) 5358-5354 (0.6%) 5348-5333 (3.2%)	16187
61		6528±29	7450±30	7504-7416 (94.3%) 7349-7339 (1.1%)	16195
62		7474±30	8290±50	8372-8276 (58.3%) 8269-8200 (37.1%)	16189
63		7434±30	8260±40	8337-8186 (95.4%)	16190
64		7941±31	8810±100	8979-8824 (42.8%) 8814-8642 (52.6%)	16191
65		8046±31	8930±80	9025-8930 (57.2%) 8924-8859 (17.7%) 8834-8778 (20.5%)	16192
66		9222±33	10380±70	10497-10267 (95.4%)	16193

4.5   Fundamental Procedures of Sample Preparation

4.5.1   Preparation of Dolphin Bone

A fossil dolphin bone collected during the excavation of the Mawaki site in 1983 was analyzed by ^{14}C dating. The procedure of the sample treatment for ^{14}C dating of the dolphin bone is described briefly in the following, as summarized in Figure 4.13 (Muto, 2001; Minami et al., 2004). The bone was decalcified with 0.5M HCl and divided into two fractions: the acid soluble component (SC) and the acid insoluble component (DB: decalcified bone). Gelatin was extracted from the DB component by heating in acidic solution at 90°C. The gelatin solution obtained was separated with a centrifuge and then lyophilized (GC-DB). The insoluble residue after gelatin removal (Insol. Res. after GC ext.) was also retained for ^{14}C measurement. A portion of the gelatin thus obtained was hydrolyzed with 6 M HCl at 110°C for 24 h. Then, the solid part was removed by centrifugation, and the filtered hydrolysate was treated with XAD-2 resign. The XAD-treated component was eluted with HCl, evaporated, and lyophilized (XAD-GC-DB). Two aliquot parts of the DB component were treated with 0.1 M NaOH, one for 2h (A-DB (2h)) and the other for 48 h at room temperature, to get rid of any humic acid contamination. In addition, the 48 h NaOH treatment was performed in two ways: one without changing the NaOH solution (A-DB (48h)) and one in which the NaOH solution was changed once during the treatment (A-DB (48h-A.C.). Gelatin components were extracted from A-DB (2h), A-DB (48h) and A-DB (48h-A.C.) using a method similar to the one described above, and labeled as GC-A-DB (2h), GC-A-DB (48h) and GC-A-DB (48h-A.C.), respectively. Finally, all of these carbonaceous fractions were combusted in a sealed evacuated bottle with CuO as an oxidizer at 900°C and changed to CO_2 (Figure 4.14 and 4.15). The liberated CO_2 was purified cryogenically using liquid N_2 and other coolants. The purified CO_2 was then reduced to graphite using a powder iron catalyst under a hydrogen atmosphere, and the mixture of graphite

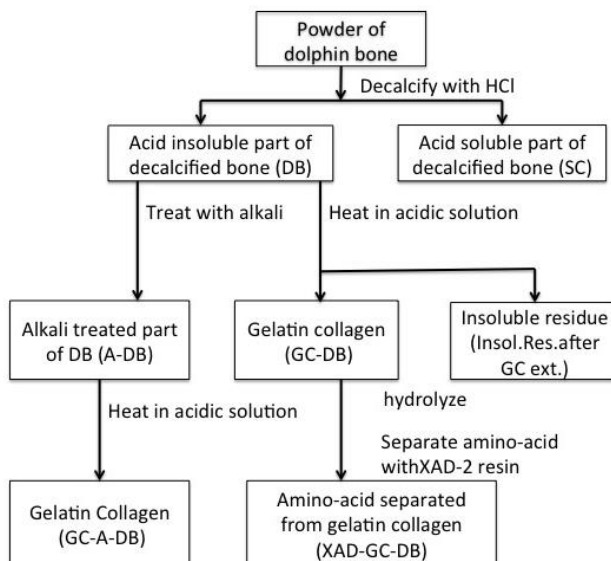and iron powder was pressed into an aluminum cathode for ^{14}C analysis by AMS.

Figure 4.13   *Procedure of extracting carbonaceous fractions from dolphin bones for AMS ^{14}C dating.*

4.5.2   Preparation of Plant, Wood and Shell Samples

Typical samples for ^{14}C dating, such as shell, plant, wood and charred wood samples were pretreated in a routine way (Minami and Nakamura, 2000; Nakamura et al., 2004; Nakamura et al., 2013). (Figures 4.14 and 4.15). Shell samples were cleaned with distilled water as well as diluted HCl (0.6 M) in an ultrasonic cleaner, and then dried and powdered. The shell powder was decomposed with 85% H_3PO_4 in an evacuated bottle to produce CO_2 (Nakamura et al., 2007). Plant, wood and charred wood samples were processed chemically with a 1.2 M HCl-1.2 M NaOH solution-1.2 M HCl (acid-base-acid) treatment and combusted to CO_2. The liberated CO_2 was then converted to graphite as described in the previous section.

Figure 4.14   Photo of glass-line vacuum system used for sample preparation.
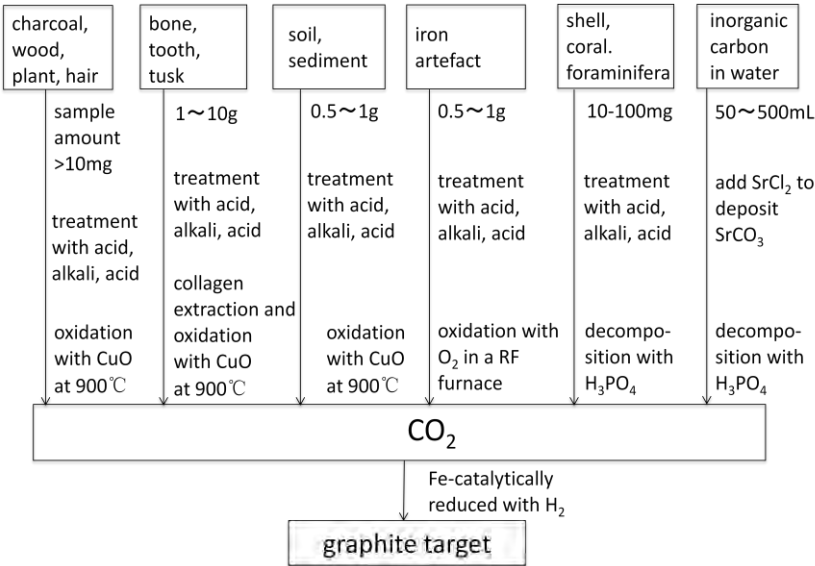

Figure 4.15   Sample preparation for ^{14}C measurement with AMS.

4.6 ^{14}C Measurement by AMS

All three carbon isotopes, ^{12}C, ^{13}C and ^{14}C, of the graphite targets prepared from the unknown-age sample, with the NIST HOxII standard and ^{14}C blank material (commercially available oxalic acid synthesized from fossil fuel,

No. 57952 from Kishida Ltd., Japan), were measured with an AMS system (HVEE Model-4130 AMS) at Nagoya University (Nakamura et al., 2004). The measured $^{14}C/^{12}C$ and $^{13}C/^{12}C$ ratios were used to correct carbon isotopic fractionation and to calculate the sample conventional ^{14}C age. The obtained ^{14}C age was calibrated to a calendar date using the calibration program OxCal 4.2.4 (Bronk Ramsey, 2009) and the IntCal13 or Marine13 calibration dataset (Reimer et al., 2013). We estimated the correction value of the local marine carbon reservoir effect, ΔR, for the sediment samples from cores C4, C5 and C6, as is discussed later in the section. The obtained ΔR values were somewhat unreliable with rather large errors, but because the ΔR values were almost consistently zero, within ±1σ error, we adopted ΔR=0 for calibration of the marine samples collected from the Mawaki site.

4.7   Results

4.7.1   Age Determination of Dolphin Bones
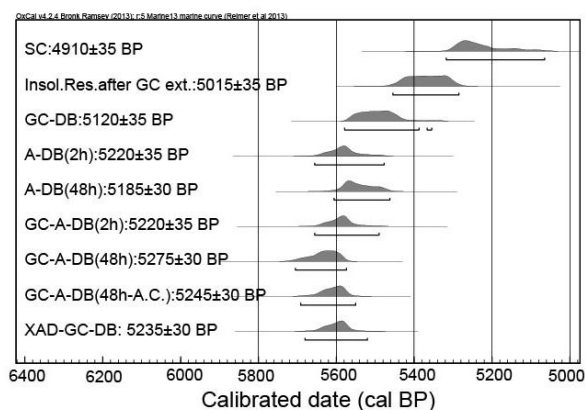
Figure 4.16   *Calibrated ^{14}C ages for nine different carbonaceous fractions separated from dolphin bones excavated at the Mawaki site.*

For ^{14}C measurements of dolphin bone samples, nine carbonaceous fractions collected by the treatment method shown in Figure 4.13 were used. The fraction

yield, CO_2 yield, C/N ratio, $\delta^{13}C$ value by IRMS, ^{14}C age, and calibrated age ranges for each carbonaceous fraction are listed in Table 4.1 and the probability density distributions against calendar date of ^{14}C ages obtained for the nine carbonaceous fractions are shown in Figure 4.16. The ^{14}C ages and their calibrated ages converged to 5,230-5,270 ^{14}C BP and 5,580-5,650 cal BP, respectively, when the carbonaceous fractions that were dated were separated from more essential and genuine parts of the dolphin bones.

4.7.2 Core Samples

Figure 4.17 *Calibrated age vs height for terrestrial and marine samples from sediments C-3, C-4, C-5, C-6 and C-8 cored at the Mawaki site.*

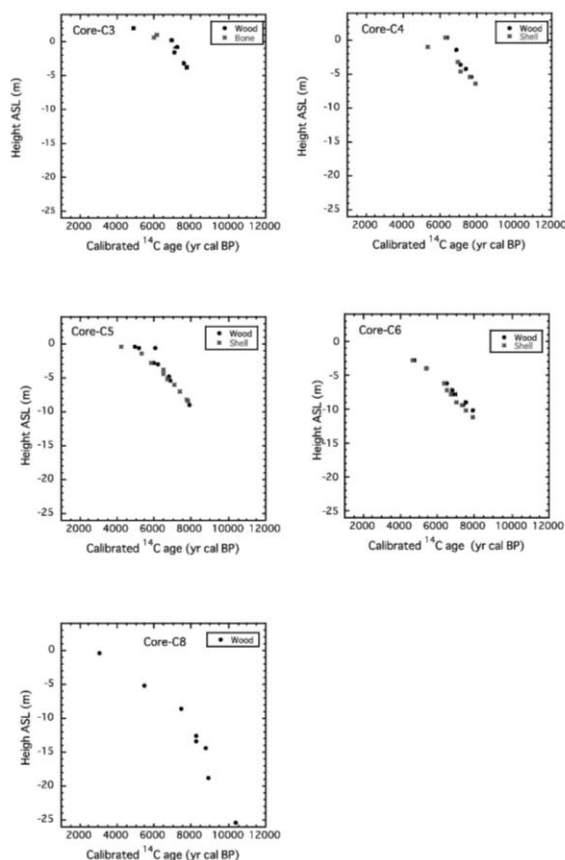The ^{14}C ages and the calibrated dates of terrestrial material (wood, plant, charcoal), marine shells and dolphin bones collected from core sediments C3, C4, C5, C6, C8 and B3, as well as wood samples from an outcrop at a trench dug along the C-line drilling (D2 in Figure 4.11) are listed in Tables 4.2, 4.3, 4.4, 4.5, 4.6 and 4.7. The calibrated ages are plotted against sample height above mean sea level (ASL) in Figure 4.17. The sample height ranged from +2 m ASL to -25.5m ASL, and the calibrated ages ranged from 3,000 cal BP to 10,400 cal BP, covering the full Holocene period.

Table 4.7   *Additional newly measured data from B3 and D2.*

No.	Sample No.	Core No.	Depth	Height above sea level	Sample Material	δ^{13}C by AMS
			(m)	(m)		(‰)
			0.00	4.59		
67	B3-1S	Core B3	3.12	1.47	Shell	-0.7±1.0
68	B3-2S	Core B3	3.38	1.21	Shell	0.8±1.0
69	D2-1W	C-Line trench		3.15	Wood	-24.8±1.0
70	D2-2W	C-Line trench		3.16	Wood	-26.5±1.0
71	D2-3W	C-Line trench		3.13	Wood	-27.5±1.0
72	D2-4W	C-Line trench		3.16	Wood	-24.6±1.0

Table 4.7   *Continue.*

No.	δ^{13}C by IRMS	^{14}C age (±σ)	Calibrated age (mean±σ)	Calibrated age range (±2σ)		Lab No.
	(‰)	(yr BP)	(cal yr BP)	(cal yr BP)(Prob.)		(NUTA2-)
67		4832±26	5140±70	5258-5024 (95.4%)		21532
68		6314±27	6770±50	6866-6682 (95.4%)		22221
69		1149±27	1060±60	1174-1157 (7.6%) 1150-979 (87.8%)		21689
70		2959±29	3120±50	3211-3020 (93.9%) 3015-3005 (1.5%)		21690
71		2959±29	3120±50	3211-3020 (93.9%) 3015-3005 (1.5%)		21691
72		2245±28	2240±60	2341-2296 (27.9%) 2269-2155 (67.5%)		21694

4.8   Discussion

4.8.1   Age of Dolphin Bones

As listed in Table 4.1 and shown in Figure 4.16, the ^{14}C ages and also their calibrated ages converged to 5,230-5,270 ^{14}C BP and 5,580-5,650 cal BP, respectively, when the carbonaceous fractions dated were collected from more genuine part of the dolphin bones. The SC fraction in the dolphin bone, collected as the acid soluble part just after decalcification with 0.5 M HCl, showed evident contamination with younger carbonaceous materials. The acid insoluble fraction after decalcification (Insol. Res. after GC ext. in Figure 4.13) was also contaminated with younger carbonaceous materials, and the contaminants could not be removed even by gelatin collagen separation (GC-DB). The GC-DB fraction showed younger age than the alkali treated fractions (A-DB, GC-A-DB) or amino-acid fraction separated with XAD treatment (XAD-GC-DB). Normally, alkali treatment removes humic acid contaminants from bone samples, and alkali treatment seemed essential for the chemical cleaning of the dolphin bone sample from the Mawaki site. As mentioned previously, the ^{14}C ages and the calibrated ages of the dolphin bone from the Mawaki site ranged from approximately 5,230-5,270 BP and 5,580-5,650 cal BP, respectively. This age of dolphin bone is consistent with the chronology established with other samples from the cored sediments, which is discussed by Takemura et al. (this volume).

4.8.2   Age-Height Relation Plot of Bored Sediment Samples

Using the ^{14}C ages and the calibrated dates of charcoal, wood and plant fragment samples that were collected from the C3, C4, C5, C6 and C8 cored sediments, height-age relations were obtained for the sediments. In the calibration of the ^{14}C ages to calendar dates for the marine samples, the correction value of the local marine carbon reservoir effect, ΔR, peculiar to the

area of the Mawaki site was assumed to be zero, and this assumption produced no particular temporal discrepancy. Because the height-age relations were smooth, except for a few ^{14}C ages, we considered that the obtained relations are acceptable (Figure 4.17). Some exceptional ages may be the result of reworking of the samples during sedimentation.

The age-height relations for sediment samples from cores C3, C4, C5, C6 and C8, which correspond to the most distant to the most proximal from the seashore (Figure 4.11), are summarized in Figure 4.18. Sediments older than 8,000 yr cal BP accumulated only at C8. Additionally, C8 sediments accumulated until less than 1,000 cal yr cal BP. Contemporaneous sediments accumulated at higher horizons as the location of sedimentation moved away from the shoreline, although the age-height relations for sedimentation in cores C6 and C8 are almost identical for overlapping periods.
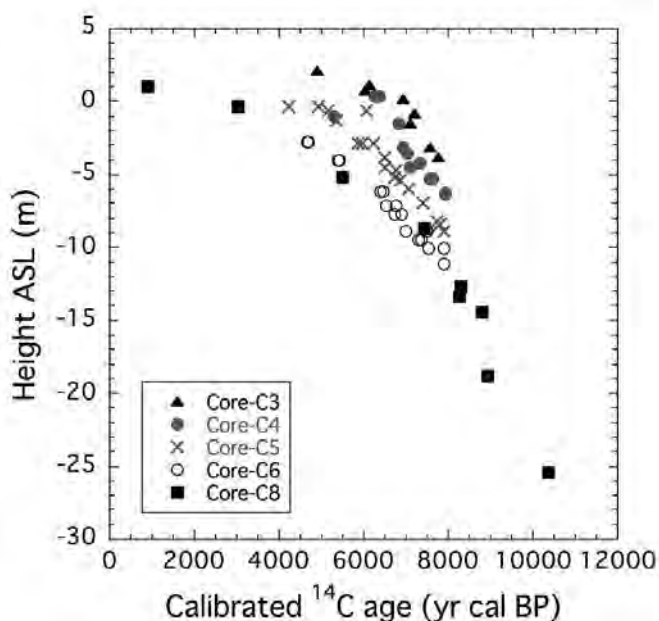

Figure 4.18 *Age-height relation of sediment samples from bored core C3, C4, C5, C6, C8.*

4.8.3 Comparison of ^{14}C Ages of Terrestrial and Marine Materials
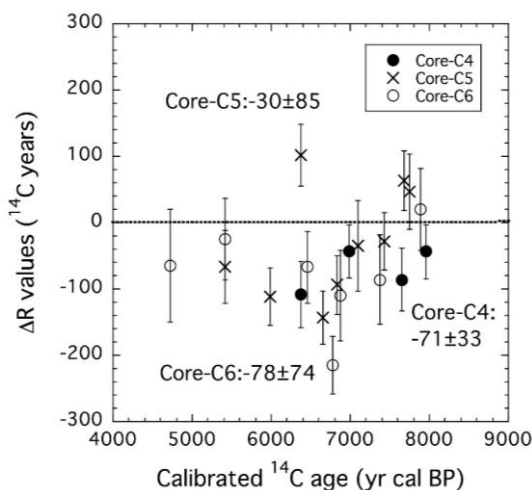

Figure 4.19 *Time dependence of the ΔR values for C4, C5 and C6 cored sediments.*

Based on the ^{14}C ages of terrestrial materials, height-age relations were determined for the sediments of cores C4 and C5. As the height-age relations were considerably smooth, with the exception of a few ^{14}C ages, we accepted that the obtained height-age relations describe the real relations. Then, the terrestrial ^{14}C ages were estimated at the depths where shell samples were collected, and pairs of terrestrial and marine ^{14}C ages were prepared. From the terrestrial ^{14}C ages thus obtained by interpolation, marine model ^{14}C ages were calculated and compared with real marine ^{14}C ages of shell samples to evaluate the local marine reservoir correction value ΔR (Figure 4.9). For core C6 sediment, both terrestrial and marine samples were selected from the identical horizons (Table 4.5), and the local marine reservoir correction values, ΔR, were calculated in the similar way. The results are illustrated in Figure 4.19. From the Mawaki samples, we obtained the time dependence of the ΔR values in the temporal range covered by the cored sediments (4,600-8,000 cal BP), as shown in Figure 4.19. The ΔR values tend to be more negative during the Holocene marine transgression period (6,000-7,000 cal BP), except for one ΔR value for

C5 core (Itoh et al., 2011). The well-mixed surface ocean water supplied by the warm Kuroshio Current might have contributed to this negative value of ΔR (weaker marine carbon reservoir effect). The average ΔR values for cores C4, C5 and C6 were calculated, excluding the unacceptable values more negative than -300 ^{14}C years that are quite different from the global marine reservoir correction value (ΔR = 0), to be -71±33, -30±85 and -78±74 ^{14}C years, respectively. Recent studies on the marine carbon reservoir effect for samples from Japan are summarized in Nakamura et al. (2016).

4.9   Summary

We measured ^{14}C ages for sediment cores B3, C3, C4, C5, C6 and C8, as well as for wood samples collected from an outcrop at a trench dug along the C-line drilling, to analyze paleoenvironmental change around the Mawaki archeological site, especially the temporal progression of Holocene ocean transgression and successive retreat. To also make use of ^{14}C ages for marine samples, we checked the local marine carbon reservoir effect and discovered that the reservoir effect is negligible at the moment, because the obtained correction values of the local marine carbon reservoir effect, ΔR, were consistent with zero within large experimental errors. We thus reached the following conclusions.

(1) Core C8 located nearest the seashore accumulated Holocene sediments from 10,400 cal BP until 900 cal BP.

(2) The ^{14}C ages obtained from several carbonaceous fractions collected from dolphin bone suggested that alkali treatment is essential to chemically clean dolphin bone samples from the Mawaki site. The ^{14}C ages and their calibrated ages for the alkali-treated fractions from the dolphin bone collected at the Mawaki site ranged 5,230-5,270 ^{14}C BP and 5,580-5,650 cal BP, respectively.

(3) The temporal change of the correction value of the local marine carbon

reservoir effect ΔR was analyzed for sediments from cores C4, C5, and C6, and it was recognized that the ΔR values tend to be more negative during the Holocene marine transgression period (6,000-7,000 cal BP).

Reference

[1]   Arnold, J. R., & Libby, W. F. (1949). Age determination by radiocarbon content: checks with samples of known age. Science, 110, 678-680.

[2]   Bronk Ramsey, C. (2009). Bayesian analysis of radiocarbon dates. Radiocarbon, 51 (1), 337-360.

[3]   Hughen, K. A., Baillie, M. G. L., Bard, E., Beck, J. W., Bertrand, C. J. H., Blackwell, P. G., Buck, C. E., Burr, G. S., Cutler, K. B., Damon, P. E., Edwards, R. L., Fairbanks, R. G., Friedrich, M., Guilderson, T. P., Kromer, B., McCormac, G., Manning, S., Bronk Ramsey, C., Reimer, P. J., Reimer, R. W., Remmele, S., Southon, J. R., Stuiver, M., Talamo, S., Taylor, F. W., van der Plicht, J., & Weyenmeyer, C. E. (2004). Marine04 marine radiocarbon age calibration, 0-26 cal kyr BP. Radiocarbon, 46(3), 1059-1086.

[4]   Itoh, Y., Takemura, K., Nakamura, T., Hasegawa, S., & Takada, H. (2011). Paleoenvironmental analysis of the Mawaki archaeological site, central japan, in relation to stratigraphic position of dolphin bones, Geoarchaeology, 26, 4, 461-478.

[5]   Minami, M., & Nakamura, T. (2000). AMS radiocarbon age for fossil bone by XAD-2 chromatography method. Nucl. Instruments and Methods in Physics Research, B172, 462-468.

[6]   Minami, M., Muto, H., & Nakamura, T. (2004). Chemical techniques to extract organic fractions from fossil bones for accurate ^{14}C dating. Nucl. Instr. and Meth., B223-224, 302-307.

[7]   Muto, H. (2001). Radiocarbon dating of fossil bone with accelerator mass spectrometry - Studies on sample preparation techniques -. Thesis for Master Degree, Graduate School of Human Informatics, Nagoya University., pp. 61. (in Japanese)

[8]   Nakamura, T., Niu, E., Oda, H., Ikeda, A., Minami, M., Ohta, T., & Oda, T. (2004). High precision ^{14}C measurements with the HVEE Tandetron AMS system at

Nagoya University. Nucl. Instr. and Meth., B 223-224, 124-129.

[9] Nakamura, T., Nishida, I., Takada, H., Okuno, M., Minami, M., & Oda, H. (2007). Marine reservoir effect deduced from ^{14}C dates on marine shells and terrestrial remains at archeological sites in Japan. Nucl. Instr. and Meth., b259, 453-459.

[10] Nakamura, T., Matsui, A., Nishida, I., Nakano, M., & Omori, T. (2013). Time range for accumulation of shell middens from Higashimyo (western Japan) and Kimhae (southern Korea) by AMS radiocarbon dating. Nucl. Instrum. Methods B294, 680-687.

[11] Nakamura, T., Masuda, K., Miyake, F., Hakozaki, M., Kimura, K., Nishimoto, H., & Hitoki, E. (2016). High-precision age determination of Holocene samples by radiocarbon dating with accelerator mass spectrometry at Nagoya University. Quaternary International 397, 250-257.

[12] Reimer, P. J., Bard, E., Bayliss, A., Beck, J. W., Blackwell, P. G., Bronk Ramsey, C., Buck, C. E., Cheng, H., Edwards, R. L., Friedrich, M., Grootes, P. M., Guilderson, T. P., Haflidason, H., Hajdas, I., Hatté, C., Heaton, T. J., Hoffmann, D. L., Hogg, A., G., Hughen, K. A., Kaiser, F., Kromer, B., Manning, S. W., Mu Niu, M., Reimer, R. W., Richards, D. A., Scott, E.M., Southon, J. R., Staff, R. A., Turney, C. S. M., & van der Plicht, J. (2013). IntCal13 and Marine13 radiocarbon age calibration curves 0- 50,000 years al BP. Radiocarbon, 55(4), 1869-1887.

[13] Stuiver, M., & Polach, H. (1977). Discussion: reporting of ^{14}C data. Radiocarbon 19(3), 355-363.

[14] Stuiver, M., Pearson, G. W., & Braziunas, T. (1986). Radiocarbon age calibration of marine samples back to 9000 cal yr BP. Radiocarbon, 28(2B), 980-1021.

[15] Stuiver, M., & Braziunas, T. F. (1993). Modeling atmospheric ^{14}C influences and ^{14}C ages of marine samples to 10,000 BC. Radiocarbon, 35(1), 137-189.

[16] Takemura, K., Takada, H., Haraguchi, T., & Itoh, Y. (2016). Holocene stratigraphy from the Mawaki archaeological site and the occurrence and significance of dolphin bones. (this volume)

Chapter 5

Analysis of Pollen and Diatoms in the Mawaki area, Noto Peninsula, During Holocene: A microscopic Perspective of the Mawaki Environment

Masaaki Kanehara

Hideki Takada

Abstract

Microfossil assemblage within the Holocene coastal deposits provides important information on environmental issues in and around archaeological sites. Pollen analysis reveals vegetation change and climate phenomena, while, diatom analysis yields data on the water ecosystem in and around archaeological sites. Preliminary data from the core samples provided insight into the environmental changes around the Mawaki site, such as changes in sea-level (one cycle of transgression to regression) and vegetation.
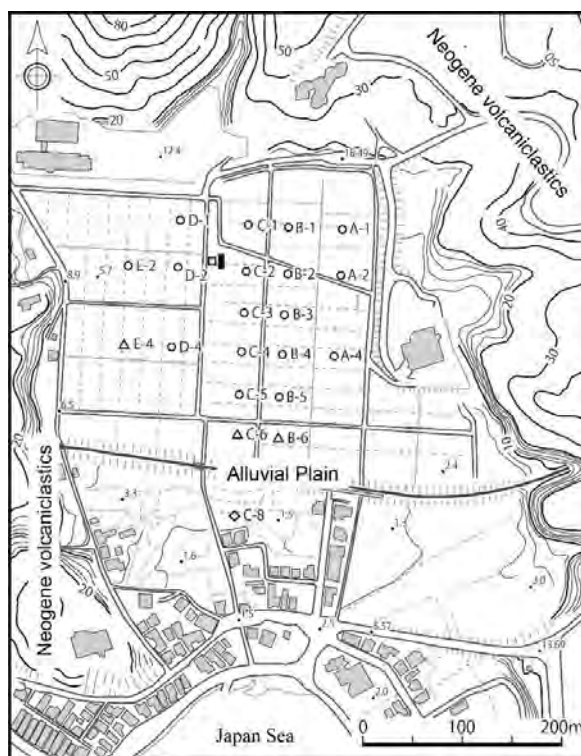
5.1　Introduction

Figure 5.1 *Borehole and geoslicer locations around the Mawaki archaeological site. Open circle: drilling in 1997 & 1998, open triangle: drilling in 2002, open rhombus: drilling in 2005, solid rectangle: geoslicer coring.*

Pollen analysis and botanical data are very important to understand the climatic environment on the basis of the reconstruction of vegetation in and around surrounding area. Additionally, diatom species lives in a wide range of aquatic conditions, as well as in planktonic and benthic habitats. Therefore, diatom assemblage of the discrete horizons is indicative of the associated environment at that time (Lowe and Walker, 1997; Nakamura, 1967, etc), and both analyses provide important information for the reconstruction of the archaeological environment. This section introduces the example from the Mawaki site.

5.2   Methods and Analytical Samples

5.2.1   Pollen Analysis

Pollen grains and spores are frequently dispersed in very large number in order to maximize the opportunities for successful pollination. Many accumulate on the ground or in water bodies, and some are subsequently incorporated and fossilized in sediments. Extraction, identification and counting of these preserved fossil grains form the basis of pollen analysis. Most pollen grains and spores are small; few exceed 80 to 100 μm in diameter, with the majority falling in the size range of 25 to 35 μm.

Samples containing fossil pollen and spores can be taken from the exposed sections by means of coring. Samples must be sealed air-tight and are usually stored in a cool place. This protects them from contamination by pollen circulating in the air. In the laboratory, following dispersal, sieving, and chemical flotation (density separation), samples are chemically treated in a variety of ways to concentrate pollen grains. Lignins and cellulose can be reduced in volume, if not entirely removed, by oxidation and accetolysis. Mineral grains may be removed by digestion in hydrofluoric acid, separation via differential centrifugation, or floating the organic detritus. The residues

containing the pollens and spores may be stained with an organic dye such as safranin which enhances the surface detail of some grains and then mounted on to glass slides on a suitable medium such as glycerine jelly. Counting is then performed at magnifications of $100\times$ to $1,000\times$, depending on the detail required for identification purposes. By traversing the slide in a systematic way, the identifiable pollens and spores can be counted until a sufficient number for interpretation has been reached. This should be high enough (e.g., 300-500 grains) to account for most of the variations in the spectrum of pollen assemblage. Identifications, which in generally can easily made up to family and genus level but less frequently to the species level, is based on distinctive exine characteristics using pollen keys, collections of photographs and laboratory reference material derived from modern pollen samples.

Where samples have been taken from a stratified sequence of sediments, such as a lake or peat sequence, an analysis of the pollen content of a single horizon will reveal a mixture of pollen types, collectively termed the pollen assemblage (pollen spectrum). Analysis of a series of horizon may show changes in pollen content which may, in turn, indicate temporal changes in vegetation cover in the area adjacent to the site. These changes are usually depicted graphically in the form of pollen diagrams which are based either on percentage values or on pollen concentration data, the latter sometimes being termed as 'absolute pollen diagrams'. Percentage pollen diagram usually take two forms. In some cases a pollen sum is selected for each level, and individual pollen and spore types are then expressed as percentages of that sum.

The interpretation of a pollen diagram is the most difficult part of pollen analysis, as it requires knowledge of pollen production and dispersal, source and deposition, preservation and the relationship between fossil pollen and former plant communities. Only when these factors have been carefully evaluated can be inferences made about former vegetation cover and, by implication, former

climatic conditions and environments.

First, not all plants produce the same quantity of pollen. Second, it is necessary to know something about the source of fossil pollen in a body of sediment. It is important to establish whether plants were growing on the bog surface or within the lake basin, around the margins of the site, in the immediate vicinity, or some distance away. Moreover, it is necessary to know some aspects of the mechanisms involved in the transport of pollen from its source to the eventual point of deposition. Third influencing factor is the nature of pollen deposition. Different settling velocities of pollen in lakes and ponds, coupled with the disturbance of sediment on the lake or bay floor, either by currents or burrowing organisms, can lead to complications in the fossil record. Equally misleading is the occurrence of redeposited or secondary pollen that has been washed into the lake by stream flow, overland flow, solifluction or collapse of the basin edge sediments, and the subsequent redistribution or material across the lake floor. These grains will clearly be of an age different from that of those arriving at the lake surface from the atmospheric pollen rain. Although they can often be distinguished from primary pollen by signs of exine deterioration, they are potential sources of confusion in the interpretation of the biostratigraphic record.

As a result, pollen stratigraphy was applied to following reconstructions: Local vegetation reconstructions, regional vegetation reconstructions, and space-time reconstructions. Analytical samples for pollen analysis were used from core samples of C-line drilling cores.

5.2.2　Diatom Analysis

Diatom remains have proved extremely useful as indicators of local habitat changes, particularly in both shallow and deep marine deposits, but also in lake sediments. The analysis of diatom flora has revealed a wide range of paleoenvironmental issues, such as changes in the water chemistry,

reconstruction of past lake level and sea-level variations and the disturbance of the ecosystem by human activities (Lowe and Walker, 1997; Ando, 1990; Asai and Watanabe, 1995; Hustedt, 1937-1938; Krammer and Lange-Bertalot, 1986-1991; Kosugi, 1986, 1988; Lowe, 1974, etc).

Diatom valves are best preserved in fine grained sediment since they can be easily damaged or destroyed in coarse-grained deposits. Samples for analysis can be obtained from vertical exposures in shallow water marine or estuarine deposits, though more frequently they are extracted from sediment cores obtained from lake, shelf seas or the deep ocean. Diatom are not susceptible to oxidation or microbial degradation, but cores for diatom analysis are usually sealed air-tight to prevent drying out of the sediment, which can lead to fracturing of the valves. Diatom frustules may be separated from the sediment matrix by a variety of laboratory procedures. Organic matter is removed by oxidation, the most common methods being digestion in H_2O_2 or in a mixture of potassium dichromate and sulphuric acid, while carbonates and certain other salts can be dissolved by heating gently in dilute hydrochloric acid.

Diatom valves are light and easily transported, and thus in estuarine sediments, for example, there is often a complex admixture of marine, brackish and freshwater forms, while lake muds may contain diatoms derived not only from the lake ecosystem, but also from inflowing streams and catchment soils. Freshwater diatoms often occur in marine sediments. Selective destruction of diatoms is another potential source of error, with complete or partial dissolution of the frustules under pressure at great depths or alkaline conditions. Also, reworked diatom frustules can sometimes be detected. Despite these problems, diatom analysis has proved to be a particularly valuable technique for environmental reconstructions.

As a result, individual diatom species can be classified on the basis of their salinity preferences as salinity is a major factor controlling distribution. Using

the specific diatom assemblage data, we can consider the aquatic environments on the basis of the salinity data such as marine, brackish and freshwater water mass, and related geographical environments.

Analytical samples for diatom analysis were used from core samples of C-line drilling cores and horizon of dolphin bone occurrence.

5.3   Reconstruction of Vegetation and Water Environment Around the Site

5.3.1   Pollen Assemblage and Interpretation of Vegetation

This section is mainly the result of pollen assemblage (Photo 5.1) from boring sample C-2 at Mawaki site (Figure 5.1 and Figure 5.2), and the result at other boring samples is shown in Figures 5.1, 5.3, 5.4, and 5.5).

The pollen assemblage from C-2 core samples is divided into four pollen zones of C-2 U-I, C-2-U-II, C-2-U-III and C-2-U-IV in ascending order.
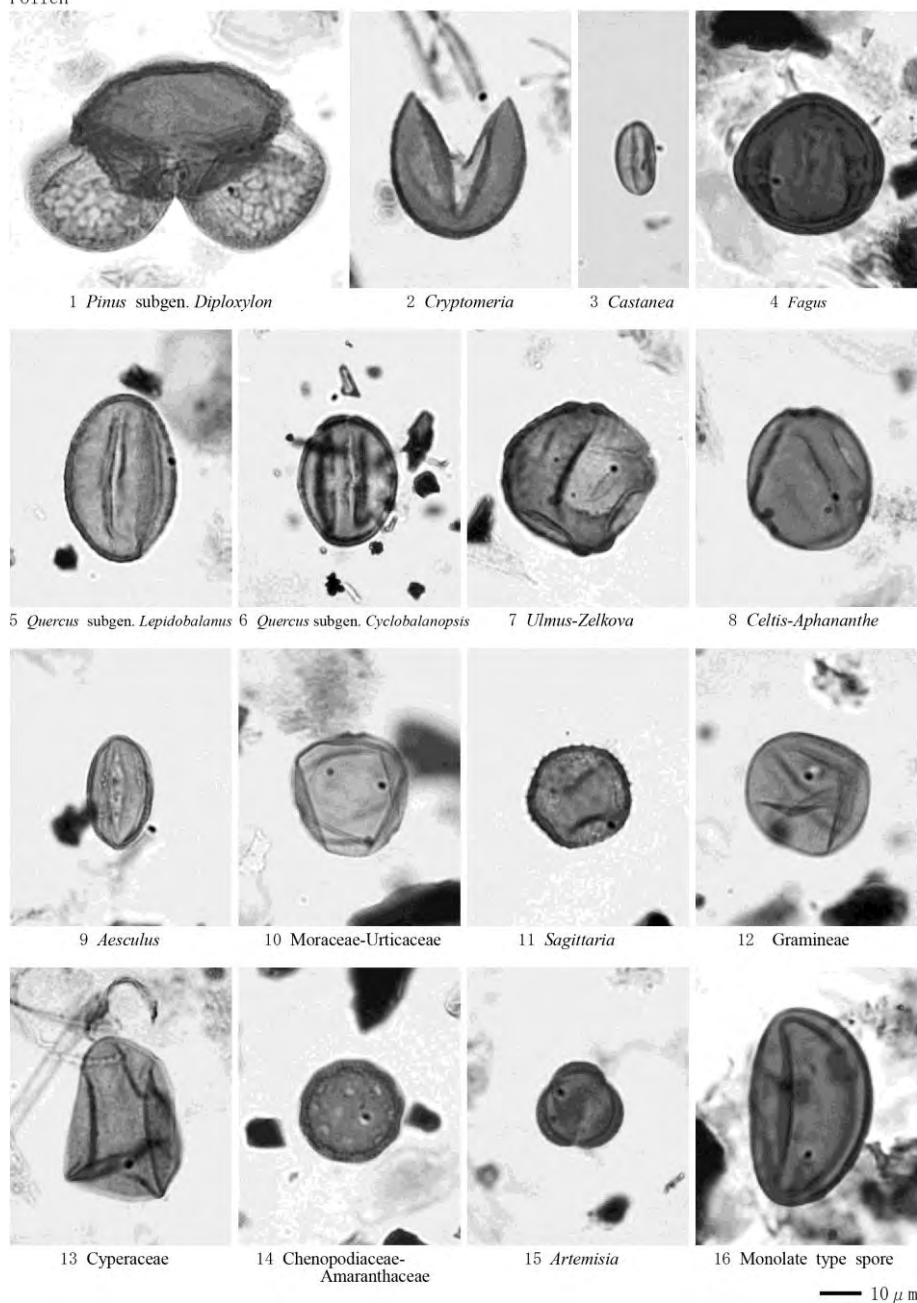
Pollen

1 *Pinus* subgen. *Diploxylon*   2 *Cryptomeria*   3 *Castanea*   4 *Fagus*

5 *Quercus* subgen. *Lepidobalanus* 6 *Quercus* subgen. *Cyclobalanopsis* 7 *Ulmus-Zelkova* 8 *Celtis-Aphananthe*

9 *Aesculus*   10 Moraceae-Urticaceae   11 *Sagittaria*   12 Gramineae

13 Cyperaceae   14 Chenopodiaceae-Amaranthaceae   15 *Artemisia*   16 Monolate type spore

━━ 10 μm

Photo 5.1 *Representative photos of pollen grains from the Mawaki Site.*
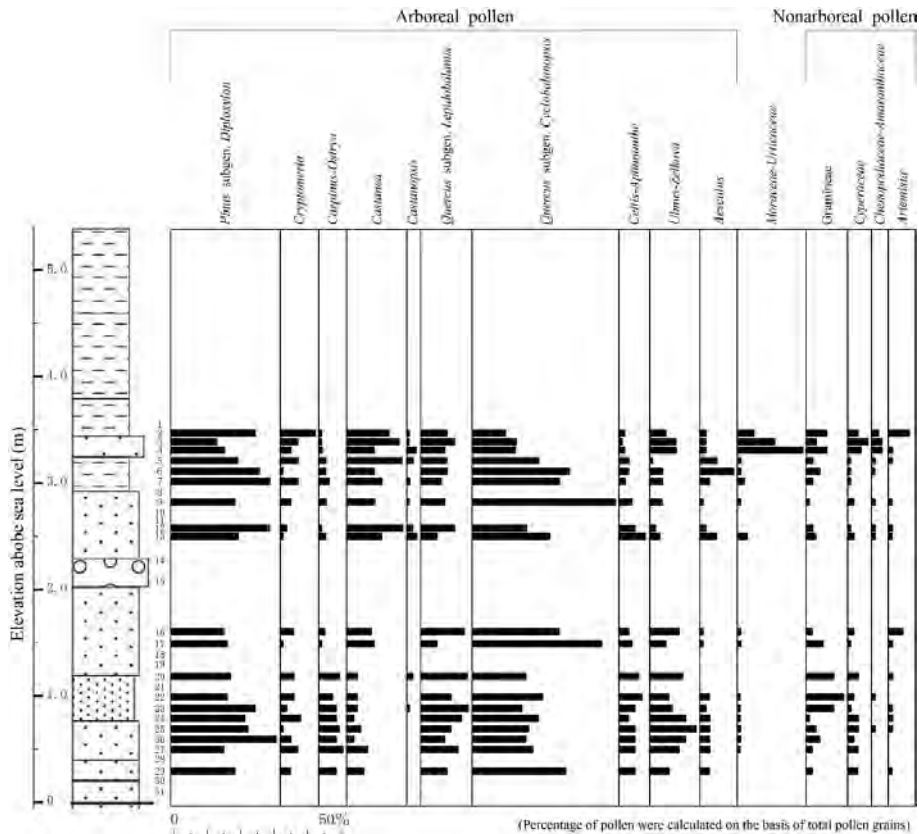
Figure 5.2 *Pollen assemblage from boring sample C-2.*

C-2-U-I zone (sample No. 18-20): Percentage of arboreal pollen is high, and Quercus (Cyclobanopsis) and Pinus are mostly occupied, and associated with broad leaf trees of Quercus (Lepidobalanus), Ulmus - Zelkova, Celtis - Aphanante, Carpinus - Ostrya, Castanea, Aesculus and Cryptomeria. Abundance of grass plant pollen is low and most of those grass pollen are Gramineae family.

C-2-U-II zone (sample No. 8-17): This zone is characterized by an increased percentage of Castanea pollen.

C-2-U-III zone (sample No. 5-7): This zone is characterized by an increased

abundance of Aesculus pollen.

C-2-U-IV zone (sample No.2-4): This zone is characterized by the decreased abundance of Quercus and increased abundance of Ulmus - Zelkova, Moraceae, Ulticacerae, Gramineae, Cyperaceae, Chenopodiaceae and Amaranthaceae.
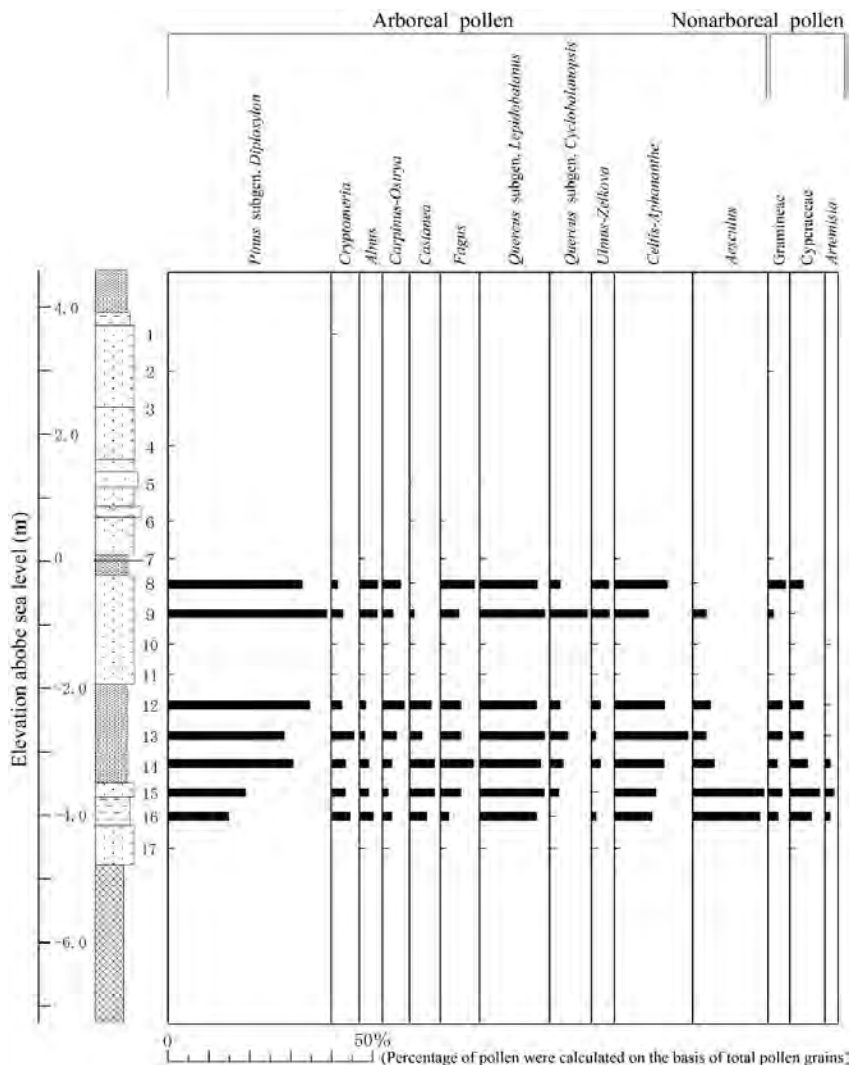

Figure 5.3 *Pollen assemblage from boring sample C-3.*

Surrounding area of Mawaki region was covered by Quercus and Pinus tree vegetation, and Pinus trees were distributed in the rock area along the shoreline and Aesculus (horse chestnut) were living along the valley. Castanea trees were distributed in and around the site, and Quercus and Celtis were present during the late and latest Jomon period. Castanea and Aesculus were the main eatable fruits for people. In the latest Jomon period, the Aesculus plant was distributed in the newly emerged humid area in front of the archeological site. Low abundance of Cryptomeria indicates a little snow near the site, and this is one of the reasons why the Mawaki archaeological site may have been used for habitations.
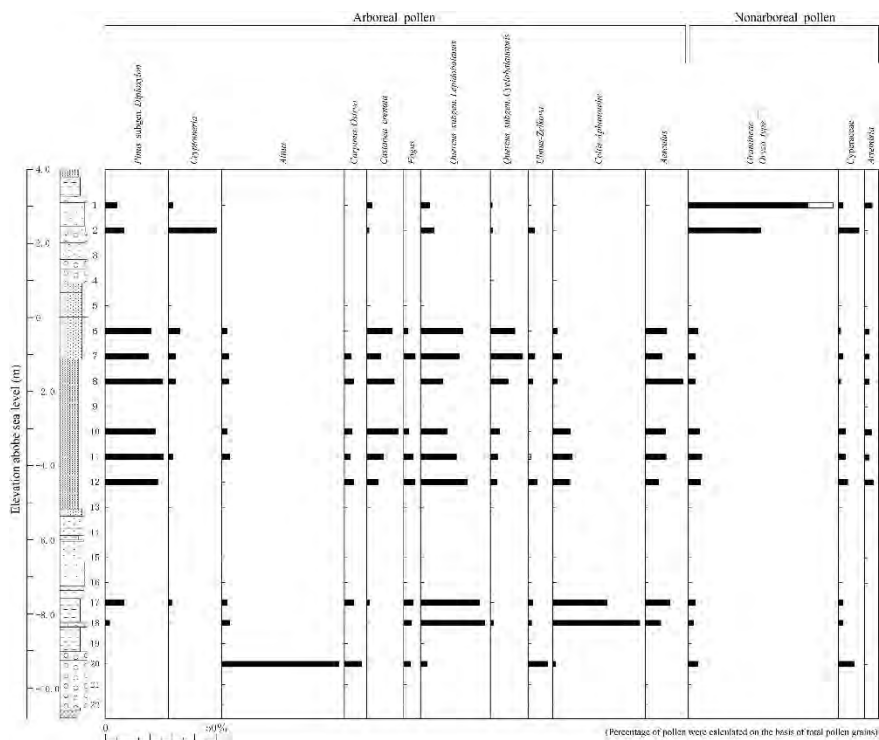

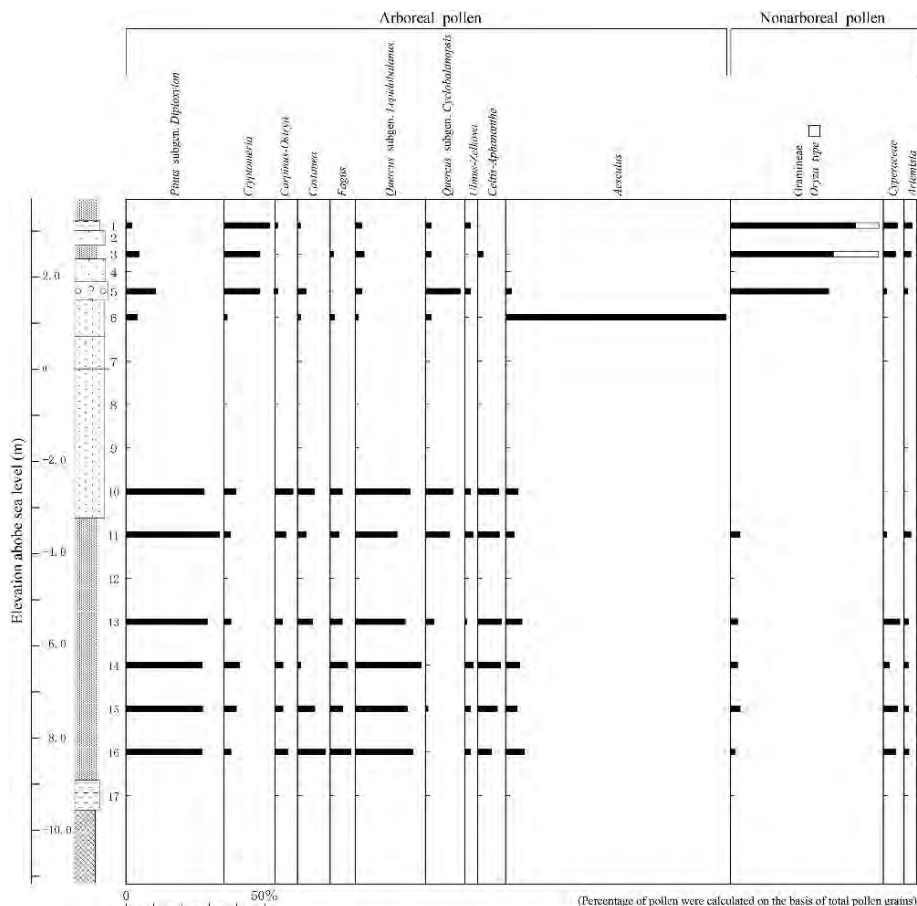***Figure 5.4***   *Pollen assemblage from boring sample C-4.*

Figure 5.5 *Pollen assemblage from boring sample C-5.*

The castanopsis group in the excavated area in 1998, having detected rather much amounts, planted in drier condition and the abundance within the marine sediments. Abundance of the Pinus group-pollen was reflected in marine sediments rather than in any other environment, and their abundance was influenced by the local vegetation at the steep slope and rock outcrops or along the shoreline.

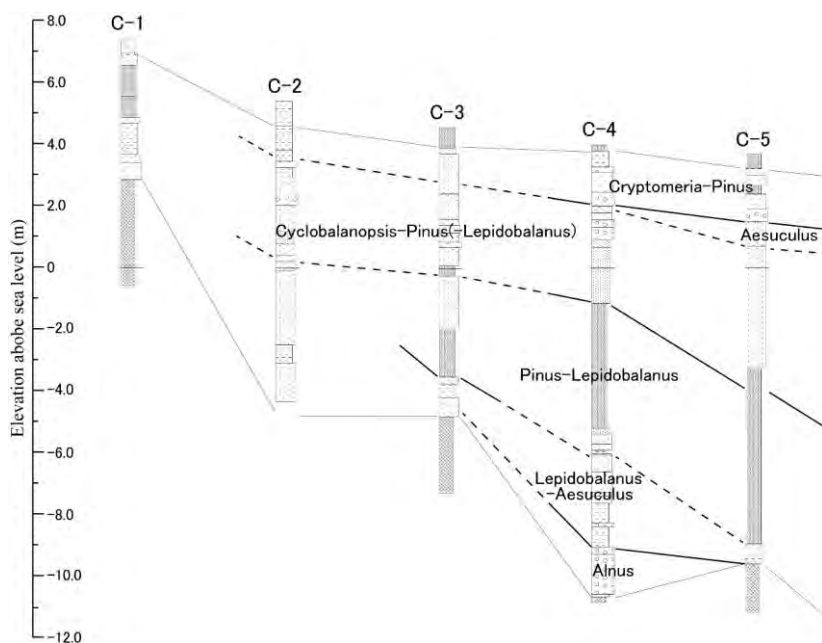## 5.3.2　Vegetational Change in and Around Mawaki Site in Space and Time

Figure 5.6　*Correlation among cores along the C-Line by pollen assemblage.*

Spatial distribution of pollen assemblage is shown along the C-Line (C-2 - C-5) in Figure 5.6. On the basis of lithological continuity, distribution of marine sediments was thicker from the hill to shoreline side. The lowest part of sedimentary sequence was composed of sandy sediments. Though the abundance of pollen grains was small, the pollen assemblage here was composed of mainly Alnus pollen. This indicates that this horizon includes sediments influenced by humic land condition. The pollen assemblage indicated a forest composed of broad-leaved deciduous trees such as Qercus, Aesculus (horse chestnut) within the clay and silty sand units (units B and C). Abundance of pollen grains was very high here. Those are composed of Lepidobalanus-Aesculus assemblage, Pinus-Lepidobalanus assemblage and Cyclobanopsis-Pinus-(Lepidobalanus) assemblage in ascending order. Abrupt

changes to uppermost part were recognized to include Cryptomeria and Pinus, which were influenced by human activity. Cultivated soil covers unconformably the sedimentary sequence during Jomon period.

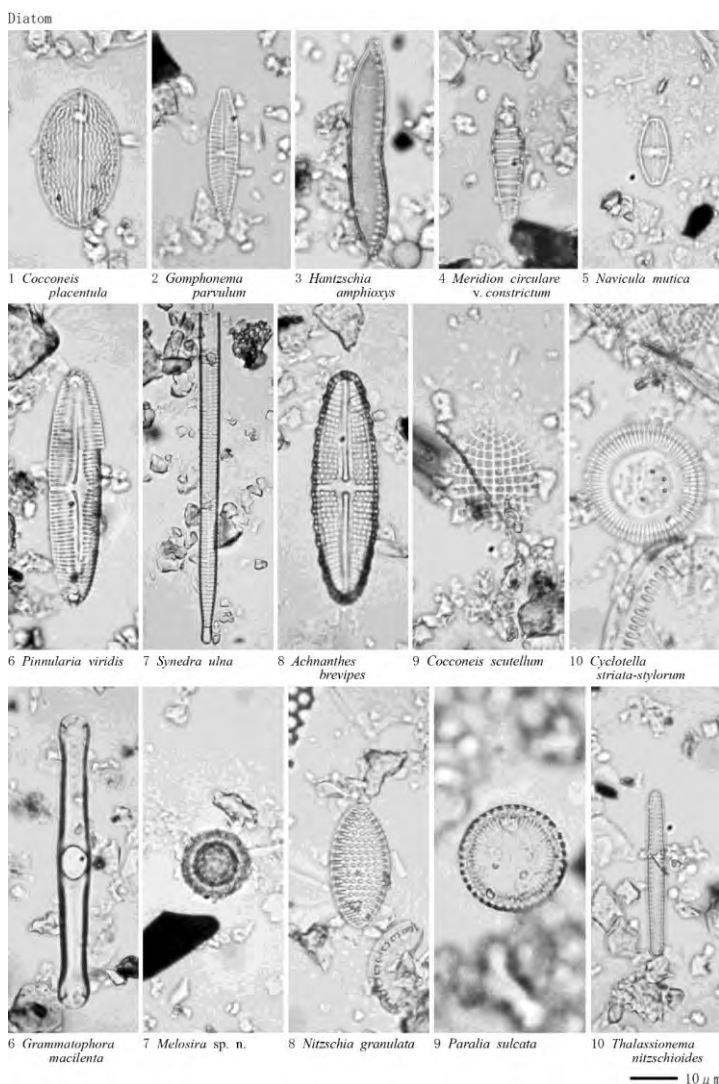### 5.3.3   Diatom Assemblage and Environmental Change

Photo 5.2   *Representative photos of diatom grains from the Mawaki Site.*

Figure 5.7 shows the result of diatom analysis (Photo 5.2) and correlation among C cores from hill side to shoreline side. Abundance of the diatom frustules grains was small in the lower part of sequence. In the middle part of sequence of boring core sediments, *Palaria sulcata* group diatoms were found. The data represent the marine environment. In the sequence of C-2, the boundary between marine environment and marshy environment was located at about 3 m above present sea level.
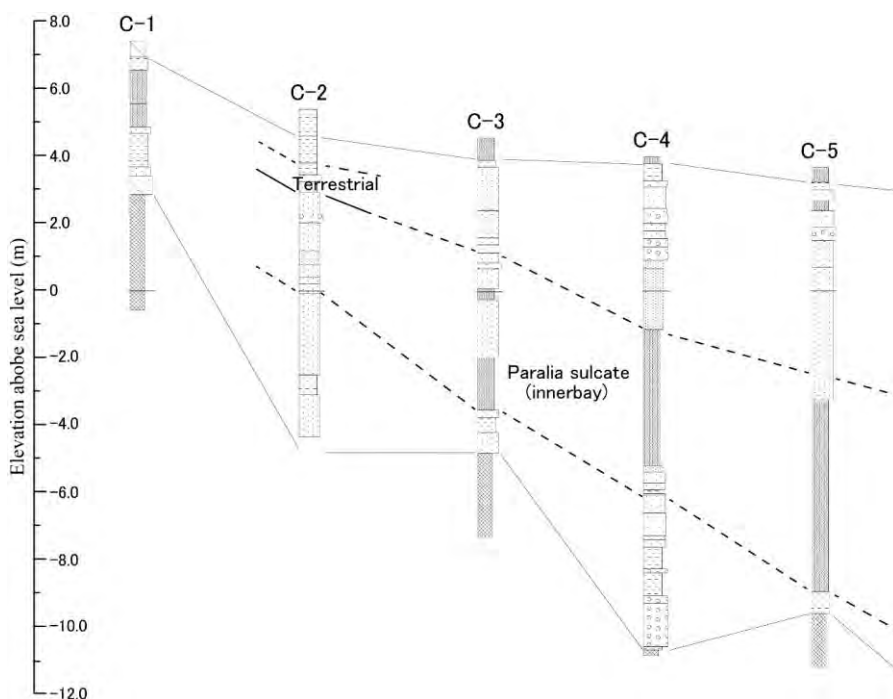
Figure 5.7 *Correlation among cores along the C-Line by diatom occurrence.*

Diatom assemblage of the sediments related with dolphin bone occurrence at the excavation site of the altitude of 3.6~4.3 m above sea level was analyzed. Composition was characterized by occurrence of terrestrial diatom and freshwater diatom associated with marine environment diatom such as *Navicula mutica* in the upper part, *Hantzschia amphioxys* and *Navicula munica* in the

middle part, and *Grammatophora oceanica*, *Hantzschia amphioxys* and *Navicula munica* in the lower part. Horizons of sediments with dolphin bones were characterized by a sedimentary environment along the shoreline based on the diatom assemblage data.
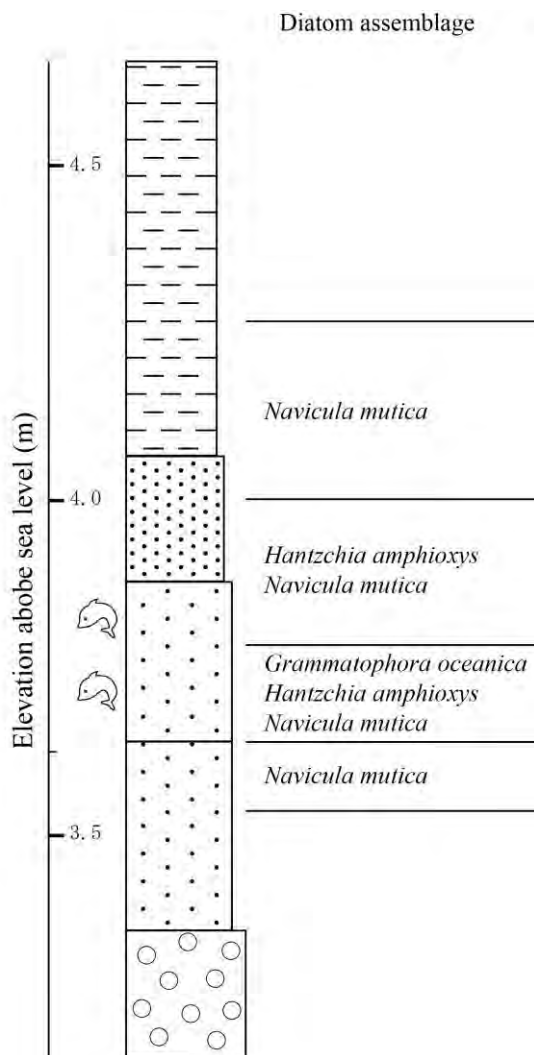

Figure 5.8   Diatom assemblage of sediments at the southwest from the excavation site.

5.4   Conclusive Remarks

Surrounding area of Mawaki region was covered by Quercus and Pinus forest vegetation, and Pinus trees were distributed in the rock area along shoreline side and Aesculus (horse chestnut) were living along the valley. Castanea were distributed in and around the site, and Quercus and Celtis were living during late and latest Jomon period. Castanea and Aesculus were main the eatable fruits for people.

In the latest Jomon period, Aesculus plants were distributed in the newly emerged humid area in front of archeological site.

Low abundance of Cryptomeria indicates a little snow near the site, and this is one of the reasons why the Mawaki archaeological site may have been used as a dwelling area during the Jomon period.

Preliminary data of pollen and diatom within the core samples provided insight into the environmental changes around the Mawaki site, such as changes in sea-level (one cycle of transgression to regression) and vegetation.

References

[1]   Ando, K. (1990). Environmental Indicators Based on Freshwater Diatom Assemblage and Its Application to Reconstruction of Paleo-environments. Ann. Tohoku Geogr. Assoc., 42, 73-88 (in Japanese).

[2]   Asai, K., & Watanabe, T. (1995). Statistic Classification of Epilithic Diatom Species into Three Ecological Groups relating to Organic Water Pollution (2) Saprophilous and saproxenous taxa. Diatom,10, 35-47.

[3]   Hustedt, F. (1937-1938). Systematische und geologishe Untersuchungen uber die Diatomeen Flora von Java, Bali und Sumatra nach dem Material der Deutschen Limnologischen Sunda-Expedition. Arch. Hydrobiol, Suppl., 15, 131-506.

[4]   Krammer, K., & Lange-Bertalot, H. (1986-1991). Bacillariophyceae 1-4.

[5]   Kosugi, M. (1986). Paleoecological Analysis Based on Terrestrial Diatoms, and Its Implications - Introduction to Japan and Its Prospects -.Japanese Journal of

Historical Botany, 1, 29-44 (in Japanese).

[6]   Kosugi, M. (1988). Classification of Living Diatom Assemblages as the Indicator of Environments, and Its Application to Reconstruction of Paleoenvironments. The Quaternary Research, 27 (1), 1-20 (in Japanese).

[7]   Lowe, J. J., & Walker, M. J. C. (1997). Reconstructing Quaternary Environments. Addison Westly Longman Limited.

[8]   Lowe, R. L. (1974). Environmental Requirements and pollution tolerance of fresh-water diatoms. 333p., National Environmental Research Center.

[9]   Nakamura, J. (1967). Pollen Analysis. Kokon Shoin, 232p. (in Japanese)

Chapter 6

Holocene Sea Level Change and Mawaki Archaeological Site

Keiji Takemura

Yasuto Itoh

Hideki Takada

Abstract

Lithological units discovered at the Mawaki Archaeological site on the Noto Peninsula were interpreted as part of a sequence in a cycle of marine transgression and regression. Dated coastal horizons were chosen to indicate former sea levels. A Holocene relative sea-level curve was generated on the basis of geological data, micropaleontological data, and ^{14}C dating, and a rapid rise from 8,800 cal yr BP to 6,000 cal yr BP and a succeeding regression of shoreline by coastal sedimentation was observed. Abundant dolphin bones lay just above the top of the sediment deposited in shallow marine environment. Cultural artifacts were found in a terrestrial deposit near the dolphin bone level that is assigned to a period of high, stable sea level after the post-glacial eustatic high-stand. Dolphin bones are associated with stone artifacts and ritual wood columns, which indicates the presence of longstanding fishery- related activities during the early Holocene on the Japan Sea coast.

6.1 Introduction

Owing to its detailed chronology of cultural materials and the Holocene coastal sediments, the Japanese Islands is an important area for Holocene environmental research in eastern Eurasia (Ota et al., 1982). However, intensive tectonic deformation along the convergent plate margin hinders the precise reconstruction of paleoenvironments. The Pacific coast of the islands has undergone intermittent co-seismic uplift as a result of plate subduction, even during the historical era (Yoshikawa et al., 1973). Although the coastal areas on the Japan Sea side of the islands also suffer considerable deformation due to the activity of adjacent tectonic lines (e.g., Okamura et al., 1995), the Noto Peninsula (Figure 6.1) in central Japan is immune to late Quaternary tectonic movements, and few active faults lie in its northern part (Research Group for Active Faults of Japan, 1991). Because the peninsula has been a low-relief

continental fragment in the Japan Sea throughout the Neogene, the shelf that surrounds it is narrow and the hydroisostatic effects on the peninsula are minimal. The local tidal range is less than 0.2 m. Thus the coastal sediments are expected to be a sensitive recorder of sea-level changes free from the uncertainties noted above (Itoh et al., 2011).

The Mawaki archaeological site is located on the eastern coast of the Noto Peninsula in central Japan (Figures 6.1 and 6.2). It is a village site with evidence of habitation from around 7,000 to 2,500 cal yr BP. The Mawaki site is surrounded by hills that are about 100 m high and is located on an alluvial plain between 4 m and 12 m above sea level. This archaeological site was discovered beneath the cultivated fields between hilly terrain and the present-day coastal residential area. Archaeological relics, such as a circular array of wood columns from the late Jomon period and tombs and human bones from the middle Jomon period, have been excavated. As an archaeological site in an embayment buried during the Holocene regression, the Mawaki site is characterized by marine animal remains. Numerous dolphin bones were excavated between 1982 and 1983 within the sediments of the late early to earliest middle of Jomon period along with abundant Jomon pottery and other remains (Takada and Takemura, this volume).
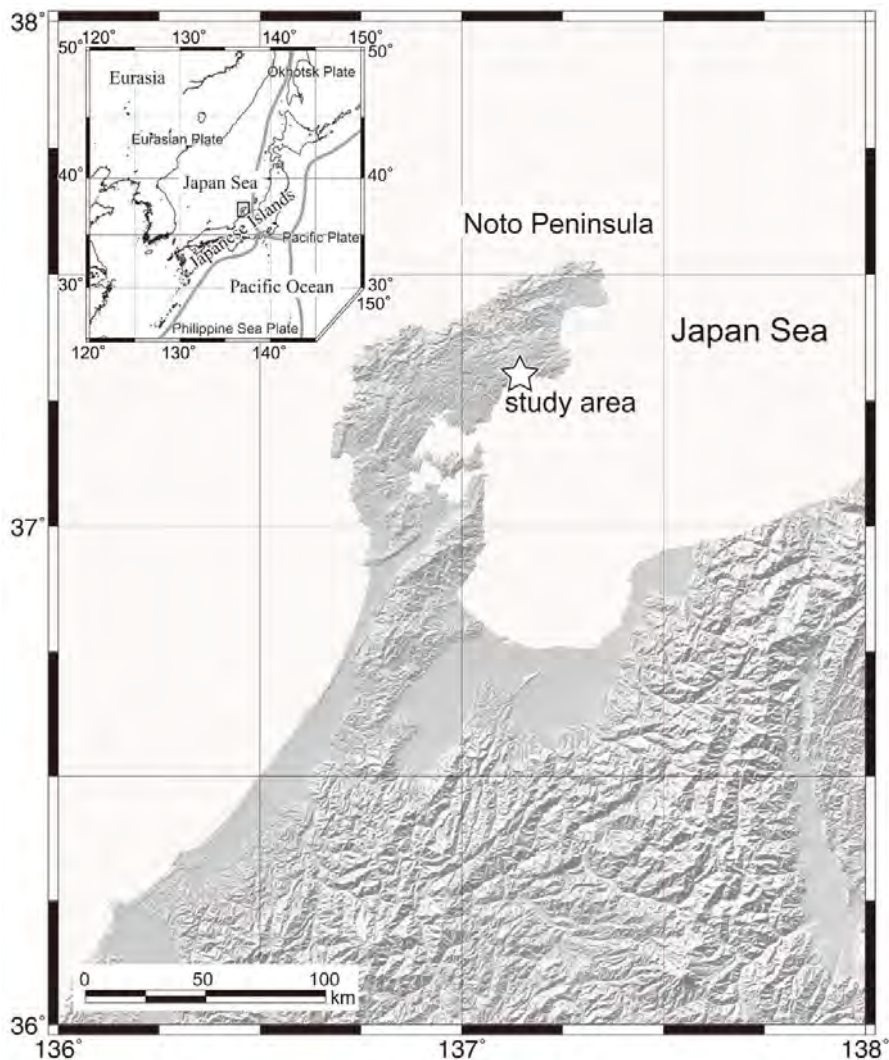
Figure 6.1 *The Noto Peninsula and coastal areas around central Japan with topographic relief on land. The star indicates our study area. (Inset) A synoptic map of the Quaternary tectonic setting around the Japanese Islands. Bold lines show the convergent plate boundary. The box around the central part of the main island of Japan encloses our study area. (Itoh et al., 2011, partly modified).*

The last deglacial sea levels have been studied in many places (Pirazzoli, 1996). The marine transgression in the Japanese Archipelago was very intensive during the middle Holocene, and there are many shell mounds

from the Jomon age along the coastal areas. In archeological terms, this transgression is commonly referred to as the 'Jomon Transgression'. Relative sea level studies have been carried out at several sites in Japan (e.g., Nakamura, 2006; Sato, 2008; Tanigawa, 2009). The occurring transgression follows a similar pattern, but the timing and altitude of high-stands of the transgression are different. Eustatic sea-level curves are generally influenced by local or regional disturbances, such as glacio-/hydroisostatic (Daly, 1934; Bloom, 1967) and tectonic (Stewart and Hancock, 1993) effects.

In this chapter, we summarize the descriptions of the lithology and stratigraphy, radiocarbon ages of borehole samples, and dolphin bones and micropaleontological information. Holocene sequences are correlated on the basis of these properties, and classified into sedimentary units corresponding to marine transgression and regression. Eustatic sea-level changes around the Japan Sea are then estimated using the depositional indicators with numerical ages.

Figure 6.2   *The modern embayment and adjacent Mawaki archaeological site on the alluvial plain.*

6.2 Interactions Between Sea Level Change and Human Activities

Transgression and regression are geological phenomena caused by the interaction between sea-level change, sediment discharge from rivers, and coastal erosion. These phenomena interact with human activities in some cases though they occur on a geological time scale that is beyond an average human's life span. Majority of the coastal plains were formed during the regression stage that succeeded the high-stand stage. Moreover, ancient civilizations developed and huge cities were settled on such coastal plains with flat land formed as a result of the regression. The evidences of the effects of the processes and speed of regression on human civilizations are evident from recent studies in the opposite direction.

The sediment discharge of the Huanghe (Yellow River) in China abruptly increased by ten times ca. 1,000 years ago (Li, 1991; Xue, 1993; Zhang, 1984). The reasons being the cultivation and deforestation is due to the increasing population in the Loess Plateau, the hinterland of the river (Saito et al., 2001). As the sediment discharge increased, regression was accelerated and as a result, huge cities, like Beijing, were developed on the large plain around the lower reach of the Huanghe. Similar accelerations of the regression are found in Changjiang (Yangtze River) in China (Chen, 1998; Hori et al., 2001; Wang et al., 1981). Such accelerations are clearly found not only in the continental big rivers, also found in small rivers, for example, the Yahagi River in central Japan (Sato and Masuda, 2010).

Though the survey area, the Mawaki site, is a small basin when compared to the big basins in continents (Figure 6.2), the Holocene sediment in this area shows transgression and regression similar to the sediment in big basins (Takemura et al., this volume) and the human activities around the basin were well studied (Takada and Takemura, this volume). Therefore, the Mawaki

archeological site was suitable for studying the interaction between human activities and geological phenomena.

6.3   Summary of Geoarchaeological Data

In this section, we present an overview history of sea level change on the basis of stratigraphy (Takemura et al, this volume), chronology (Nakamura and Takada, this volume) and paleoenvironmental information of pollen and diatom (Kanehara and Takada, this volume) at the Mawaki archaeological site, and present a precise summary of three viewpoints.

6.3.1   Lithology and Stratigraphy

A drilling survey was carried out at the Mawaki archaeological site in 1998 (see Figure 6.3). For the survey, seventeen boreholes were drilled and continuous records of the Holocene sediments and underlying basement were obtained. Most of the cultural remains found in the strata including dolphin bones have been excavated in the vicinity of borehole C-2, where the sediments are mostly subaerial. C-Line boreholes (C-1 to C-8) were selected for the collection of lithological, micropaleontological, and chronological data. These boreholes are aligned in the north-south direction, namely, from the coastal areas to the shallow marine areas of the Holocene embayment in the northern part of the Noto Peninsula. Detailed lithological descriptions and radiocarbon ages have been obtained from the core samples (Board of Education of Noto Town and Investigating Commission for Mawaki Site, 2002). Auxiliary core B-3 (Figure 6.3 for borehole location) and dolphin bone occurrence elevation with ^{14}C ages were utilized to determine the post-glacial high-stand.
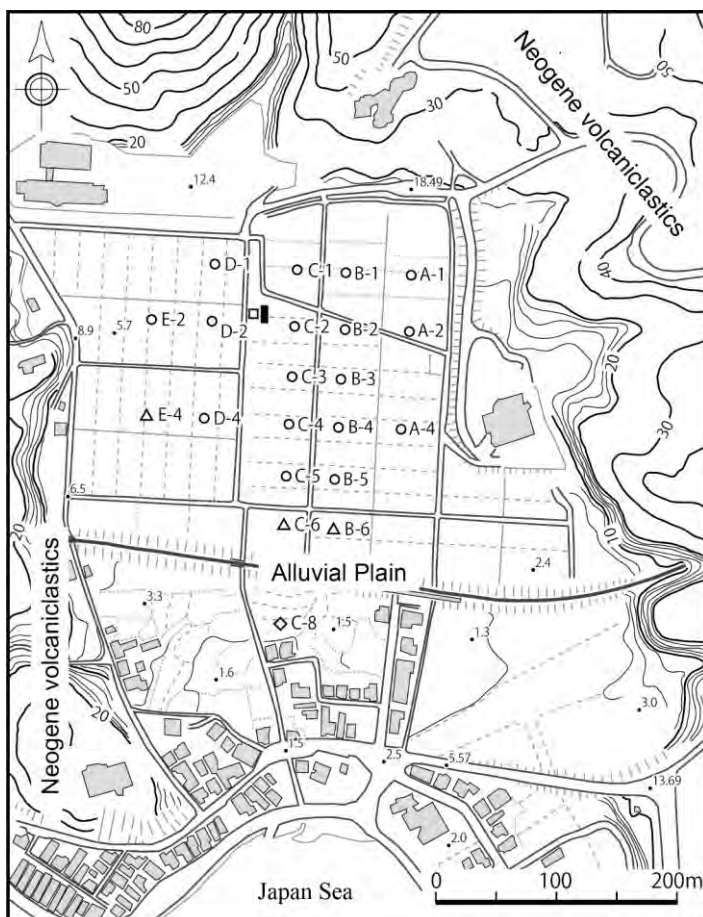
Figure 6.3 *Borehole and geoslicer locations around the Mawaki archaeological site. Open circle: drilling in 1997 & 1998, open triangle: drilling in 2002, open rhombus: drilling in 2005, solid rectangle: geoslicer coring.*

Stratigraphic data obtained from the core samples taken at Mawaki site are summarized by Takemura et al. (this volume). The lithological unit nomenclature is that of Itoh et al. (2011) as follows.

Basement: Miocene volcaniclastics composed of tuff and tuffaceous mudstone.

Unit A: Sands and gravels, poorly sorted, containing charcoal grains.

Unit B: Clays and silts with abundant remains of marine organisms, intercalations of well-sorted sandy layers, containing shell and plant fragments.

Unit C: Silty sands with gravels, well-sorted medium sands, containing abundant shells and plant fragments.

Unit D: Sands and gravels, poorly sorted, containing pottery fragments and charcoal grains.
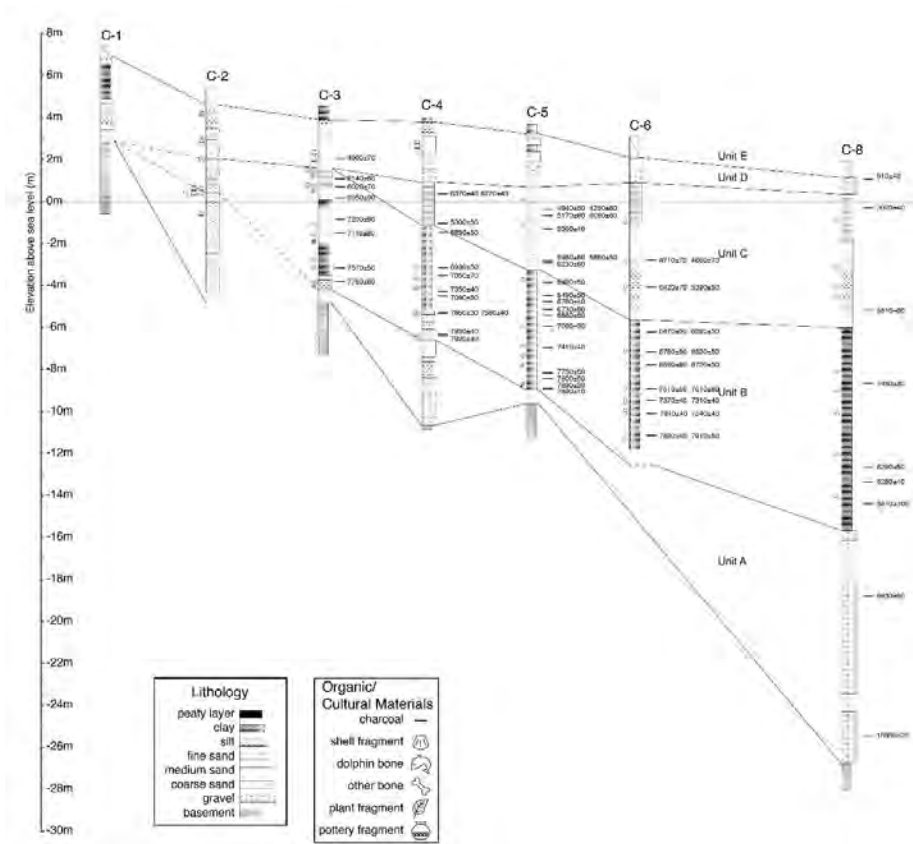
Unit E: Cultivated soil.

Figure 6.4 *Stratigraphic data for core samples along the C-Line (C-1, C-2, C-3, C-4, C-5, C-6 and C-8). The occurrence of organic/cultural materials is shown on the left side of the lithological columns. Radiocarbon dates are shown on the right side of the columns. Solid lines are the lithological boundaries of units A, B, C and D.*

Information on organic/cultural materials and radiocarbon dates (Nakamura and Takada, this volume) are placed on the left and right sides of the lithological columns, respectively, in Figure 6.4. These data are used later in the discussion of paleoenvironmental reconstruction and the recognition of former sea levels.

6.3.2   Radiocarbon Ages of Borehole Samples and Dolphin Bones

Table 6.1   *^{14}C age data related with the horizons of ancient sea levels.*

			Depth (m)	Elevation (m)	Calibration age (cal yBP)
1	C-3	wood	2.53	2.06	4900±70
2	B-3	shell	3.12	1.47	5140±70
3	Dolphin			3.50	5580-5650
4	B-3	shell	3.38	1.21	6770±50
5	C-3	wood	8.43	-3.84	7760±60
6	C-4	wood	9.30	-5.30	7650±30
7	C-4	shell	9.30	-5.30	7580±40
8	C-4	wood	10.30	-6.30	7930±40
9	C-4	shell	10.38	-6.38	7920±40
10	C-5	wood	12.60	-8.93	7890±40
11	C-6	shell	14.24	-11.14	7890±40
12	C-6	plant	14.24	-11.14	7910±50
13	C-8	plant	16.36	-14.40	8810±100

The ^{14}C ages of shell samples, wood, plant fragments and peat samples separated from sediment cores C-3, C-4, C-5, C-6 and C-8 were measured at the AMS laboratory of the Center for Chronological Research, Nagoya University (Nakamura et al., 2000). After the treatment procedure, the ^{14}C ages were obtained. The oceanic reservoir effect on marine shell samples was calibrated using a calibration program OxCal4.2.4 (Bronk Ramsey, 2009) and IntCal13 or Marine-13calibration data set (Reimer et al., 2013).

Nakamura and Takada (this volume) have estimated the correction value of the local marine carbon reservoir effect, ΔR, for sediment samples from cores C4, C5, and C6. The obtained ΔR values were less reliable with rather large

errors, and because the ΔR values were almost consistent with zero within ±1 σ error, ΔR = 0 for calibration of marine samples collected from the Mawaki site. On the basis of probability density distributions against the calendar dates of ^{14}C ages obtained for nine carbonaceous fractions from dolphin bones, ^{14}C ages and their calibrated ages were found to be around 5,580-5,650 cal yr BP, when the carbonaceous fractions dated were separated from more essential and genuine sections of the dolphin bones.

We selected thirteen carbon dating results for the reconstruction of sea level changes around the Mawaki site (Table 6.1) from the age data obtained by Nakamura and Takada (this volume) on the basis of sedimentological information.

6.3.3   Micropaleontological Information

The pollen assemblage at the site indicated a forest comprising broad-leaved deciduous trees such as Qercus and Aesculus (horse chestnut) within the clay and silty sand units (units B and C). The occurrence of pollen grains was very high within units B and C, comprising Lepidobalanus-Aesculus assemblage, Pinus-Lepidobalanus assemblage and Cyclobanopsis-Pinus-(Lepidobalanus) assemblage in an ascending order. This indicated a cycle of marine transgression.

In the middle part of the sequence of boring core sediments (Unit B), *Palaria sulcata* group diatoms were found. Additionally, in the sequence of C-2, the boundary between marine environment and marshy environment was located at about 3 m above the present sea level on the basis of diatom assemblage. Diatom assemblage of the sediments related to dolphin bone occurrence at the excavation site at an altitude of 3.6 - 4.3 m above sea level was analyzed. The composition was characterized by the occurrence of terrestrial diatom and freshwater diatom associated with marine environment diatom such as *Navicula mutica* in the upper part, *Hantzschia amphioxys* and *Navicula munica* in the

middle part, and *Grammatophora oceanica*, *Hantzschia amphioxys* and *Navicula munica* in the lower part. Based on the diatom assemblage data, horizons of sediments with dolphin bones were characterized by a sedimentary environment along the shoreline.

6.4   Discussion

Our study has established the Holocene stratigraphy around the Mawaki archaeological site. In the first part, we consider the sedimentary facies, which record a cycle of marine transgression and regression. Indicators of former sea levels have been identified during the course of paleoenvironmental interpretation. Next we present a Holocene eustatic curve along the Japan Sea coast by taking into consideration the effects of tectonic uplift. Finally, the history of the Mawaki archaeological site is described on the basis of the stratigraphic interpretation related to the sea level change.

6.4.1   Paleoenvironments

Radiocarbon ages suggest that the bottom of unit B is a marine transgressive surface. Its age ranges from 8,810 cal yr BP (C-8) to 7,760 cal yr BP (C-3) as shown in Figure 6.4, and this is suggestive of rapid onlapping sedimentation during a remarkable rise in sea-level. The altitudes and ages of coastal sediments at the base of unit B are therefore regarded as an indicator of ancient sea levels.

Unit B in the C-3 core is an upward-coarsening sequence that was deposited during the latter period of the sea-level rise. The sandy wedge of unit C is interpreted as a maximum relict barrier or relict sand-pit developed parallel to the ancient shoreline, and covered by terrestrial sediments with potteries from 4,900 cal yr BP (2.06 m above sea level). Its age is useful for the reconstruction of the sea-level.

In the C-series cores, evidence of higher sea levels has been destroyed by subsequent erosion. Instead we use the record from auxiliary core B-3 (see Figure 6.3 for location) where marine sediments containing oyster shells are preserved at the highest level (1.91 m above sea level) of the Holocene succession despite the absence of age data. Moreover, the age of dolphin bones discovered at 3.50 m above sea level, analyzed by Nakamura and Takada (this volume), are used to obtain ancient shoreline information. We interpret these to mean that the high-stand followed the deposition of transgressive unit B. Silty and well-sorted sands in cores C-4, C-5, C-6 and C-8 are interpreted as estuary and long-shore bar deposits, respectively, in a coastal system.

Using the micropaleontological data of diatom, a cycle of marine transgression and the location of the shoreline were interpreted on the basis of the occurrence of terrestrial diatom species.

6.4.2   Eustatic Sea Levels

Figure 6.5 presents a sea-level change for the Holocene constructed on the basis of the Mawaki depositional indicators described in the previous section. It is characterized by a rapid rise during the period from 8,800 cal yr BP to 6,000 cal yr BP succeeded by a minor fall around the present sea level. Such a trend is generally concordant with previous research (Fujii and Fuji, 1982) based on sea-level indicators along the Japan Sea coast. In Unit C, horizontal isochrones indicate an aggradational sedimentation pattern.

Holocene sea level change is a significant concern for Japanese archaeologists because of the significant influence it had on the waxing and waning of societies during the Jomon period. It has been suggested that the so-called 'Jomon Transgression' was related to the establishment of the Incipient to Early Jomon culture that is preserved in the form of many shell midden sites along certain Japanese coastal areas. However, relative sea levels in the

Japanese Archipelago show considerable variability (e.g., Ota et al., 1982; Moriwaki, 2004) reflecting tectonic and/or hydroisostatic controls on an active plate margin (Pirazzoli, 1996). We present an in situ sea level curve in order to discuss the paleoenvironments of the Mawaki site. Moreover, as mentioned previously, this sea level curve is mostly free from local tectonic effects and may therefore serve as a regional reference curve in East Asia.
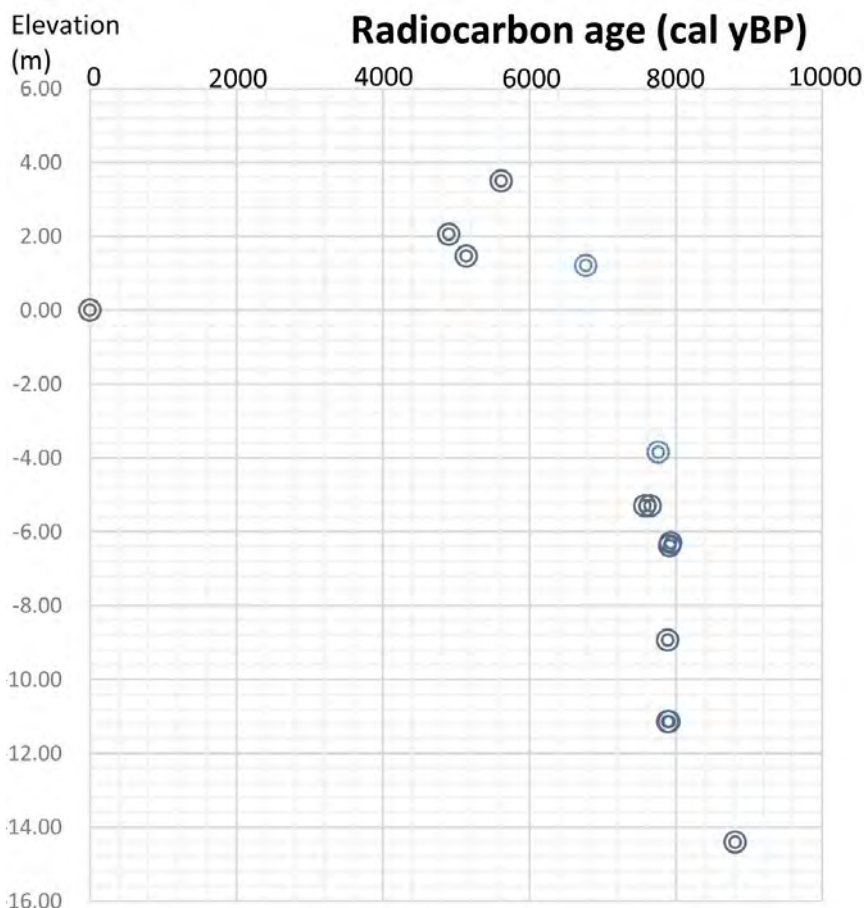

Figure 6.5 *A Holocene sea-level change plot obtained from the Mawaki Archaeological Site.*

6.4.3 History of the Mawaki Archaeological Site Related with the Discovery of Dolphin Bones

Holocene sediments from the Mawaki archaeological site on the Japan Sea coast yielded many animal bones-remains, Jomon pottery and stone remains. The most characteristic remains are dolphin bones intercalated in the strata of the late-early to early-middle Jomon period found as a discrete, stratified occurrence. These strata also contain stone implements including many flint arrowheads, stone arrows, stone knives and scrapers.

As Itoh et al. (2011) summarized, the coexistence of many dolphin bones, human stone remains and scraped wooden columns can be attributed to dolphin fishery. Abundant dolphin bones were recorded at the top of the marine sequence (boundary between units C and D) and located in the seashore environment. Cultural materials were found in a subaerial deposit (unit D) just above the dolphin bone occurrence level. A stable high sea level subsequent to the rapid post-glacial transgression resulting in a lagoonal environment and a deep inlet around the Mawaki site has been clarified on the basis of paleoenvironmental study. The Mawaki site must have been a suitable configuration for thriving fisheries-related activities from the earliest through to the latest Jomon periods. The dolphin fishery itself has continued along the coastal area till the present day (e.g., Hiraguchi, 2006).

6.5 Summary

The paleoenvironment around the Mawaki archaeological site in central Japan has been reconstructed on the basis of a geological survey by utilizing precise stratigraphic correlation and numerous ^{14}C age data. As a result, four lithological units have been identified and interpreted as a sequence in a cycle of Holocene marine transgression and regression. Relative sea-level changes in the Holocene along the Japan Sea coast are characterized by a remarkable rise between the

period from 8,800 cal yr BP to 6,000 cal yr BP and a succeeding regression of shoreline by coastal sedimentation around the present level. These changes are not attributed to local tectonic disturbance rather to a regional eustatic trend. It worth noting that horizons containing abundant dolphin bones are representative of a period of high, stable sea level after the post-glacial eustatic high-stand. Dolphin bones are associated with stone artifacts (arrowheads, knives and scrapers) and ritualistic wood columns, implying the presence of fishing activities throughout the Jomon period along the Japan Sea coast.

References

[1] Bloom, A. L. (1967). Pleistocene shoreline: a new test of isostasy. Geological Society of America Bulletin, 78, 1477-1494.

[2] Board of Education of Noto Town and Investigating Commission for Mawaki Site (2002). Mawaki Site in Noto Town, Ishikawa Prefecture - Outline of excavation report at Three to Six stages related to the improvement act of site environment as a historical site, 170pp (in Japanese).

[3] Bronk Ramsey, C. (2009). Bayesian analysis of radiocarbon dates. Radiocarbon, 51 (1), 337-360.

[4] Chen, X. (1998). Changjiang (Yangtze) River delta. Journal of Coastal Research, 14, 838-858.

[5] Daly, R. A. (1934). The Changing World of the Ice Age. New Haven: Yale University Press.

[6] Fujii, S., & Fuji, N. (1982). Postglacial sea-level changes in the Hokuriku region, central Japan. The Quaternary Research, 21, 183-193 (in Japanese with English abstract).

[7] Hiraguchi, T. (2006). People at Mawaki site with dolphin fishery. In Board of Education of Noto Town & Investigating Commission for Mawaki Site (Eds.), Mawaki Site in Noto Town, Ishikawa Prefecture - Outline of Excavation Report at Seven to Nine Stages related to the Improvement Act of Site Environment as a Historical Site (pp.147-158) (in Japanese).

[8] Hori, K., Saito, Y., Zhao, Q., Cheng, X., Wang, P., Sato, Y., & Li, C. (2001). Sedimentary facies and Holocene progradation rates of the Changjiang (Yangtze) delta, China. Geomorphology, 41, 233-248.

[9] Itoh, Y., Takemura, K., Nakamura, T., Hasegawa, S., & Takada, H. (2011). Paleoenvironmental analysis of the Mawaki archaeological site, central Japan, in relation to stratigraphic position of dolphin bones. Geoarchaeology, 26 (4), 461-478.

[10] Kanehara, M., & Takada, H. (2016). Analysis of pollen and diatoms in the Mawaki area, Noto Peninsula, during Holocene: A microscopic perspective of the Mawaki environment (this volume).

[11] Li, Y. (1991). Changes of the abandoned Huanghe delta. Geographical Research, 10, 29-38.Maeda, Y. (1976). The sea level changes of Osaka Bay from 12,000 BP to 6,000 BP. Journal of Geosciences, Osaka City University, 76, 43-58.

[12] Moriwaki, H. (2004). Kaimenhenka to koukogaku (Sea level changes and archaeology). In Y. Yasuda (Ed.), Handbook on Geoarchaeology (pp. 135-143). Tokyo: Asakura Shoten (in Japanese).

[13] Nakamura, T. (2006). Holocene sea level changes and paleogeography of the central part of the San-in District, Japan. The Quaternary Research, 45, 407-420 (in Japanese).

[14] Nakamura, T., Niu, E., Oda, H., Ikeda, A., Minami, M., Takahashi, H., Adachi, M., Pals, L., Gottdang, A., & Suya, N. (2000). The HVEE Tandetron AMS system at Nagoya University. Nuclear Instruments and Methods in Physics Research, B172, 52-57.

[15] Nakamura, T., & Takada, H. (2016). Radiocarbon dating of Holocene sediments at the Mawaki site by accelerator mass spectrometry (this volume).

[16] Okamura, Y., Watanabe, M., Morijiri, R., & Satoh, M. (1995). Rifting and basin inversion in the eastern margin of the Japan Sea. The Island Arc, 4, 166-181.

[17] Ota, Y., Matsushima, Y., & Moriwaki, H. (1982). Notes on the Holocene sea-level study in Japan - On the basis of "Atlas of Holocene Sea-level Records in Japan" -. The Quaternary Research, 21, 133-143 (in Japanese with English abstract).

[18] Pirazzoli, P. A. (1996). Sea-Level Changes: The Last 20,000 Years. Chichester: John Wiley & Sons.

[19] Reimer, P. J., Bard, E., Bayliss, A., Beck, J. W., Blackwell, P. G., Bronk Ramsey, C., Buck, C. E., Cheng, H., Edwards, R. L., Friedrich, M., Grootes, P. M., Guilderson, T. P., Haflidason, H., Hajdas, I., Hatté, C., Heaton, T. J., Hoffmann, D. L., Hogg, A., G., Hughen, K. A., Kaiser, F., Kromer, B., Manning, S. W., Mu Niu, M., Reimer, R. W., Richards, D. A., Scott, E. M., Southon, J. R., Staff, R. A., Turney, C. S. M., & van der Plicht, J. (2013). IntCal13 and Marine13 radiocarbon age calibration curves 0- 50,000 years al BP. Radiocarbon, 55(4), 1869-1887.

[20] Research Group for Active Faults of Japan (1991). Active Faults in Japan: Sheet Maps and Inventories, Revised Edition. Tokyo: University of Tokyo Press (in Japanese with English abstract).

[21] Saito, Y., Zuosheng, Y., & Hori, K. (2001). The Huanghe (Yellow River) and Changjiang (Yangtze River) deltas: a review on their characteristics, evolution and sediment discharge during Holocene. Geomorphology, 41, 219-231.

[22] Sato, H. (2008). Reconstruction of Holocene sea-level change along the coast of Harimanada in the eastern part of the Seto Inland Sea, western Japan. The Quaternary Research, 47, 247-259 (in Japanese).

[23] Sato, T., & Masuda, F. (2010). Temporal changes of a delta: Example from the Holocene Yahagi delta, central Japan. Estuarine, Coastal and Shelf Science, 86, 415-428.

[24] Stewart, I. S., & Hancock, P. L. (1993). Neotectonics. In P. L. Hancock (Ed.), Continental Deformation (pp. 370-409). Oxford: Pergamon Press.

[25] Takada, H., & Takemura, K. (2016). An overview of the Mawaki Archaeological Site with a focus on its archaeological significance (this volume).

[26] Takemura, K., Takada, H., Haraguchi, T., & Itoh, Y. (2016). Holocene stratigraphy from the Mawaki Archaeological site and the occurrence and significance of dolphin bones (this volume).

[27] Tanigawa, K. (2009). Stratigraphic and sedimentary environment of the recent deposits and Holocene relative sea level changes in the lower Maruyama River Plain, Hyogo Prefecture, Japan. The Quaternary Research, 48, 255-270 (in Japanese).

[28] Wang, J., Guo, X., Xu, S., Li, P., & Li, C. (1981). Evolution of the Holocene Changjiang delta. Acta Geologica Sinica, 55, 67-81 (in Chinese with English

abstract).

[29] Xue, C. (1993). Historical changes in the Yellow River delta, China. Marine Geology, 113, 321-329.

[30] Yoshikawa, T., Sugimura, A., Kaizuka, S., Ota, Y., & Sakaguchi, Y. (1973). Geomorphology of Japan. Tokyo: University of Tokyo Press (in Japanese).

[31] Zhang, R. (1984). Land-forming history of the Huanghe river delta and coastal plain of North Jiangsu. Acta Geographica Sinica, 39, 173-184.

Short Introduction to the Book

An archaeological site provides us with affluent information on climatic and geologic phenomena during late Pleistocene and Holocene. It is pursued by means of extensive research integrating stratigraphy, paleontology, geochronology and geophysics. Through such multidisciplinary approach, the authors attempt to describe life of the ancients on post-glacial Far East, which has never been understood in the framework of long-term environmental changes.

Short Biography of the Author

Yasuto Itoh - He is the Professor of the Graduate School of Science of Osaka Prefecture University. He conducts research into tectonics, stratigraphy and paleomagnetism, and has published about 100 papers in the field of backarc opening processes, deformation mode of active plate margins, quantitative assessment of active faults, paleoenvironment of East Asia and mechanism of sedimentary basin formation. He is a member of the Integrated Research Project for Active Tectonics by the Ministry of Education, Culture, Sports, Science and Technology (MEXT), Japan.

Hideki Takada – He graduated from Nara University in the course of Department of the Preservation of Cultural Properties, Faculty of Letters, and now is the Counselor and Director of the Mawaki Site Jomon Museum of Headquarters of Education, Noto Town, Ishikawa Prefecture. He has been engaged in the excavation and archaeological researches of Mawaki Archaeological site of Noto Peninsula since 1981.

Keiji Takemura – He received a PhD in Kyoto University related to geological science, and now is the Professor of the Graduate School of Science of Kyoto University. He conducts research into stratigraphy, active tectonics, tephrochronology and geothermal sciences, and has published more than 300 papers (half in English) in the field of Quaternary sciences.